Thesis for Master of Science degree in Molecular Biosciences

Main field of study in molecular biology

DNA damage induced changes to Golgi apparatus morphology: Visual analysis of Golgi apparatus morphological change and analysis of effect on proteoglycan synthesis and sorting in MDCK cells.

Kim Bache-Mathiesen

Department of Biosciences

The Faculty of Mathematics and Natural Sciences

University of Oslo

October 2015

2015

DNA damage induced changes to Golgi apparatus morphology: Visual analysis of Golgi apparatus morphological change and analysis of effect on proteoglycan synthesis and sorting in MDCK cells.

Kim Bache-Mathiesen

http://www.duo.uio.no/

Print: University Print Centre, University of Oslo

Acknowledgements

The work presented in this thesis was carried out at the Deparment of Biosciences, University of Oslo, under the supervision of D.Sc. Gunnar Dick and professor D.Sc. Kristian Prydz.

Words cannot express the gratitude I have for my two supervisors D.Sc. Gunnar Dick and professor D.Sc. Kristian Prydz. You have shown me more patience than I deserve, and have helped guide me through a bumpy part of my life with your amazing teaching, understanding and advice. Kristian you have not only supported me with your knowledge and advice since your first lecture in advanced cell biology in 2011, but through group presentations and participating courses over the years, you have also helped me largely overcome my fear of giving presentations to groups of my peers. I know I have not been the easiest master student moving through your group, and my humble thanks are not enough. Thank you both for everything.

I would also like to thank the other members of the Prydz-group both from past and present. Ravi Adusumalli, you have always given me your invaluable assistance in understanding and performing experimental protocols when I am working late in the lab. Linn Kristin Akslen-Hoel, in combination with Kristian Prydz, you introduced me to the working lab environment, and taught me all the rudimentary knowledge and routines I needed for all cell lab related work.

I would also like to thank Frode Militzow Skjerdal for his help teaching me the confocal microscope and the use of the analytical tools available.

I want to thank the managers at Outland AS where I work in the weekends, Simen Josefsen and Ellen Guldberg, for their continued patience and understanding, and who have provided financial aid and giving me time off from work to focus on my studies whenever I need it.

Last, but not least, I would like to thank my family for having supported me through the last 6 years of my university degree. Especially my sister Lena Bache-Mathiesen, who has often taken time away from her own studies to listen to my complaints and help me get through presentations and exams.

Oslo, October 2015

Kim Bache-Mathiesen

List of content

Abbreviations

A	Ampere
Api	Apical
Baso	Basolateral
BFA	Brefeldin A
BSA	Bovine serum albumin
COP	Coat protein complex
cpm	Counts per minute
CPT	Camptothecin
CS	Chondroitin sulphate
CSPG	Chondroitin sulphate proteoglycans
Ctrl	Control
dH_2O	Distilled water
DMEM	Dulbecco's modified Eagle's medium
DMSO	Dimethyl sulfoxide
DNA	Deoxyribonucleic acid
Doxo	Doxorubicin
DS	Dermatan sulphate
EDTA	Ethylenediaminetetraacetate
ER	Endoplasmic reticulum
ERGIC	ER-Golgi intermediate compartment
FBS	Fetal bovine serum
GAGs	Glycosaminoglycans
Gal	Galactose
GalNAc	N-acetyl-galactosamine
Glc	Glucose
GlcNAc	N-acetyl-glucosamine
GlcNS	N-sulphated-glucosamine
GlcA	Glucuronic acid
GFP	Green fluorescent protein
HS	Heparan sulphate
h	Hour(s)
IdoA	Iduronic acid
KDEL	Lys-Asp-Glu-Leu sequence
KS	Keratan sulphate
M	Molar
mCi	Millicurie
MDCK	Madin-Darby canine kidney
mg	Milligram
min	Minutes
mL	Milliliter
mM	Millimolar
mm	Millimeter
nm	Nanometer
P/S	Penicillin / streptomycin
PAPS	3'-phosphoadenosine 5'-phosphosulphate
PAPST1	3'-phosphoadenosine 5'-phosphosulphate transporter-1
PBS	Phosphate buffered saline
PG	Proteoglycan
PTM	Post-translational modification
RNA	Ribonucleic acid
RPM	Rotations per minute
SDS	Sodium dodecyl sulphate
SDS-PAGE	Sodium dodecyl sulphate – polyacrylamide gel electrophoresis
SG-GFP	Serglycin-GFP
SG-KDEL-GFP	Serglycin-KDEL-GFP
SRP	Signal recognition particle
t	Time
TGN	*Trans*-Golgi network
UV	Ultraviolet
V	Volt
x g	Times gravity
µl	Microliter
µM	Micromolar
µm	Micrometer
VTC	Vesicular-tubular clusture

Abstract

The Golgi apparatus is the main transportation and sorting organelle system for proteins entering the secretory pathway. It is involved in the modification of N-linked glycans, and it is the site for several types of O-linked glycosylation. One such mechanism is the synthesis of glycosaminoglycans (GAGs), which are attached to acceptor protein cores at specific glycosylation sites. The resulting proteoglycan (PG) can have multiple GAGs of various types and lengths. These GAGs are heavily sulphated in the Golgi apparatus by the universal sulphate donor 3'-phosphoadenosine 5'-phosphosulphate (PAPS), which is transported into the Golgi lumen by the Golgi transmembrane proteins 3'-phosphoadenosine 5'-phosphosulphate transporter 1 (PAPST1) and 2. Glycan moieties have earlier been shown to work as sorting signals in polarized epithelial cells, and influences whether a protein core is destined for the apical or basolateral side of the epithelium. In this thesis, we have studied changes in the Golgi morphology in Madin-Darby canine kidney (MDCK) cells as a result of chemically induced DNA damage, and how such morphological change affects synthesis and sorting of sulphated PGs in the cell line. Morphological studies were carried out using fluorescent confocal imaging of MDCK II cells expressing the Golgi transmembrane PAPST1 protein with a GFP tag in the presence of the DNA damaging agents doxorubicin (Doxo) or Camptothecin (CPT). The results show an increase in relative Golgi area in MDCK II cells post treatment with Doxo or CPT.

Synthesis and secretion studies were carried out using metabolic labeling by incubating filter-grown MDCK II cells with ^{35}S-sulphate. In these studies we observed possible reduction in sulphated macromolecules in the apical medium, the basolateral medium and the cell lysate.

1 Introduction

1.1 Golgi apparatus form and function

Proteins that pass through the secretory pathway will pass through the Golgi apparatus and either be integrated in the plasma membrane, secreted or transported to endosomes or lysosomes. The secretory pathway originates in the endoplasmic reticulum (ER) where the proteins are synthesized. After completion of the polypeptide constituting the protein core, the proteins receive variable post-translational modifications (PTMs), such as glycosylation, as they move along the pathway. Several of these proteins are important for the cell's structure and function, and as such, changes in their synthesis and modification can affect normal cell structure and function. Further, these changes can potentially lead to a transformation of normal cells into cancer cells. Changes in the Golgi apparatus structure and (biochemical) environment have been observed in cancer cells (Kellokumpu et al. 2002; Li & Wang 1989; Schulenberg et al. 2003). It is therefore interesting to study the connection between DNA damage that often leads to cancer and the Golgi apparatus structure and function.

DNA damage can result in changes to the final gene products and the regulation of their synthesis and function. This can further lead to changes in the cells form and functions, including changes in the Golgi apparatus structure. It is of interest whether these changes have an effect on proteoglycan (PG) synthesis. Further, more research is needed on whether certain changes to the form and function of the Golgi apparatus could act as a mediator between DNA damage and cancer development. For example, changes in the glycosylation of epidermal growth factor receptors (EGF-receptors), cadherins and other important proteins have been observed to lead to transformation of cells (Przybylo et al. 2002; Lin et al. 2015).

1.1.1 Proteins path through the secretory pathway

Secretory proteins usually have an N-terminal signal sequence that is recognized by a signal recognition particle (SRP) in the cytoplasm. This signal is recognized as soon as it is translated from the ribosome and causes the translation to halt until the SRP-ribosome complex binds to an SRP receptor in the ER membrane. This causes the release of the SRP and the ribosome recruits additional ER membrane proteins to help facilitate the translation and translocation through the ER membrane (Walter & Johnson 1994).

Within the ER lumen newly translated proteins will be able to undergo N-linked glycosylation, disulfide bond formation, protein folding and quality control. These secretory proteins then leave the ER at ER exit sites in direction of the Golgi apparatus, involving coat protein complex II (COPII) coated vesicles (Bannykh et al. 1996; Mogelsvang et al. 2004). Transport between the ER and Golgi apparatus is observed to involve pre-Golgi structures known as vesicular-tubular clusters (VTCs) or the ER-Golgi intermediate compartment (ERGIC). This membrane cluster can be identified by the lectin ERGIC-53, and exhibits different properties from both the ER and the *cis*-Golgi compartments (Saraste & Kuismanen 1984; Schweizer et al. 1991; Sannerud et al. 2006).

The detailed mechanisms of how the Golgi apparatus resides as a permanent structure, as well as facilitating dynamic transport of cargo, are still unclear. Different models are suggested, as described in section 1.1.3 below. The ERGIC will either incorporate with an existing *cis*-Golgi *cisterna* or participate in the construction of a new *cis*-Golgi *cisterna*. When entering the *cis*-Golgi apparatus, secretory proteins will then travel through the *cis*- and *medial*-Golgi apparatus, where O-linked glycosylation occurs, as well as trimming and possible branching of N-linked glycans, along the way to the *trans*-Golgi network (TGN). In the TGN, proteins will be sorted and transported to their target destinations, the plasma membrane, for secretion or transport to endosomal/lysosomal compartments.

1.1.2 Golgi apparatus structure, size and localization

Golgi apparatus structure as observed in the transmission electron microscope (TEM), shows several *cisternae* organized into stacks localized in the perinuclear area. In vertebrate cells, the Golgi *cisternae* and stacks are all one single entity termed the Golgi ribbon (Wei & Seemann 2010; Mogelsvang et al. 2004). Many vesicles can be observed around the Golgi apparatus, and different models have been suggested to explain their purpose.

The size and shape of the Golgi complex has high variability, depending on the organism and cell type. The Golgi apparatus may consist of individual Golgi *cisterna*, as found in certain yeast cell types, or the stacks themselves can be made of from 2-3 *cisterna* up to 30 in certain euglenoids (Prydz et al. 2008). The Golgi apparatus is usually located in the perinuclear region. There are exceptions; however, nerve cells have been observed to have Golgi outposts at dendritic branch points, while some *Drosophila* cell types have been observed to have individual stacks distributed throughout the cytoplasm (Prydz et al. 2008).

1.1.3 Golgi apparatus models and transport

There are several models for how secretory proteins move through the Golgi *cisternae* and how resident Golgi proteins are retained in their compartments (Glick & Luini 2011; Prydz et al. 2008). Further sorting implications are considered in epithelial cell types that require strict sorting to apical and basolateral cell surfaces, or sorting routes that bypass the Golgi apparatus entirely (Prydz et al. 2013). This has implications when performing studies with the Golgi apparatus, as Golgi apparatus form and function is relatively complex and to some degree unknown. Different models can attribute and explain certain things, for example how large proteins like procollagen can move through the Golgi complex, but no model explains all observations made to date.

1.1.3.1 Stable compartments model

In the stable compartments model, the Golgi apparatus sub-compartments are believed to have a unique and stable set of resident Golgi proteins. A secretory protein would enter the *cis*-Golgi in COPII-coated vesicles, and would move from one compartment to the next in COPI-coated vesicles. Resident Golgi proteins would then be retained in their selective compartments through exclusion from COPI-coated vesicles in anterograde traffic. However, variations of this model have suggested a bidirectional COPI traffic where escaped resident Golgi proteins are returned through retrograde traffic (Orci et al. 2000).

1.1.3.2 Cisternal maturation model

The cisternal maturation model suggests that the COPII vesicles and VTCs fuse together to form the ERGIC, which will mature into a *cis*-Golgi *cisterna*, which then gradually matures into a *trans*-Golgi *cisterna*. This concludes with a fission of the *cisterna* into secretory vesicles and other types of carriers. COPI vesicles would in this model traffic the resident Golgi proteins from older to newer (retrograde) *cisternae*. A variant of this model explains why tubules are formed between stacks, where resident Golgi proteins and smaller secretory cargo proteins can be transported anterogradely and retrogradely through the Golgi apparatus in membrane tubules.

1.1.3.3 Other noteworthy proposed models for Golgi apparatus function.

In the rapid partitioning model, the Golgi apparatus operates as one compartment with both

processing and export domains. Secretory proteins arriving from the ER will rapidly disperse into the complete Golgi apparatus through rapid partitioning of vesicles and tubules.

The rim progression model proposes that the center of the Golgi *cisternae* are static (Lavieu et al. 2013), while proteins in transit through the Golgi apparatus are located at the cisternal rims. Secretory proteins are therefore only moving anterogradely from the rims of the Golgi *cisternae*, either in tubules or COPI vesicles.

In the cisternal progenitor model, the Golgi apparatus has stable compartments with distinct domains defined by Rab GTPases (Glick & Luini 2011; Pfeffer 2010). These domains can undergo Rab conversion, resulting in a transient "homeotypic" fusion with cisterna in adjacent stacks. Secretory cargoes can move forward through the resulting connection. Alternatively, a rab domain could pinch off from a cisterna to create a "megavesicle", which would then fuse with a later cisterna in the same Golgi stack.

1.1.4 Protein sorting signals in the Golgi apparatus

1.1.4.1 ER retention

Proteins that are native to the ER are subjects to ER retention mechanisms. Several transmembrane proteins of the ER possess a C-terminal lysine, lysine, any amino acid, and any amino acid (KKXX) signal, which allows them to incorporate into retrograde COPI trafficking vesicles. Soluble ER proteins contain a C-terminal Lys-Asp-Glu-Leu (KDEL) signal that favors the binding of the protein to a transmembrane KDEL receptors in the Golgi apparatus or ERGIC, which enables the packaging of the protein into COPI retrograde vesicles. Other possible retention mechanisms, are based on the length of the transmembrane domain of proteins being slotted into cholesterol rich (compared to ER) COPII vesicles, or formation of protein multimers in the ER.

1.1.4.2 Golgi signal sorting and protein transport

The current, dominating view is that, once a protein has entered the Golgi apparatus, the primary sorting station is in the TGN. However, some studies challenged this view. Most proteins that enter the secretory pathway have an N-terminus signal peptide, often cleavable, that acts as a signal for ER entry. Other signals for guiding the proteins to their proper destinations reside elsewhere in the protein sequence or in post-translationally added structures, like glycans.

1.1.5 Changes in Golgi morphology after induced DNA damage

When DNA is damaged, a pathway involving GOLPH3, MYO18A, F-actin and DNA-PK causes a rapid dispersal of the Golgi apparatus (Farber-Katz et al., 2014) in mammalian cell lines. This dispersal is independent of dispersal that can be observed under apoptosis.

GOLPH3 is essential for normal Golgi morphology, and functions with F-actin to create a tensile force for efficient tubule and vesicle formation (Ng et al. 2013; Dippold et al. 2009). This requires the ability for GOLPH3 to link *trans*-Golgi membrane to F-actin through the interaction with MYO18A. GOLPH3's localization to the *trans*-Golgi requires binding with phosphatidylinositol 4-phosphate. Under chemically induced DNA damage, DNA-PK phosphorylates GOLPH3 on residues T143 and T148. This increases the interaction with MYO18A, results in increased interact action with F-actin, and causes the Golgi apparatus to disperse (Farber-Katz et al., 2014). Dispersal of the Golgi apparatus is still noticeable over 30 days post treatment with DNA damaging agents. This pathway is shown to be required for normal survival following DNA damage, and overexpression of GOLPH3 confers resistance to killing by DNA damaging agents.

1.2 Golgi apparatus dependent glycosylation and proteoglycan synthesis

Proteoglycans (PGs) are a diverse group of macromolecules that are made up of a protein core with at least one, but usually many, covalently attached glycosaminoglycan (GAGs). These are long, unbranched polysaccharides. The function of a PG is often determined by the GAG chains and their further modification pattern, as the GAGs can have a variety of functions, from structural support to cell signaling. Since the protein core can have active and enzymatic domains, they are able to perform several roles at the same time. GAGs have also shown to influence sorting in polarized epithelial cells (Prydz & Dalen 2000). Commonly, PGs are either inserted into the plasma membrane or secreted to the extracellular environment.

1.2.1 Proteoglycan synthesis

The PG protein core is translated in the ER, as most PGs are secreted or membrane bound. They then follow the secretory pathway through the Golgi apparatus, where O-linked glycosylation occurs and extensive glycan modifications are conducted.

1.2.1.1 Activation and transport of nucleotide-sugars.

The sugars involved in GAG synthesis are activated nucleotide-sugars in the cytoplasm. These nucleotide-sugars are created by removal of pyrophosphate from uridine-5'-triphosphate (UTP) by a glucosyltransferase. This, in turn, releases energy which is then used by the glucosyltransferase to attach a sugar, like glucose-1-phosphate, onto the uridine-5'-monophosphate (UMP), which results in a UDP-sugar, for example UDP-glucose. Then these nucleotide-sugars have to be transported into the Golgi lumen by transmembrane nucleotide-sugar transporters before they can be used in O-linked glycosylation or branching of N-linked glycans.

1.2.1.2 Attachment of the tetrasaccharide linker

With the exception of keratan sulphate (KS), which is an N- or O-linked proteoglycan, synthesis of other proteoglycans is initiated with a tetrasaccharide linker located on a serine (Ser) residue followed by a glycine on the surface of a protein core. This tetrasaccharide linker is initiated by the addition of a xylose (Xyl) β(1->O-serine), followed by addition of two galactose units, D-galactose (Gal) β(1->4), Gal β(1->3) and a D-glucuronic acid (GlcA) β(1->3). The following structure represents the tetrasaccharide linker: ->GlcAβ(1–>3)Galβ(1–>3)Galβ(1–>4)Xylβ(1->O)Ser.

1.2.1.3 Attachment of alternating carbohydrate dimers to the linker region

The GAG chain extends from the linker tetrasaccharide by the addition of two alternating monosaccharides. For the heparan sulphate (HS) PGs, the monosaccharides are alternating GlcA and N-acetyl-glucosamine (GlcNAc), ->GlcAβ(1->4)GlcNAcα(1->4). Heparin is created by the epimerization of the GlcA in HS to iduronic acid (IdoA) and further sulphation, ->IdoA(2S)α(1->4)GlcNS(6S)α(1->4).

Chondroitin sulphate (CS) is created by the addition and repetition of alternating GlcA and N-acetyl-galactosamine (GalNAc) to the tetrasaccharide linker, ->GlcAβ(1->3)GalNAcβ(1->4).

Moreover, dermatan sulphate (DS) is created by epimerization of the GlcA in CS to IdoA, ->IdoAβ(1->3)GalNAcβ(1->4).

For KS, an oligosaccharide linker region can be both N-linked or O-linked, followed by the repeating disaccharide of ->Galβ(1 >4)GlcNAcβ(1->3).

1.2.1.4 Sulphation of glycosaminoglycans

3-phosphoadenosine 5'-phosphosulphate (PAPS) is synthesized in the cytoplasm by PAPS synthase and transported into the Golgi lumen by PAPS transporter 1 (PAPST1) and 2. Sulphation of GAGs is then carried out by the sulphotransferases in the Golgi lumen that transfer sulphate from PAPS onto a –OH in a sugar moiety, the -N-acetyl moiety in the GAG chain, or sulphation of tyrosine on the protein core. A single sugar can have multiple sulphation sites. The GalNAc carbohydrate can be unsulphated GalNAc, or sulphated as GalNAc(4S), GalNAc(6S), or GalNAc(4S,6S). GlcA can be unsulphated or sulphated as GlcA(2S), and IdoA can likewise by unsulphated or sulphated as IdoA(2S). GlcNAc can be unsulphated, sulphated as GlcNAc(6S), or the acetyl group is replaced with a sulphate as N-sulphated glucosamine (GlcNS) or GlcNS(6S). Galactose, which is only present in KS, can be unsulphated or sulphated as Gal(6S).

The utilization of the possible sulphation sites can vary along GAGs, with less sulphated regions in between more highly sulphated domains. Coupled with the variations in the protein core, the epimerization of GlcA to IdoA and addition of N-linked glycosylation, all of which can be a target for sorting signals in the Golgi apparatus, make PGs good candidate cargo molecules for studies of Golgi apparatus function.

Table 1.2.1: Glycosaminoglycan structure and sulphation

This table illustrates which hexose and hexosamine that participates in each GAG disaccharide. Further, it shows where sulphation can occur, and the link between the disaccharides.

GAG	Hexuronic acid / Hexose	Hexosamine	Linkage
Chrondroitin sulphate (CS)	GlcA / GlcA(2S)	GalNAc / GalNAc(4S) / GalNAc(6S) / GalNAc(4S,6S)	->GlcAβ(1->3)GalNAcβ(1->4)
Dermatan sulphate (DS)	GlcA / IdoA / IdoA(2S)	GalNAc / GalNAc(4S) / GalNAc(6S) / GalNAc(4S,6S)	->IdoAβ(1->3)GalNAcβ(1->4)
Heparan sulphate (HS)	GlcA / IdoA / IdoA(2S)	GlcNAc / GlcNS / GlcNAc(6S) / GlcNS(6S)	->GlcAβ(1->4)GlcNAcα(1->4)
Heparin	GlcA / IdoA(2S)	GlcNAc / GlcNS / GlcNAc(6S) / GlcNS(6S)	->IdoA(2S)α(1->4)GlcNS(6S)α(1->4)
Keratan sulphate (KS)	Gal or Gal(6S)	GlcNAc / GlcNAc(6S)	->Galβ(1->4)GlcNAcβ(1->3)

1.3 Epithelial cell structure and polarized sorting

Cells lining the cavities and organs of the body, called epithelial cells, adhere together to form tight monolayers with the help of tight junctions. Such monolayers form borders between two distinct environments, where molecules cannot freely pass between. Epithelial cells therefore

display a polar organization, where the cell membrane is divided into apical and basolateral domains facing the different environments.

1.3.1 Madin-Darby canine kidney cells

For this thesis, the Madin-Darby canine kidney cell line was used. This is an established model cell line for studies of epithelial cells. Growing cells on filters allows *in vitro* studies of an epithelial cell monolayer, with the apical and basolateral environments above and below the filter, respectively. The MDCK cells form a tight monolayer on the filter and do not allow the passage of molecules from one medium reservoir to the other, unless transport occurs actively through the cells. MDCK cells both synthesize and secrete the PGs of the CS and HS type (Stoops & Caplan 2014; Svennevig et al. 1995), and exhibit polarized sorting.

1.3.2 Golgi apparatus morphology in MDCK cells

During a cultivation period of MDCK cells on an adherent surface, the morphology and location of the Golgi apparatus changes (Bacallao et al. 1989). After one day of plating, single cells are observed to have adhered to the growth surface, and have microtubules radiating from a perinuclear region containing the centrosomes and the Golgi apparatus. After further growth, the cells will have reached confluence, and formed tight junctions close to the substratum. At this point, the Golgi complex has spread around the nucleus. After five days of incubation the cells will have reached their final polarized state, being columnar in shape, while the tight junctions will have moved approximately 10 microns upward from the basal location. The Golgi complex will have formed a ribbon-like convoluted structure located in the apical and perinuclear region.

1.3.3 Polarized protein sorting in epithelial cells

Epithelial cell polarity has an effect of protein sorting. As the cell membrane is divided into two distinct domains, proteins have to be targeted to the correct membrane domain to uphold the polarized organization. In general, sorting signals identified that direct transmembrane proteins to the basolateral membrane are embedded in the cytoplasmic tail of the protein core structure, while apical signals can be more diverse.

Upon leaving the Golgi apparatus, secretory proteins may be sorted directly to the cell surface or pass through endosomal compartments (Futter et al. 1995). Additionally, there are endosomal compartments that specialize in trafficking to the apical and basolateral membrane, respectively (Brown et al. 2000; Sheff et al. 1999). The sorting process can be even more complex since subdomains may exist within the plasma membrane, for instance where a transmembrane protein could be targeted for insertion into a lipid raft in the apical membrane, or into a ciliary region (Garcia-Gonzalo & Reiter 2012).

Precisely where along the secretory pathway most sorting decisions take place is still a topic for discussion. Sorting has been proposed to mainly take place in the TGN in MDCK cells (Simons K & Wandinger-Ness A. 1990). In more recent studies in yeast and mammalian cells there are indications that laterally segregated lipid microdomains might form as early in the secretory path as the ER and/or *cis*-Golgi region (Sarnataro et al. 2004; Muñiz & Riezman 2000; Morsomme et al. 2003). There is also evidence of Golgi apparatus bypass routes, as mentioned in section 1.1.3, that would require sorting to take place already in the ER or ERGIC (Prydz et al. 2013).

1.3.4 Modification of GAGs as an effect on signal sorting in epithelial cells.

Earlier studies have shown that chondroitin sulphate proteoglycans (CSPGs) are preferentially transported to the apical surface (Kolset et al. 1999), while HS has been found to be secreted mainly basolaterally (Mertens et al. 1996; Svennevig et al. 1995; Kolset et al. 1999).

Serglycin-GFP is secreted from MDCK cells with mainly CS GAG modification. This PG has been utilized as a model PG for studies of trafficking in MDCK II cells. In these studies it has been observed that the CS on Serglycin-GFP has a higher degree of sulphation when secreted basolaterally compared to the counterpart secreted apically (Tveit et al. 2005).

Further sulphation studies have been performed by changing the expression levels of the transmembrane Golgi resident protein PAPST1. Increasing the expression level of PAPST1 (with a GFP tag), increases the amount of available PAPS in the lumen of the Golgi apparatus, and has been shown to increase the sulphation of CS in the apical pathway (Dick et al. 2008). Performing a knock-down experiment where the expression of PAPST1 is reduced

leads to an increase in sulphation level of a particular HSPG in the basolateral pathway (Dick et al. 2015).

O-glycosylation with glycans of the mucin type has also been shown to be important for apical sorting by treatment with glycosylation inhibitors (Slimane et al. 2000)

2 Materials and Methods

2.1 Cell culture work

The cells used in this thesis were adherent Madin-Darby canine kidney epithelial (MDCK) cells. The MDCK II cell line is one of two subclones of the original cell line derived from dog kidney, originating either from the distal tubule or the collecting duct of the nephron, and is widely used as a model system for studies of polarized epithelia (Herzlinger et al. 1982; Simons K & Wandinger-Ness A. 1990; Bacallao et al. 1989). Various cell strains expressing different recombinant proteins have been established within the research group after stable transfection and clonal selection and are utilized in this work (listed in table 1).

MDCK cells were for maintenance purposes grown in 75 cm^2 flasks with ventilated caps containing 20 ml of complete growth medium; Dulbeccos's modified Eagle's Medium (DMEM), containing 5 % fetal calf serum (FCS) and (1 %) penicillin/streptomycin (P/S). We kept the cells in an incubator at 37°C with 5 % CO_2 in the incubator atmosphere.

We performed cell culture work in a laminar cell culture hood in a designated cell lab.

Table 2.1.1 List of MDCK cell lines used in the investigation.
This table describes the cell lines that will be used in this thesis.

Cell Line	**Description.**
MDCK II	Cells from later passages of MDCK.
MDCK II Serglycin-GFP	MDCK II cells stably expressing serglycin with a C-terminal GFP tag.
MDCK II Serglycin-KDEL-GFP	MDCK II cells stably expressing serglycin with a GFP tag and a KDEL ER-retention signal.
MDCK II PAPST1-GFP	MDCK II cells stably expressing PAPST1-GFP.

2.1.1 Expansion of cells: Trypsination of MDCK II cells grown in 75 cm^2 flasks

When adherent MDCK II cells have grown to confluency in 75 cm^2 flasks, we expanded them to new flasks, to avoid inhibition of further growth and division in confluent epithelial cell layers. Ethylenediaminetetraacetic acid (EDTA) was used to open tight junctions creating gaps in the otherwise tight monolayer. This in turn allows apically added Trypsin to diffuse through the monolayer and cleave proteins in the basolateral domain. Some of these proteins help the cells adhere to the flask, and this detaches them and suspends the cells into the medium.

Protocol:

- Remove medium from the bottle.
- Wash cells with 10 mL Phosphate-buffered saline (PBS) containing EDTA.
- Add 5 mL Trypsin-EDTA to each bottle. Remove after 3-5 min, or when cells are beginning to round up.
- Add 2 mL Trypsin-EDTA and leave the cells in incubator for 10-15 min, or until all the cells have detached.
- Add 10 mL of complete growth medium to the flask, and resuspend the cells.
- Transfer cells to new bottles. If transferring to new 75 cm^2 flasks, then transfer 2 mL of the cell suspension to each flask containing 20 mL of fresh complete growth medium.

Protocol for growth of cells on 35 mm MatTek glass bottom dishes:

MDCK II cells were plated on 35 mm dishes with a central glass coverslip for studies using confocal microscopy. This procedure involves an extra step to remove Trypsin from the cell medium. The cells are detached with Trypsin as in the protocol above.

Protocol:

- After resuspension in 10 mL of complete growth medium, transfer the cells to centrifugation tubes.
- Centrifuge at 1500 x g 4-5 min.
- While centrifuging, add 2 mL of medium to each MatTek 35 mm dish.
- Remove supernatant from tubes and resuspend the cell pellet in 10 mL of complete growth medium.
- Add 0.5 mL of cell suspension to each 35 mm MatTek dish.

2.1.2 Cryopreservation and retrieval of cryopreserved cells

To allow us to store cells at a low temperature for a longer period of time, we used dimethyl sulfoxide (DMSO) in the medium, which works as a cryopreservative by keeping ice crystals from forming and lysing the cells during freezing.

Protocol, cryopreservation:

- Grow cells in 75 cm^2 flasks before trypsination (2.1.1).
- Transfer the cell suspension to a 15 mL or 50 mL sterile centrifugation tube.
- Centrifuge cells at 1500 x g for 5 min.
- Remove supernatant.
- Add 1 ml of complete medium with 10 % DMSO to the pellet, and resuspend pellet.
- Transfer cell suspension to a cryotube and place in a -80 °C freezer.
- After minimum 2 h, transfer the ampule to liquid nitrogen.

Protocol, retrieval of cryopreserved cells:

- Thaw the ampule of cells in a water bath at 37 °C.

- Immediately after thawing, add to 75 cm^2 cell culture flask containing 20 mL of complete growth medium.

- Incubate for 24 h to achieve fully adherent and confluent cell layer.

2.1.3 Growing cells on filters – for studies of polarized transport

Epithelial cells, like the MDCK II cell line, are polarized and have two distinct membrane domains that are separated by tight junctions, the apical and the basolateral membrane domains. To allow epithelial cells to polarize in an *in vivo*-like manner, we grew the cells on porous filters. The nutrition uptake from the medium underneath the filter-grown cell layer induces formation of a polarized monolayer. When the cells are grown to confluency, apically secreted macromolecules are segregated by the tight monolayer of filter-grown cells from the basolaterally secreted macromolecules. Passage of macromolecules between the cells of the monolayer is restricted due to the tight junctions.

Protocol:

- Grow cells in 75 cm^2 flasks before trypsination (Section 1.3).

- Transfer cell suspension to a 15 mL or 50 mL tube for centrifugation.

- Centrifuge at 1500 x g for 5min.

- Remove supernantant and resuspend pellet in 10 mL complete growth medium.

- Add 90 mL of complete growth medium to an autoclaved glass petri dish with 6 polycarbonate filters (each with an area of 4.7 cm^2) in appropriate filter holders.

- Add 1.6 mL of cell suspension to each filter.

- Incubate for 3-4 days to allow formation of a tight cell layer on the filter.

Protocol, treatment with doxorubicin or Camptothecin

- Add 2 mL of complete growth medium with chosen concentration of Doxo or CPT to (basolateral) wells in a fresh 6 well plate.

- Add 1 mL of complete growth medium with chosen concentration of Doxo or CPT to (apical) filters, while transferring filters to new wells.

- Incubate for chosen length of time (4 h to 24 h) to allow for studies of Golgi dispersal.

Protocol, incubating with ^{35}S-sulphate:

- Add 2 mL of sulphate-reduced medium with 2 % FBS and the chosen concentration of Doxo or CPT to (basolateral) wells in a fresh 6 well plate.

- Add 1 mL of complete growth medium with chosen concentration of Doxo or CPT apically to filters, while transferring filters to new wells.

- Incubate for chosen period of time (4 h to 24 h) to allow for studies of Golgi dispersal.

2.1.4 ^{35}S-sulphate metabolic labeling of filter-grown cells.

We labeled the filter grown cells with the ^{35}S radioactive isotope to allow us to study synthesis, sorting and modification of PGs and glycoproteins. PGs carry GAGs that are sulphated to various degrees in the Golgi apparatus. By using medium with reduced non-radioactive sulphate and added radioactive ^{35}S-sulphate, it is possible to determine the amount of sulphated macromolecules synthesized during a labeling period. Information concerning sorting and transport of labeled macromolecules will then be gathered by analysis of the apical medium, the basolateral medium and the cell lysate.

Sulphate is mainly taken up from the basolateral (blood) side of epithelial cells. We therefore only added the ^{35}S-sulphate to the basolateral medium at a concentration of 0.2 mCi/ml. We used sulphate free medium (Gibco: RPMI 16040) supplemented with 2 % FBS.

Protocol:

- Add 2.0 mL of sulphate reduced medium containing 0.2 mCi/ml of ^{35}S-sulphate and working concentrations of Doxo or CPT to basolateral wells on a new 6-well plate.

- Add 1 mL of sulphate reduced medium with working concentrations of Doxo or CPT to the filters while transferring to the new 6-well plate.
- Incubate (18 h to 24 h).
- Transfer filters to new 6-well plates on ice.
- Remove and store apical and basolateral medium for analysis.
- Wash cell filters with 2.0 mL of PBS apically and 2.5 mL PBS basolaterally for 15 min on tilt table 2 times.
- Lyse cells with 1.5 mL 1 % Nonidet P-40 (NP-40) lysis buffer on apical filter on tilt table for 30 min.

2.2 Biochemical analysis of sorted ^{35}S-sulphate labeled macromolecules.

2.2.1 Isolation of metabolically labeled macromolecules

Non-incorporated ^{35}S-sulphate had to be removed before further analysis, so it would not interfere with detection of the labeled macromolecules during scintillation counting and phosphorimaging of SDS-PAGE gels. We performed gel filtration with Sephadex G-50 Fine of cell media and lysates. While macromolecules were eluted, non-incorporated sulphate was left behind in the disposable columns.

Protocol:

- Prepare columns by adding 10 mg/mL Sephadex G-50 Fine suspended in dH_2O until columns are 4.0 mL in volume.
- Load 1.0 mL of dH_2O through the gel first, to make sure it has settled.
- Prepare apical samples which contain less than 1mL of medium by adding 1.0 mL of PBS.
- Load columns carefully with 1.0 mL of sample, so as not to disturb the gel.

- Add 1.5 mL of dH2O or PBS for elution, and collect eluate.

2.2.2 Scintillation counting

After gel filtration, it is possible to determine the amount of ^{35}S-labeled macromolecules in each sample. The scintillation counter will detect nuclear disintegrations in the added scintillation fluid through emission of energy from molecules present in the scintillation fluid. The prior excitation takes place when scintillation molecules are hit by a β-particle emitted from ^{35}S. Since the scintillation counts per minute (cpm) reports detected excitation, it is not an exact count of the number of nuclear disintegrations. These results will give a relative indication of how many ^{35}S labeled macromolecules there are present in our samples.

2.2.3 SDS-PAGE: Separation of molecules by molecular mass

Polyacrylamide gel electrophoresis separates molecules according to their molecular mass in a gel when an electric current is applied. SDS is negatively charged and binds to proteins with a fairly fixed ratio, making all the proteins in a sample negatively charged and thus able to move in the same direction in an electric field.

For this thesis, premade BioRad SDS-PAGE gradient (4-12 %) gels were used, these gels give a good range of separation of larger PGs in the upper half of the gels.

Protocol:

- Prepare 30 μL of each sample in Eppendorf tubes.
- Add 2 μL (20 x) XT reducing agent and 10 μL (4 x) XT sample buffer to each sample.
- Heat samples at 96 °C for 5 min.
- Spin samples down in a table top centrifuge at 1500 x g for 5 min.
- Place gels in the electrophoresis chambers.
- Add (1 x) XT-MOPS Running buffer until you reaching the marked lines on the chambers. Tilt gels to remove any bubbles that might accumulate underneath the gels.

- Load 40 µL of each sample to each well, if using 12+2 well gels. Alternatively, load 30 µL if using 18+2.
- Run gels at 90 A per gel for 90 min (should start out at around 120 V), or until blue dye has reached the bottom of the gel.
- When complete, remove the gels from their chambers, and use a spatula to release the gel from the plastic cassette and mark the orientation of the gels.
- Slide the gel off the plastic cover, and into fixation solution.

2.2.4 Fixation and drying of gels.

Fixation keeps the protein fixed in the gel at their location by preventing the diffusion of the proteins through the gel. Once the gel is in the fixation solution, it can be kept there for minimum an hour, but also up to several days. It is also possible to bathe the gels in a signal amplification solution. However, we find that this is not necessary for ^{35}S-detection.

Protocol:

- Fix solution is made of 1 part methanol, 1 part acetic acid, and 5 parts of water.
- Place the gels in a container with fixation solution.
- Leave for minimum 30 min on a tilt table.
- Transfer the gels to new containers with dH_2O, and leave on a tilt table for 15 min to wash away the fixation solution.
- (Optional) Incubated 15-30 min in Amplify on tilt table for increased detection sensitivity.

After fixation, the gel needs to be dried before it can be further analyzed by phosphorimaging. This is done by placing the gels on a piece of filter paper in a vacuum sealed gel dryer for 4 h at 70 °C, or until there is no remaining liquid in the tubing to the vacuum pump. After which, the gel will be adhered to the paper.

2.2.5 Detection: Phosphorimaging

To visualize radioactively labeled macromolecules in SDS-PAGE gels, we use a Typhoon Phosphorimager. This is done by first clamping the gel filter paper to phosphor screens that absorb the beta particles from the dried gel for 24 h. We then scan the screens to get a measure of the size distribution and quantity of ^{35}S labeled macromolecules. The resulting images were then analyzed using the computer program ImageQuant. Figure 2.2.5.1 illustrates how lanes are marked (Figure 2.2.5.1.A) and how the program quantifies the signal peaks and areas under curves after lane marking and background subtraction (Figure 2.2.5.1.B). The results can then be exported as a numerical measurements to excel.

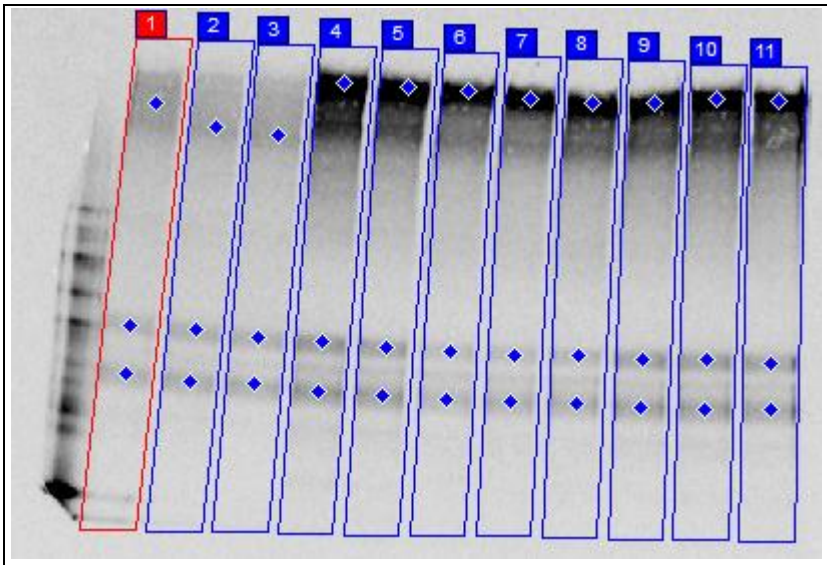

A) Marking of lanes.

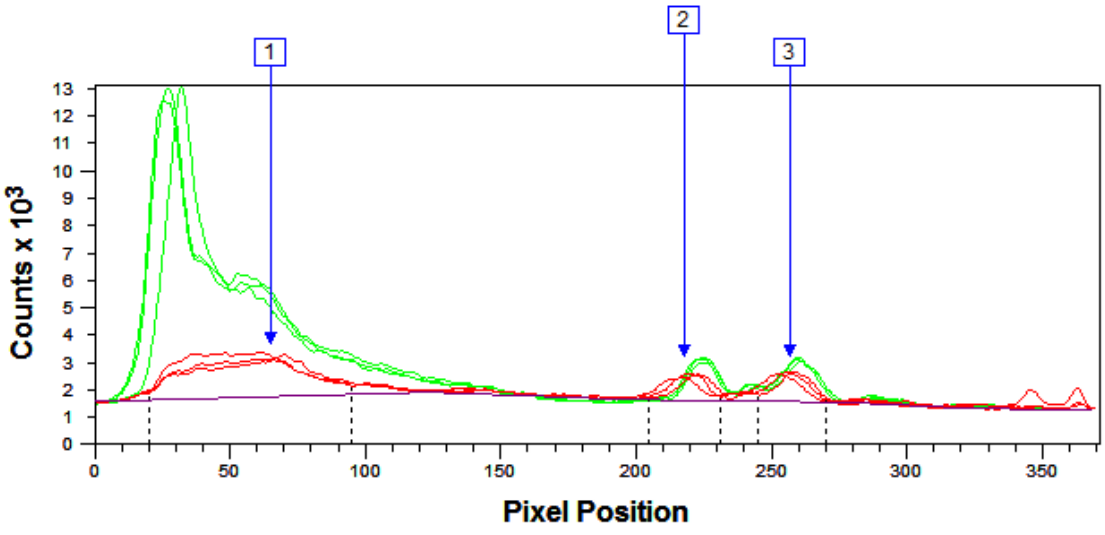

B) Signal detection in lanes.

Figure 2.2.5.1: Example of ImageQuant and signal detection.

This illustrates lane marking and measurement of signals from the lanes. The red curves represent the lanes 1, 2 and 3 from A, and the green curves represent lanes 4, 5 and 6. The numbers in the blue boxes are labeled peaks from one of the lanes. The purple line represents the background noise from the gel picture, and is deducted from the calculated area under the curves.

2.3 Cellular imaging

2.3.1 Live imaging – end point

Every sample used for visualization in the confocal microscope for this thesis, had their images taken in a z-stack series. This allowed for selecting the plane with the highest Golgi complex dispersal. In most cases, the highest x and y dispersal can be found around the cell center, or slightly apical to this region. Whenever a comparison was done between one selected sample picture and another, the areas with the highest dispersal were chosen. When two or more pictures were used to compare a sample, one picture was usually chosen from the bottom of the cell. This is done to showcase any possible z-plane dispersal. Bias is avoided by the fact that images from control cells are also chosen based on maximum Golgi dispersal. The only exception to the z-stack rule, is when doing time lapse microscopy. The images in the time-lapse series are scanned in one plane only. The objective used in this thesis was 60X in oil with 1.35 numerical aperture. GFP was scanned using 488 nm excitation and 510 nm emission detection.

Image analysis was done for the most part in ImageJ with the Bio-Formats package.
3D rendering and analysis was done with iMaris.

2.3.1.1 Kalman filter and sequential imaging

The microscope settings we used for every image were the kalman filter and sequential image taking. Kalman setting was set to 4 in all pictures with the exception of time-lapse. When we took 4 pictures for each color channel, and take an average of the signaling between those 4.

This helps to reduce background noise and sharpens the signals. Taking the pictures sequentially between the lasers wavelengths helps to reduce bleed-through of signals from one channel to the other. All cells in this section were grown in 35 mm MatTek glass bottom culture dishes, all imaging was done live, and all pictures were taken using the inverted Olympus FLUOVIEW FV1000 confocal laser scanning microscope.

2.3.2 Fluorescent marker: Hoechst 33258

The Hoechst dye binds to the minor groove of double stranded DNA, and it is membrane permeable and will bind to DNA and stain the nucleus in live cells. The interaction with DNA gives a fluorescent complex with maximum absorbance at 352 nm and maximum excitation at 461 nm, compatible with both the RFP and GFP spectra.

Protocol:

- Grow MDCK II cells to confluency in 35 mm MatTek glass bottom dishes or on polarized filters.
- Add 1 μM of Hoechst 20 min prior to visualization.
- Wash with 1.0 mL PBS, two times.
- Add 1.0 mL Phenol-red free medium to dish.
- Image in fluorescence confocal microscope using 405/422 nm.

2.3.3 BODIPY® TR Ceramide complexed to BSA

The ceramide glycolipid precursor forms a complex with BSA, making it possible to add this lipophilic fluorescent marker directly to a protein-free cell medium. After uptake, the fluorescent sphingolipids will be incorporated into cellular membranes, but will most prominently be present in Golgi membranes, as reported by ThermoFisher. This marker has maximum absorbance at 589 nm and maximum excitation at 617 nm.

Protocol:

- Grow MDCK II cells to confluency in 35 mm MatTek glass bottom dishes or on polarized filters.
- Incubate in 5.0 μM of BODIPY-TR-Ceramide-BSA in serum-free medium for 30 min prior to visualization.
- Wash with 1.0 mL PBS, two times.
- Add 1.0 mL Phenol-red free medium to the dish.
- Image in fluorescence confocal microscope using 559/583 nm.

2.3.4 CellLights Golgi-RFP, BacMam 2.0

This marker is a transient transfection which leads to the expression of the Golgi apparatus localized protein N-acetylgalactosaminyltransferase (GalNAc-T) with an RFP tag. This localization is potentially more towards the *trans*-Golgi region than towards the *cis*-Golgi side. It has maximum excitation at 555 nm and maximum emission at 584 nm.

Protocol:

- Grow MDCK II cells to 70 – 80 % confluency in 35 mm MatTek glass bottom dishes or on polarized filters.
- Add Golgi-RFP to a concentration of 30 parts per cell (PPC) Golgi-RFP 24 h prior to visualization (calculate by assuming a maximum cell density of 10^6 cells in 35 mm dish).
- If needed, add 1x BacMam enhancer and incubate for 1 h.
- Wash with 1.0 mL PBS.
- Add 1.0 mL Phenol-red free medium to dish.
- Image in confocal microscope using 559/583 nm.

2.4 Cell viability assays

For this thesis, we used chemically induced DNA damaging agents in concentrations that could kill the cells or cause apoptosis (Tacar, Sriamornsak & Crispin R Dass 2013; Dippold et al. 2009; Liu et al. 2000). The biochemical experiments were conducted on whole populations of cells in a dish or on a filter, therefore a cell viability assay was needed to establish reproducible and reliable experimental conditions.

2.4.1 Viability assay: Trypan blue stain

One cell viability assay is the Trypan blue exclusion test, which works on the premise that dead cells have leaky and permeable membranes. This allows water-soluble molecules to pass into the cell interior and stain the cells in a blue color. Live and viable cells will have a solid non-blue core. These can then be manually counted under a microscope or one can employ an automatic cell counter. We employed the Countess™ automated cell counter for this task.

Protocol:

- Add CPT or DOXO depending on amount being tested, for the required period of time.
- Remove the medium after the incubation.
- Wash cells with 1 mL of PBS with EDTA.
- Add 0.5 mL of Trypsin-EDTA.
- Incubate for 15 min, or until all cells have detached from the substratum.
- Add 2 mL of cell growth medium, then transfer to centrifugal tubes.
- Centrifuge at 1500 rpm for 5 min.
- Remove supernatant and resuspend pellet in 1mL of cell growth medium
- Add 10 µL of the cell suspension to a new tube.
- Add 10 µL of Trypan blue (0.4 %) and mix well by pipetting.

- Remove 20 μL of Trypan blue stained cell suspension and add to Countess™ cell counter slide.

- Insert slide into Countess™, focus the counter properly (live cells have a bright center, dead cells have a dark center) and count the cells.

2.4.2 Viability assay: Propidium iodide assay

Propidium iodide (PI) is a membrane impermeable compound with fluorescent properties when interacting with nucleic acids, interlacing with DNA between guanine and cytosine. It has an excitation maximum of 535 nm and emission maximum at 617 nm, when bound to DNA in aqueous solution. It also binds to RNA in the same manner.

Protocol:

- Grow MDCK II cells to confluency in 35 mm MatTek glass bottom dishes.

- Add Doxo or CPT at working concentrations and incubate for 24 h.

- Add 300 mL of 0.5 mM PI, incubate for 60 min.

- Wash with 1 mL of PBS.

- Add 1 mL of Phenol-red free medium.

- Image in confocal microscope using 488/604.

2.5 DNA damaging agents, growth media and solutions

2.5.1 DNA damaging agents

Doxorubicin:

Doxorubicin (Doxo) is a drug used in cancer chemotherapy, which intercalates into DNA and inhibits the progression of topoisomerase II, as it stabilizes the topoisomerase II complex after having introduced a break in the DNA strands. Doxo can also induce apoptosis through the Bcl-2/Bax pathway (Tacar, Sriamornsak & Crispin R. Dass 2013). It has also been reported that Doxo may lead to an increase in free radical production (Rossi 2013).

Camptothecin:

Camptothecin (CPT) has analogues used in cancer chemotherapy. The mechanism of action is to bind and stabilize the topoisomerase I DNA complex, which prevents DNA from re-ligating (Liu et al. 2000).

2.5.2 Growth media

Complete MDCK II cell growth medium:

Lonza DMEM 4.5 g/L glucose w/ L-glutamine. DMEM is a growth medium that contains four times the concentration of amino acids, vitamins and supplementary components compared to the Basal Medium Eagle (BME). We also modified this with 5 % fetal calf serum (FCS) and 1 % penicillin / streptomycin (P/S) to prevent infections and optimize growth conditions.

Reduced sulphate medium:

Gibco RPMI 1640. This medium has all sulphate removed and extra magnesium chloride ($MgCl_2$). We also add 2 % FCS to make it more compliant with our MDCK II cells.

Phenol red free medium:

Gibco Opti-MEM (1X). This medium has increased L-Glutamine, HEPES and no phenol red, to reduce background when imaging.

2.5.3 Solutions

Fix solution:

1 part methanol, 1 part acetic acid, and 5 parts of water.

Lysis buffer with NP-40:

1 % (5 mL) Nonidet P-40, 2 mM (0.3722 g) EDTA, 35 µg/ml (17.5 mg) PMSF, 150 mM (18.75 mL of 4 M) NaCl and 50 mM (25 mL of 1 M) Tris-HCl (pH 7.5). Adjust volume to 500 mL using MQ water.

10 x PBS:

2.62 g NaH_2PO_4 x H_2O, 14.42 g NaH_2PO_4 x $2H_2O$, 87.66 g NaCl. Mix NaH_2PO_4 x H_2O and NaH_2PO_4 x $2H_2O$ with 300 mL dH_2O while stirring. Add NaCl stepwise. At the end, add dH_2O to 1 L. Adjust pH to 7.4 before autoclaving.

10 x PBS with EDTA:

2.62g NaH_2PO_4 x H2O, 14.42 g NaH_2PO_4 x $2H_2O$, 87.66 g NaCl and 18.64 g EDTA. Mix NaH_2PO_4 x H_2O and NaH_2PO_4 x $2H_2O$ with 300 mL dH_2O while stirring. Add NaCl stepwise, then EDTA. At the end, add dH_2O to 1 L. Adjust pH to 7.4 before autoclaving.

Cryomedium:

Add sterile filtered 10 % DMSO to complete cell growth medium with 10 % FBS.

3 Results

3.1 Visualizing the Golgi apparatus: Cell lines and Golgi markers.

Since DNA damaging agents have been reported to cause changes in Golgi morphology and in the localization of certain Golgi-associated proteins in HeLa cells (Farber-Katz et al. 2014), we wanted to address whether proteoglycan (PG) synthesis is affected by such treatment, since PG synthesis is a major function of the Golgi apparatus in mammalian cells, and changes in PG synthesis are also observed during cancer development. We aim at studying this in non-transformed MDCK cells. In these cells, we have good knowledge of PG synthesis (Prydz & Dalen 2000; Grøndahl et al. 2009), and the cell line is derived from an epithelium, which is the starting point of most cancer types.

3.1.1 CellLight Golgi-RFP, BacMam 2.0 marker experiments

A straightforward way to visualize the Golgi apparatus is by transfecting MDCK II cells with CellLight® Golgi-RFP (Figure 3.1.1.1) according to the manufacturer's instruction (Section 2.3.4: CellLights Golgi-RFP). To easily visualize the cells in a cell monolayer and to have a reference for the Golgi apparatus staining in each cell, we also added Hoechst stain to the incubations. Therefore, the nucleus of each cell is visualized, making it possible to observe the nuclear size and shape.

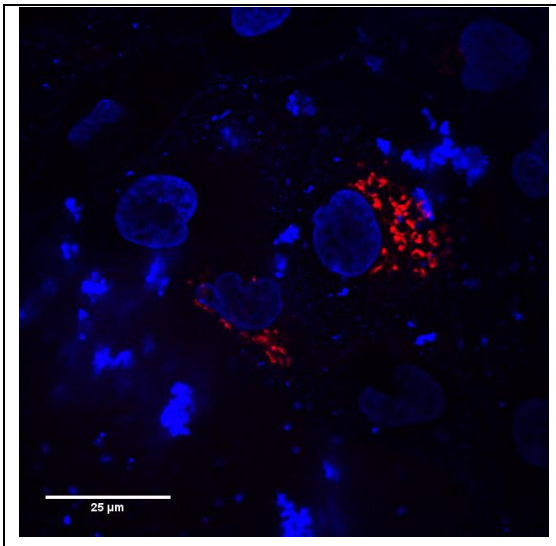

Figure 3.1.1.1: MDCK II cells transfected with CellLight Golgi-RFP, BacMam 2.0. MDCK II cells were grown to from 70 % to 80 % confluency and incubated for 24 h with 30 PPC CellLight Golgi-RFP, followed by incubation with 10 mg/µL Hoechst for 20 min prior to visualization. Scale bar; 25 µm.

As can be observed in the above figure, a low percentage of the cells have been transfected with the CellLight Golgi-RFP, BacMam 2.0 reagent. Changing concentrations and incubation times did not seem to give significant improvement. It is well known that MDCK cells are not easily transfected in the transient mode. ThermoFisher reports that certain cell types might benefit from a BacMam enhancer kit to increase the expression of BacMam reagents in mammalian cells.

It is not clearly explained on the manufacturer's website what the effect of the enhancer would be, but it seems to require that the transfection already has taken place. It does not seem to increase the transfection efficiency, as the enhancer only helps increase the expression level. According to the manufacturer, the transfection vector is the baculovirus. Transgenes under the promoter are expressed, but the baculovirus genes and their promoters are not recognized in mammalian cells. We decided to perform an experiment with CellLight Golgi-RFP, BacMam 2.0 treated with the BacMam enhancer (Figure 3.1.1.2).

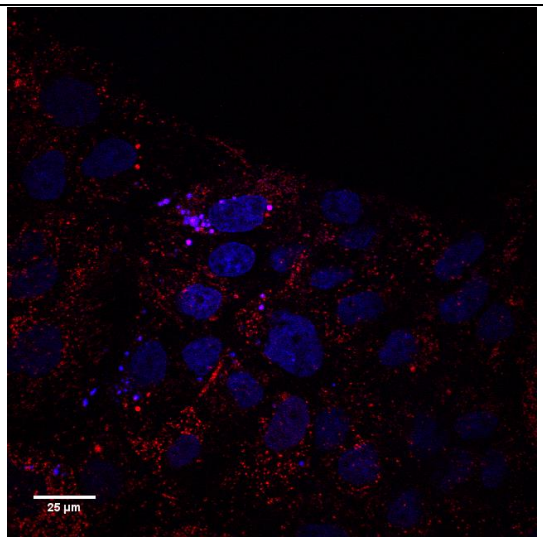

Figure 3.1.1.2: MDCK II cells transfected with CellLight Golgi-RFP, BacMam 2.0 with 1X BacMam enhancer.

MDCK II cells were grown to from 70 % to 80 % confluency and incubated with 30 PPC CellLight Golgi-RFP for 24 h, and then treated with 1 x BacMam enhancer solution for 1 h. This was followed by incubation with 10 mg/µL Hoechst 20 min prior to visualization. Scale bar; 25 µm.

As can be seen in Figure 3.1.1.2, after transfection, the RFP signal was now distributed in vesicle-like structures throughout the cytoplasm of the cells. This is not a typical Golgi apparatus localization, evem if the Golgi morphology in MDCK cells is changing significantly during polarization of the epithelium (Bacallao et al. 1989). We therefore decided to do a second experiment with the BacMam enhancer present (Figure 3.1.1.3).

An issue with respect to the concentrations of Golgi-RFP required, was that a 35 mm dish may contain up to 10^6 cells, and calculating the amount of Golgi-RFP revealed that it would require around 360 µL of reagent for effective use, which is a high cost for one individual experimental point. To work around this issue, we decided to test lower concentrations than recommended.

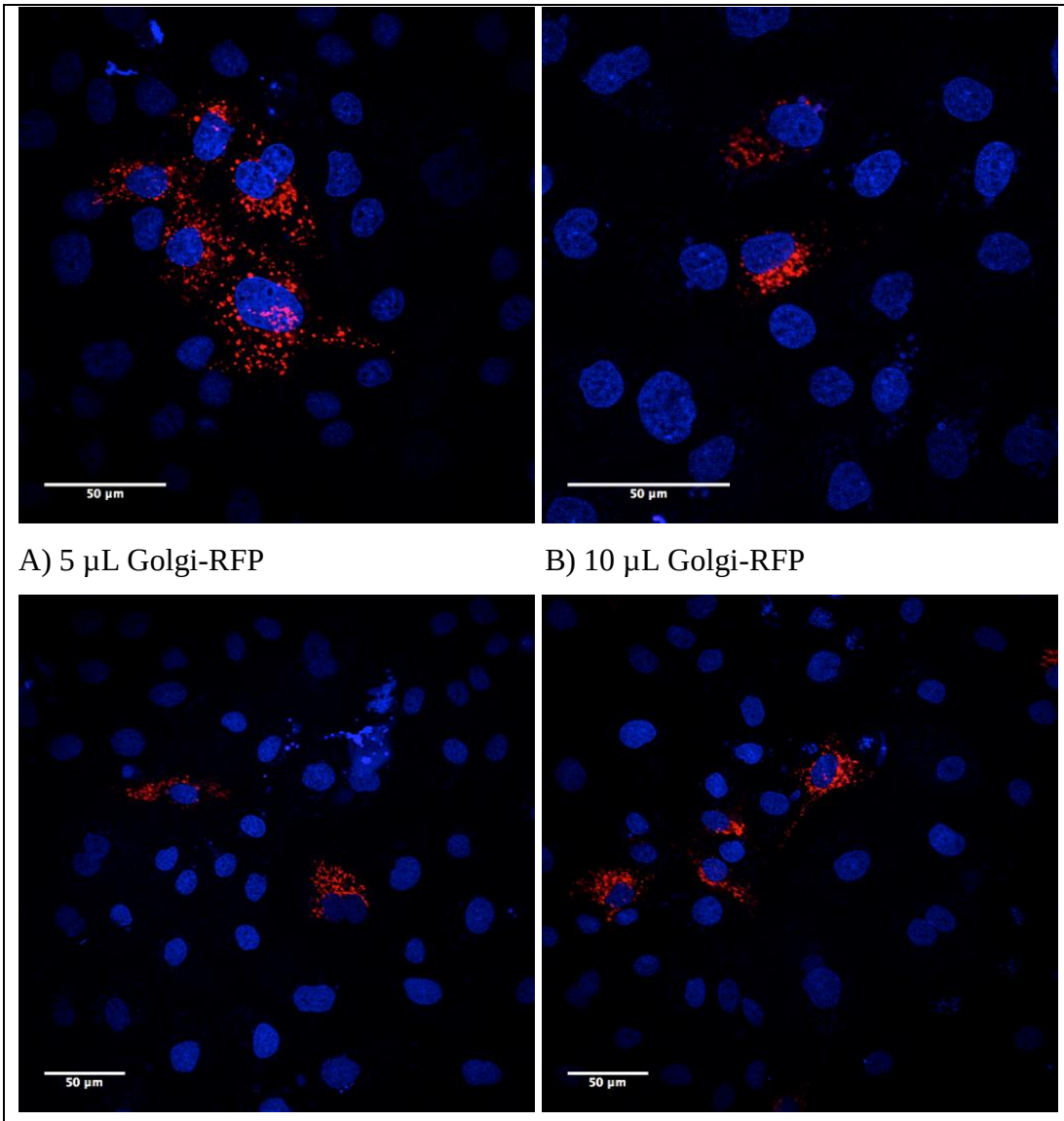

A) 5 µL Golgi-RFP B) 10 µL Golgi-RFP

C) 20 µL Golgi-RFP D) 40 µL Golgi-RFP

Figure: 3.1.1.3: MDCK II cells transfected with CellLight Golgi-RFP, BacMam 2.0. MDCK II cells were grown to from 70 % to 80 % confluency, and then incubated for 24 h by the listed volumes of CellLight Golgi-RFP, BacMam 2.0, then incubated with 1x BacMam enhancer for 1 h, and finally incubated with 10 mg/µL Hoechst for 20 min prior to visualization. Scale bar; 50 µm.

The highest transfection efficiency was obtained at the lower concentration tested (Figure 3.1.1.3). However, the Golgi-RFP reagent did not transfect the majority of the MDCK II cells, making this a sub-optimal choice of Golgi apparatus marker for this cell line.

3.1.2 BODIPY® TR Ceramide complexed to BSA marker experiments

Another marker test was carried out with BODIPY® TR Ceramide complexed to BSA (BODIPY-TR-Ceramide-BSA) (Figure 3.1.2.1). As was the case for Golgi-RFP, the available stock solution from the manufacturer did not allow for a large number of experiments. A stock solution of 150 µL with a stock concentration of 0.5 mM, with a working concentration of 5.0 µM allowed for fifteen experiments with 1.0 mL of medium. We therefore decided to test incubation with lower concentrations of the reagent or with less growth medium.

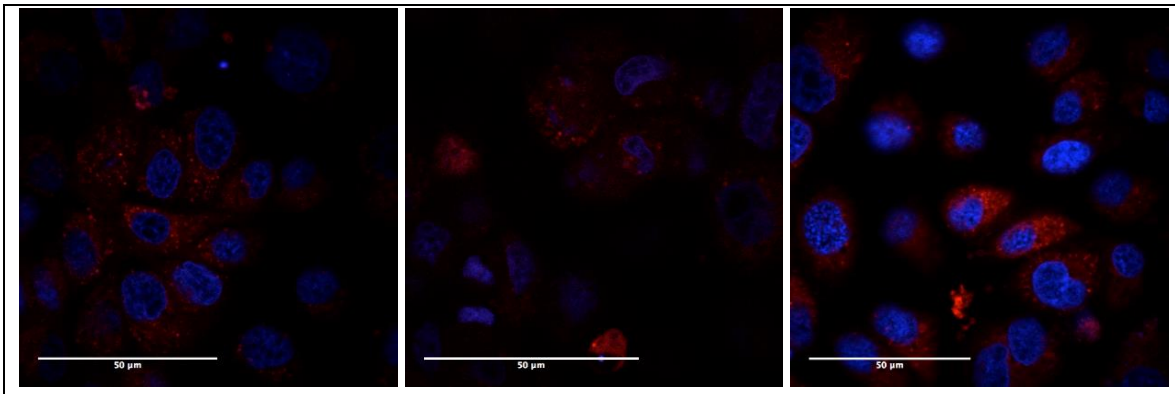

A) 0.5 µM in 0.5 mL medium B) 0.25 µM in 1,0mL medium C) 0.5 µM in 1.0 mL medium.

Figure 3.1.2.1: MDCK II cells treated with Bodipy-TR-Ceramide-BSA.
MDCK II cells were grown to confluency, then treated for 30 min with the indicated concentrations of Bodipy-TR-Ceramide-BSA stock solution, then incubated with 10 mg/µL Hoechst for 20 min prior to visualization. Scale bar; 50 µm.

After treatment with BODIPY-TR-Ceramide-BSA treatment we observed that the 5 µM marker (5 µl BODIPY-TR-Ceramide-BSA) in 500 µl medium was sufficient to give a visible signal similar to what was expected for Golgi membranes (Figure 3.1.2.1). Working with medium volumes down to 500 µL is possible for a thirty minute incubation, but it is not ideal as it is difficult to ensure that the whole cell layer in a 35 mm dish is covered. The protocol for future BODIPY-TR-Ceramide-BSA marker experiments would therefore use 1 mL of medium at 5.0 µM.

Worth noting is that there is a significant background signal when using this type of marker. For future experiments with Golgi apparatus dispersal, we would expect a noticeable reduction in the signal peaks, and that the concentrated signal in the Golgi apparatus area disappears into the background signal. Because experiments with a high background signal

are not optimal, we would have to try and find a more specific marker for Golgi apparatus visualization, while this marker could be used in the interim and as a complementary method.

To perform experiments with inducers of DNA-damage over time with observation of Golgi apparatus morphology, we addressed the longevity of the BODIPY-TR-Ceramide-BSA signal. We had a possible interest in incubating cells for up to 72 h. Therefore, a 35 mm dish with MDCK II cells was incubated with 10.0 µM ceramide reagent for 72 h before observing in the microscope (Figure 3.1.2.2).

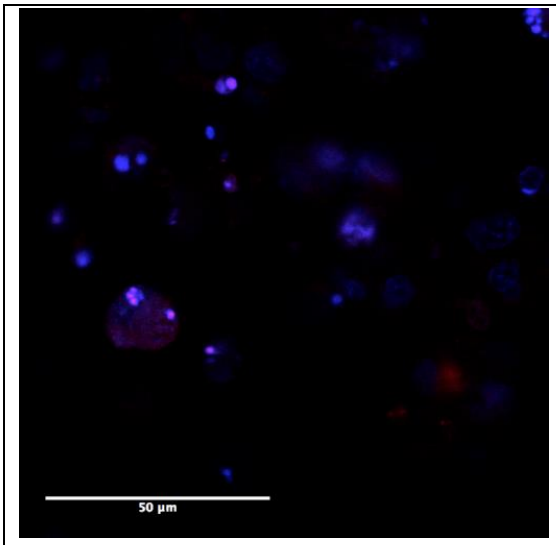

Figure 3.1.2.2: MDCK II cells treated with Bodipy-TR-Ceramide-BSA, incubated for 72h.

MDCK II cells were grown to full confluency, treated for 30 min with 5.0 µM Bodipy-TR-Ceramide-BSA marker, and then incubated with 10 mg/µL Hoechst for 20 min. This was followed by a 72 h incubation period prior to imaging. Scale bar; 50 µm.

Results indicate that the BODIPY-TR-Ceramide-BSA marker needs to be refreshed if long incubation periods are of interest (Figure 3.1.2.2).

3.1.3 MDCK II cells expressing Serglycin-GFP and SG-KDEL-GFP

An alternative approach was to take advantage of MDCK II cells stably expressing fluorescent proteins with predominant or partial Golgi apparatus localization. An available cell line (Tveit et al. 2005) was MDCK II cells expressing Serglycin-GFP (Figure 3.1.3.1). Serglycin-GFP (SG-GFP) is a protein core with GAG modification sites and follows the secretory pathway to the cell surface, where the recombinant PG is secreted. We can therefore

expect some signal in the ER, which becomes more concentrated in the Golgi apparatus, and also in vesicles trafficking between the Golgi apparatus and the cell membrane.

As shown in Figure 3.1.3.1.A, employing a cargo molecule that marks the complete secretory pathway is concentrated in the Golgi apparatus, but does also significantly label other organelles that would give a background labeling in Golgi apparatus dispersal studies. Incubation of the cells with 2.0 µM of the DNA damaging agent doxorubicin (Doxo) (Figure 1.3.1.B) for 24 h indicates some dispersal, but this is difficult to visualize consistently or to quantify.

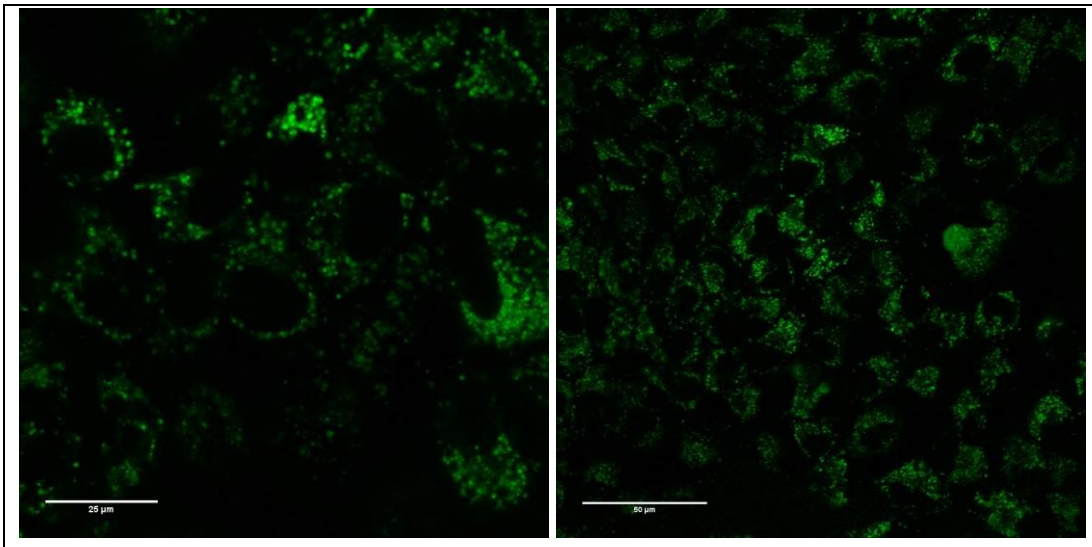

A) Ctrl B) Doxo, 2.0 µM

Figure 3.1.3.1: MDCK II cells expressing SG-GFP incubated with 2 µM Doxo.
MDCK II Serglycin-GFP cells were grown to confluency, then incubated with 2 µM Doxo for 24 h, and finally with 10 mg/µL Hoechst for 20 min prior to visualization. Scale bar; 50 µm.

We next investigated the possibility of using MDCK II cells expressing SG-GFP with a C-terminal KDEL ER retention signal (SG-KDEL-GFP). This KDEL sequence motif (Lys-Asp-Glu-Leu), mediates retrograde transport from the Golgi apparatus and the ER-Golgi intermediate compartment back to the ER (Stornaiuolo et al. 2003). We should therefore be able to visualize the Golgi apparatus, the ER, the ER-Golgi intermediate compartment and vesicles.

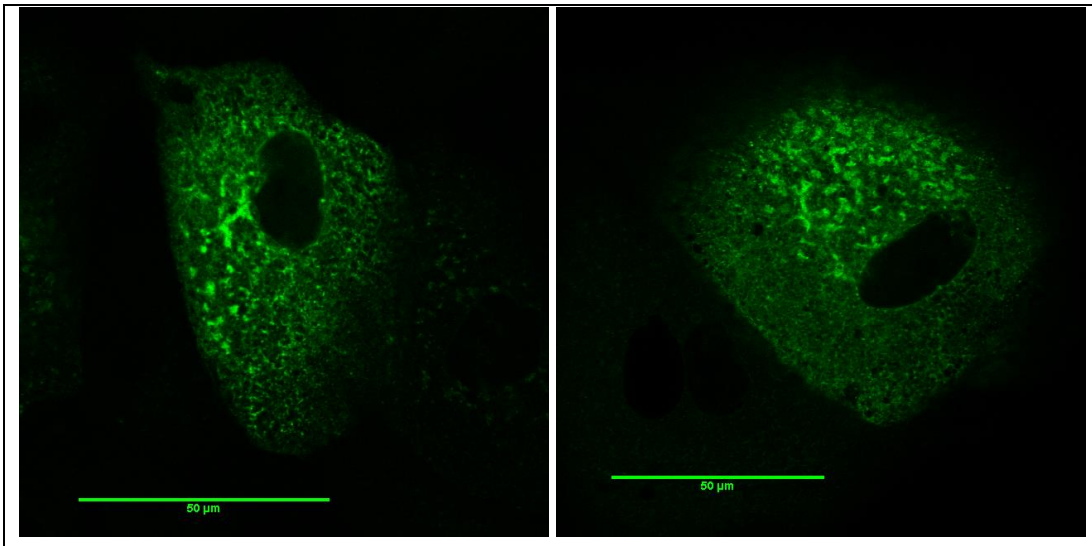

A) Ctrl B) Doxo, 2.0 µM

Figure 3.1.3.2: MDCK II cells expressing SG-KDEL-GFP, incubated with 2 µM Doxo. MDCK II Serglycin-KDEL-GFP cells were grown to confluency, then incubated with Doxo for 24 h, and finally with 10 mg/µL Hoechst for 20 min prior to visualization. Scale bar; 50 µm.

After 24 h of incubation, the cells were visualized in the confocal microscope. Obviously, SG-KDEL-GFP gives a relatively dispersed signal also in untreated MDCK II cells, with no clear profile of the Golgi apparatus. A comparison with Doxo treated cells shows putatively some more dispersal in treated cells, but this is difficult to quantify (Figure 3.1.3.2, comparing A to B).

3.1.4 MDCK II cells expressing PAPST1-GFP

The 3'-phosphoadenosine 5'-phosphosulphate transporter 1 (PAPST1) transports 3'-phosphoadenosine 5'-phosphosulphate (PAPS) from its site of synthesis in the cytoplasm into the lumen of the Golgi apparatus where PAPS is the donor of sulphate to sulfotransferases. PAPST1 is therefore localized to Golgi membranes. We thus regarded the MDCK II cell line expressing PAPST1 with a GFP tag (Dick et al. 2008) as a promising cell line for studies of changes in the Golgi apparatus morphology. PAPST1 localizes mostly to the *trans*-Golgi region, and may therefore not give a representative view of the entire Golgi apparatus. It is a membrane-spanning protein, so it will remain in Golgi membranes during morphological changes.

Figure 3.1.4.1 shows that visualization of PAPST1-GFP in MDCK II cells reveals a typical Golgi apparatus pattern. Further experiments with addition of Doxo and Camptothecin (CPT) indicated significant Golgi dispersal upon treatment with these DNA damaging drugs. The MDCK II cell line expressing PAPST1-GFP was therefore a good candidate cell line for studies of changes in Golgi apparatus morphology.

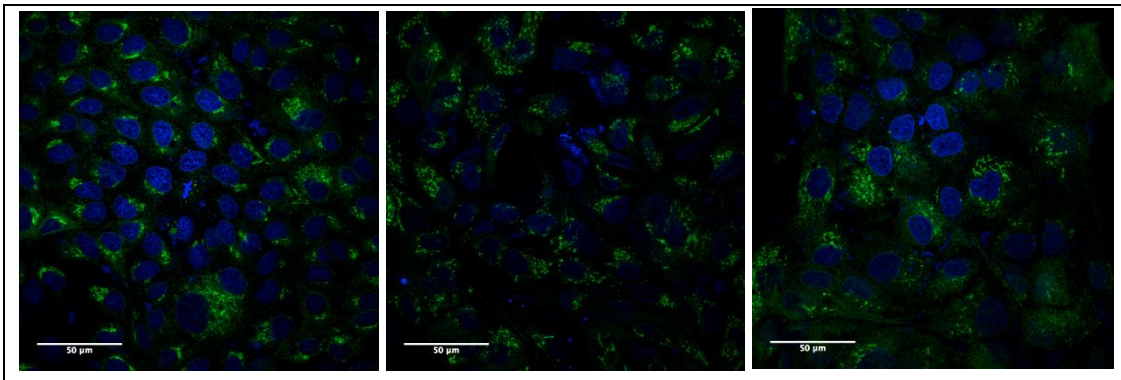

A) Ctrl: B) Doxo, 2.0 µM C) CPT 4.0 µM

Figure 3.1.4.1: MDCK II cells expressing PAPST1-GFP incubated with Doxo. MDCK II PAPST1-GFP cells were grown to confluency. Doxo and CPT treated cells underwent 4 h incubation at the indicated concentrations, followed by 20 h incubation without drug, and finally with 10 mg/µL Hoechst for 20 min prior to visualization. Scale bar; 50 µm.

The only disadvantage of this cell line seems to be a relatively slow growth rate, requiring several days extra compared to non-transfected MDCK II cells to reach a confluent cell layer. However, there is an advantage in not needing incubation time with a Golgi marker prior to drug treatment. Certain marker experiments in this thesis have required up to a 48 h incubation time, mainly due to transient transfection to express a Golgi marker. The transient transfection reagents, often lipid-based, may also influence the morphology of cytoplasmic organelles.

3.2 Incubation with DNA damaging agents and changes in the Golgi apparatus morphology

The aim for this thesis was to investigate possible changes in the Golgi apparatus morphology in MDCK II cells upon incubation with DNA damaging agents. It has recently been shown that inducers of DNA damage, like doxorubicin (Doxo) and Camptothecin (CPT) also affect Golgi morphology dramatically (Farber-Katz et al. 2014). What is important to know about Golgi morphology in polarized epithelial MDCK cells, is that under optimal conditions when the cell layer becomes completely confluent, the Golgi apparatus will move to the apical part of the cell, residing in a perinuclear position, above the nucleus (Bacallao et al. 1989). In less confluent cells, that are flatter than the columnar epithelium, the Golgi apparatus is condensed so that it will predominate to one side of the nucleus. What we expect after treatment with DNA damage inducing agents (Farber-Katz et al. 2014), is that Golgi markers will be more widely distributed in the cytoplasm than in control cells, with less concentrated signal in the perinuclear area, and a more dispersed signal around the whole nucleus. In our attempt to induce this phenomenon, we used the two DNA topoisomerase inhibitors, doxorubicin and Camptothecin (Section 2.5.1: DNA damaging agents).

3.2.1 Induction of changes in Golgi morphology, visualized with Golgi-RFP, BacMam 2.0.

After completing our first investigation of suitable Golgi markers (Section 3.1 Visualizing the Golgi Structure), we decided to investigate the effect of Doxo on Golgi morphology with CellLight Golgi-RFP, BacMam 2.0 as the marker of the distribution of Golgi apparatus components (Figure 3.2.1.1) in MDCK II cells. What was immediately apparent was that the Golgi morphology in cells treated to express CellLight Golgi-RFP seemed dispersed already in untreated cells (Figure 3.2.1.1.A). CellLight Golgi-RFP could be observed in a vesicle-like pattern all around the nucleus. Cells grown on 35 mm glass bottom dishes might not have a perfect tight monolayer, therefore these cells might not be as polarized as they would be when grown *in vivo* or on filter, and it follows that Golgi morphology might not be exactly as expected from a 3 – 4 day growth period. However, some of the cells display a more typical Golgi morphology and in particular there is a progression towards more dispersal from the lowest (2.0 µM) to the highest (4.0 µM) Doxo concentrations (Figure 3.2.1.B-D).

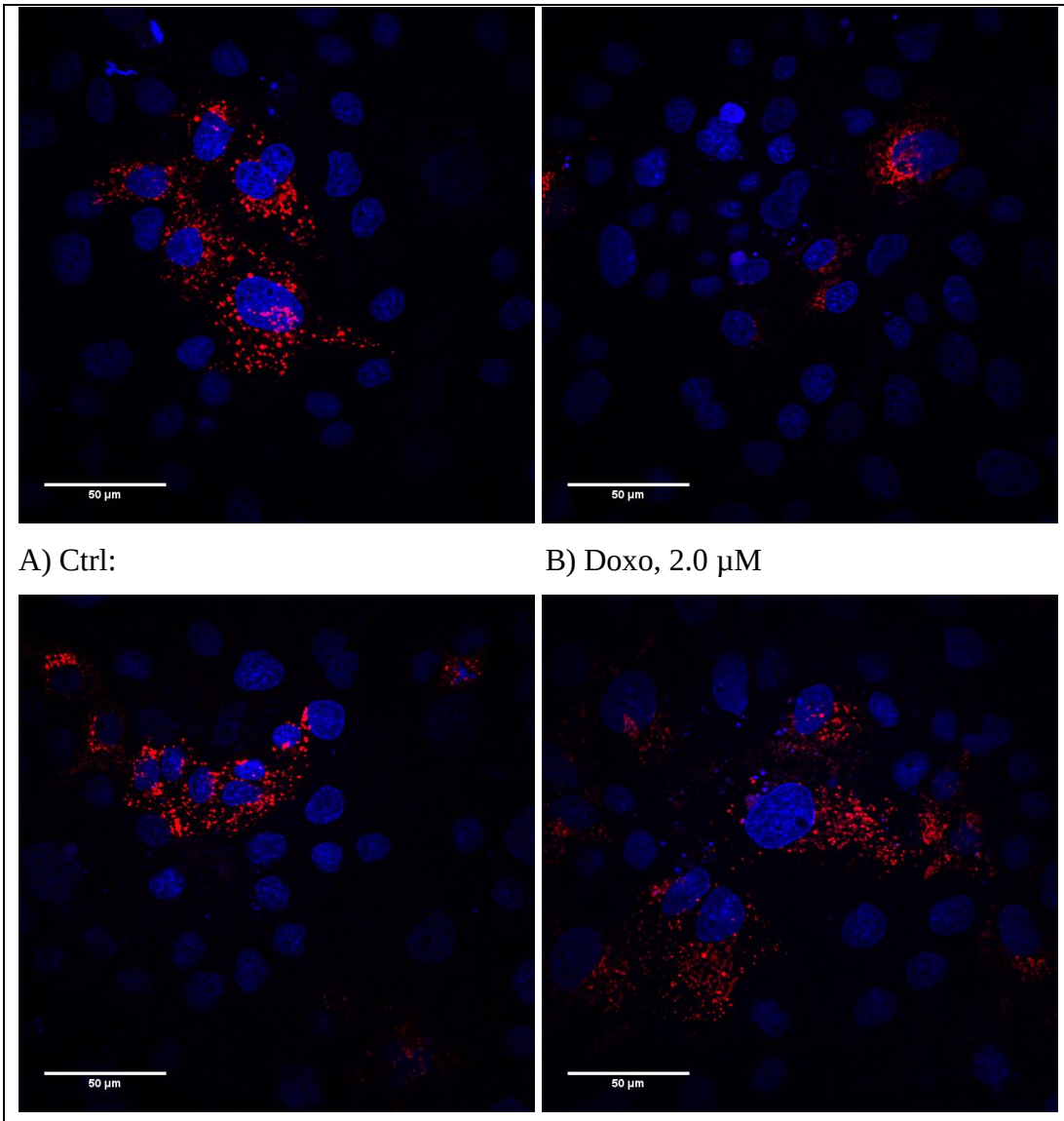

A) Ctrl: B) Doxo, 2.0 µM

C) Doxo, 3.0 µM D) Doxo, 4.0 µM

Figure 3.2.1.1: Effect of Doxo treatment on Golgi apparatus morphology in MDCK II cells, visualized by Golgi-RFP, BacMam 2.0.

MDCK II cells were grown to from 70 % to 80 % confluency in culture dishes with a coverslip at the center, then incubated with Golgi-RFP, BacMam for 24 h, followed by Doxo treatment for 6 h at the indicated concentrations, then 10 µg/mL Hoechst was added 20 min prior to visualization in the confocal microscope. Scale bar; 50 µm.

3.2.2 The effect of Doxo treatment on Golgi apparatus morphology in MDCK II cells using BODIPY TR Ceramide as the Golgi marker.

Due to sub-optimal expression of Golgi-RFP, the effect of Doxo on Golgi apparatus morphology in MDCK II cells was also investigated using BODIPY TR Ceramide as the

Golgi marker. An issue with the ceramide-based marker is a significant background signal, as the ceramide-based marker in addition to incorporating into Golgi membranes labels the plasma membrane and intracellular vesicles to some extent.

As can be observed in Figure 3.2.2.1, the ceramide marker displays a brighter staining in the perinuclear Golgi region than in the remaining cytoplasm in untreated cells and partially in cells treated with 1.0 µM Doxo, while at higher Doxo concentrations, the labeling seems more dispersed. Still, there is quite large cell-to-cell variation in Golgi morphology, also in control cells, and some loss of cells from the monolayer after treatment with 3.0 µM Doxo, made quantification of changes in Golgi morphology difficult.

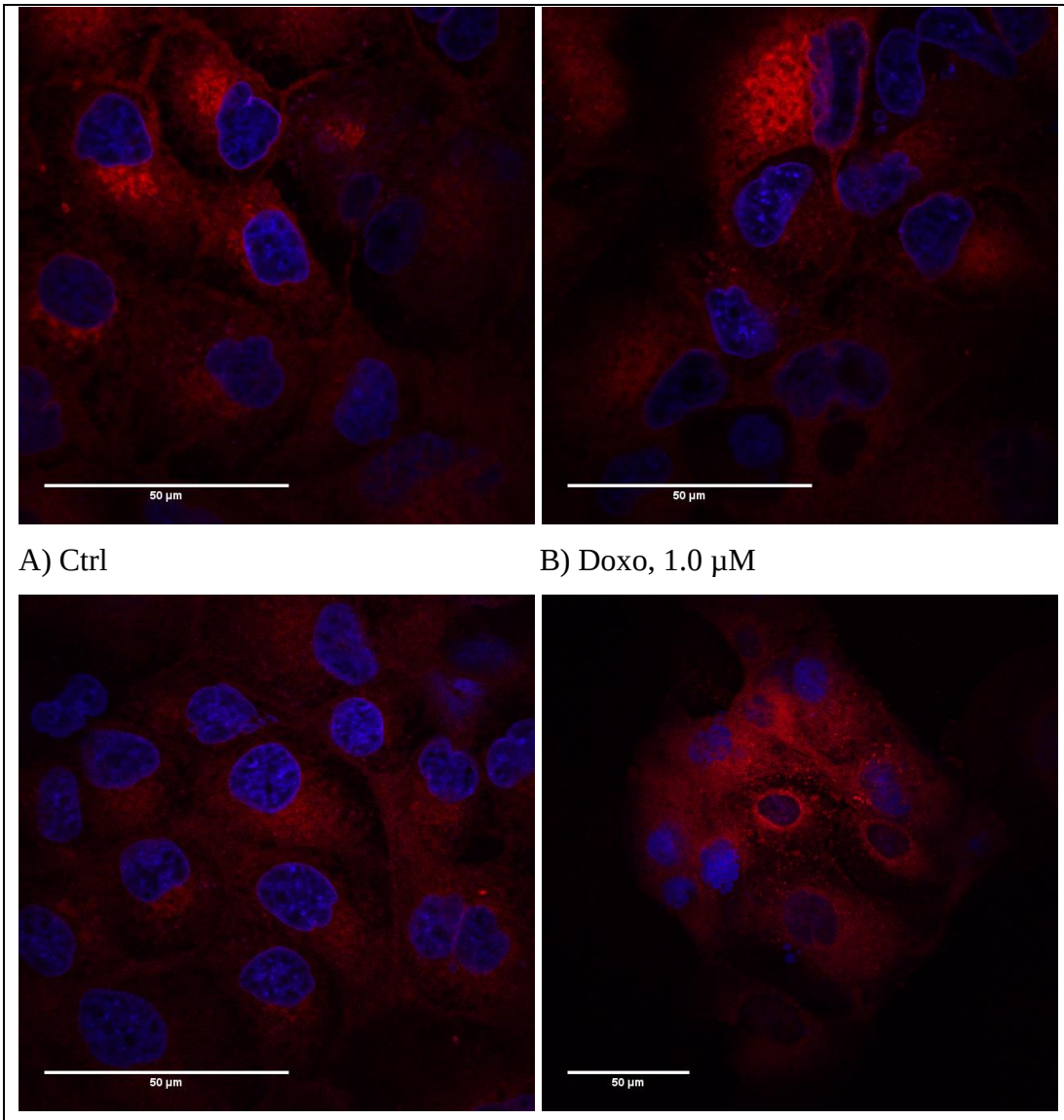

A) Ctrl B) Doxo, 1.0 µM

C) Doxo, 2.0 µM D) Doxo, 3.0 µM

Figure 3.2.2.1: Effect of Doxo treatment on Golgi apparatus morphology in MDCK II

cells using BODIPY TR Ceramide as the Golgi membrane marker.
MDCK II cells were grown to confluency, treated with Doxo for 6 h, incubated for 30 min with BODIPY TR Ceramide, and finally incubated for 20 min with 10 µg/mL Hoechst prior to visualization. All images were taken using the same laser strength. Scale bar; 50 µm.

Due to some loss of cells at the higher Doxo concentrations, in the next experiment, the effect of lower concentrations of Doxo on the morphology of the Golgi apparatus was tested. Farber-Katz et al. demonstrated changes in Golgi morphology at concentrations below 1 µM. Since they have reported that DNA damage leads to cell death via apoptosis, following the GOLPH3 signaling cascade, and the fact that Doxo has been reported to increase cell death via apoptosis following the Bcl-2/Bax pathway (Tacar, Sriamornsak & Crispin R. Dass 2013), lower concentrations were tested to potentially identify an experimental window where Golgi dispersal is induced without significant loss of cells. Farber-Katz et al. were able to detect changes in Golgi morphology after 4 h of Doxo treatment of HeLa cells (Farber-Katz et al. 2014). We therefore decided to treat MDCK II cells for 6 h in the following experiment.

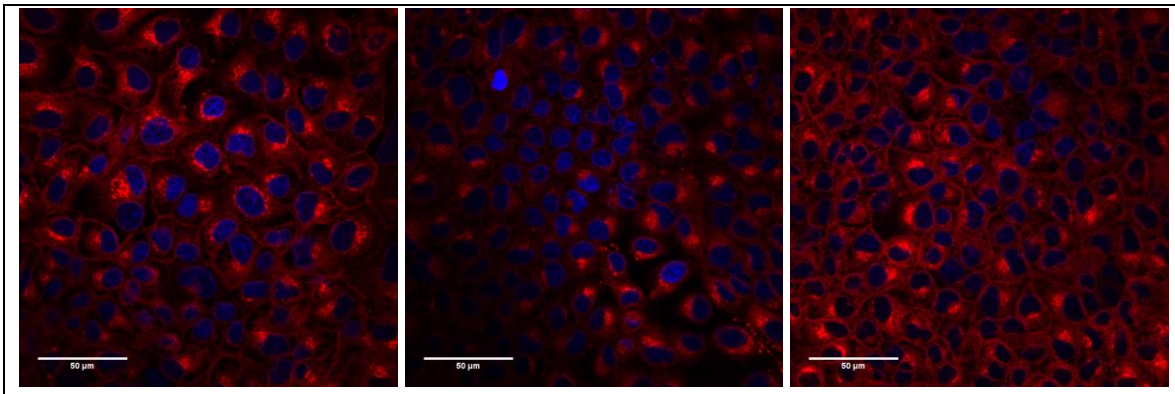

A) Ctrl B) Doxo, 0.05 µM C) Doxo, 0.25 µM

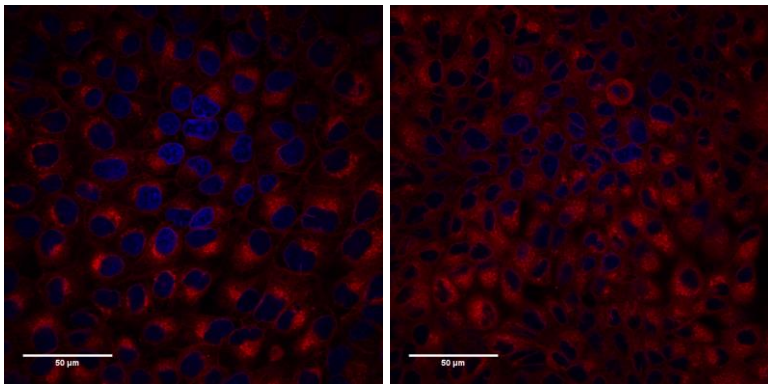

D) Doxo 0.5 µM E) Doxo 0.75 µM

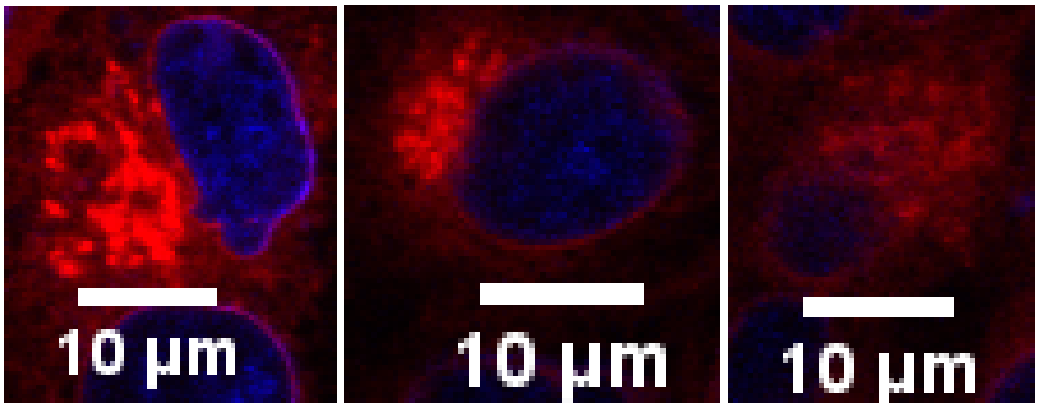

Ctrl Doxo, 0.5 µM Doxo, 0.75 µM

F) Higher magnification

Figure 3.2.2.2: Treatment of MDCK II cells with Doxo and observation of Golgi morphology after 6 h, using BODIPY TR Ceramide as marker.

MDCK II cells were grown to confluency, treated with Doxo or not for 6 h, then incubated for 30 min with BODIPY TR Ceramide, and finally for 20 min with 10 µg/mL Hoechst, prior to visualization. All images were taken using the same laser strength. A-E scale bar; 50 µm, F scale bar; 10 µm.

While 0 – 0.5 µM Doxo gave a predominant perinuclear localization of the lipid-based Golgi marker, the marker dispersal was observable after 6 h in the presence of 0.75 µM Doxo (Figure 2.1.3.E), particularly evident at a higher magnification (Figure 2.1.3.F). A reduction in the signal seemed to occur already at 0.5 µM Doxo.

3.2.3 Doxo treatment of MDCK II cells expressing PAPST1-GFP

Based on the experiments addressing visualization of the Golgi apparatus by fluorescence (Section 3.1: Visualizing the Golgi Structure), MDCK II cells stably expressing PAPST1-GFP were found to be a suitable cell line for studies of Golgi morphology. The first incubations with Doxo were carried out for 30 h. This long incubation time might reduce cell survival (Section 3.3: Cell viability), but should indicate whether a given Doxo concentration leads to Golgi dispersal, as observed for HeLa cells by Farber-Katz et al. (Farber-Katz et al. 2014) where the relative Golgi area was tripled after this incubation time.

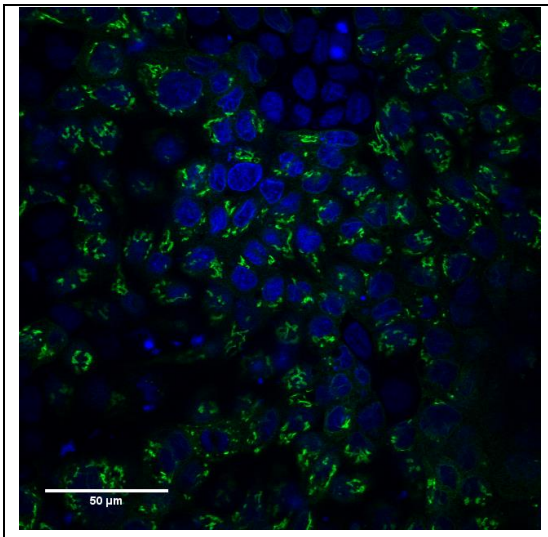

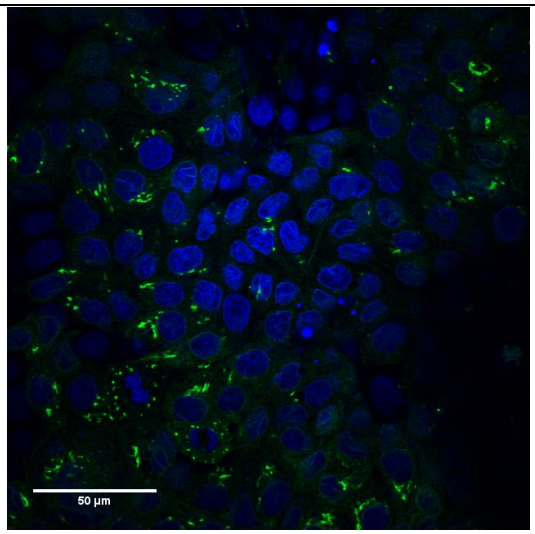

A) Ctrl: Middle plane Basal, lower plane

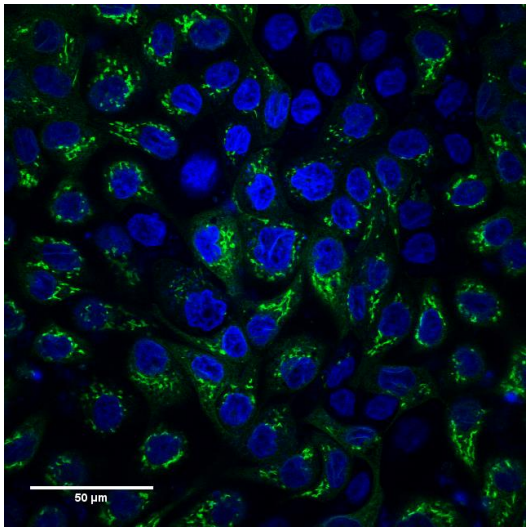

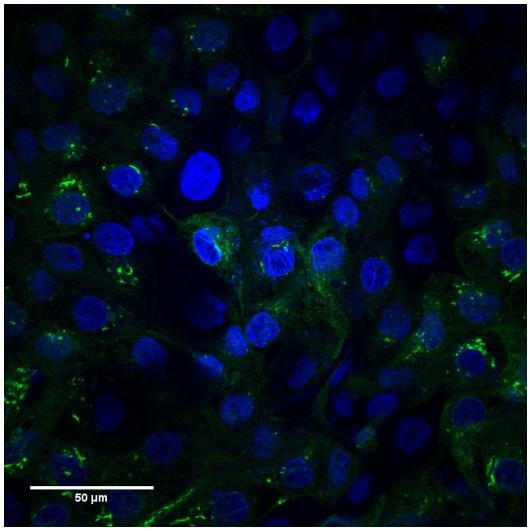

B) Doxo, 2.0 µM: Middle plane Basal, lower plane

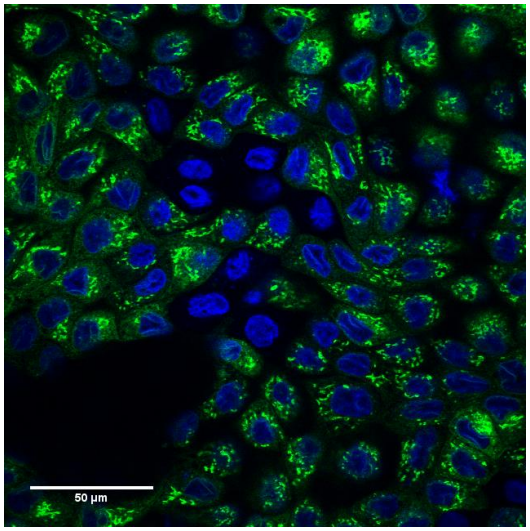

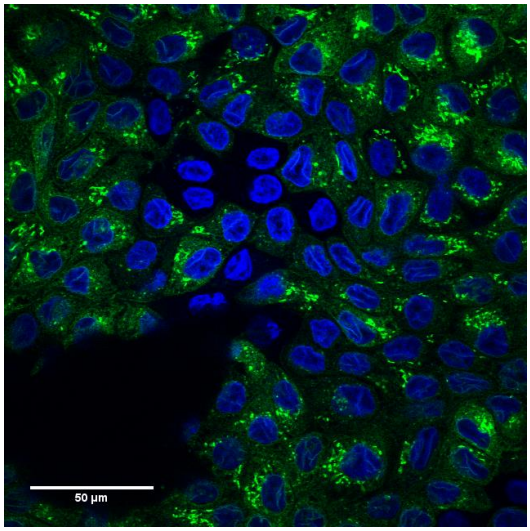

C) Doxo, 5.0 µM: Middle plane Basal, lower plane

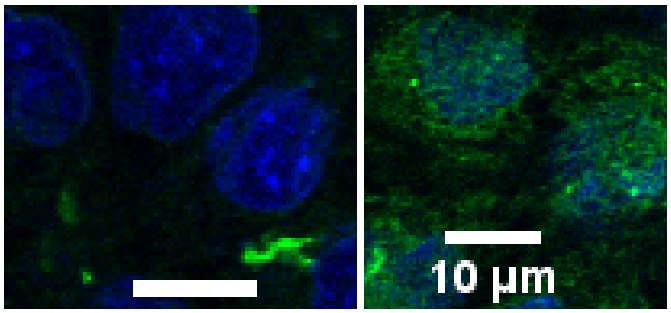

Ctrl: Doxo, 5.0 µM:

D) Higher magnification of Basal, lower plane:

Figure 3.2.3.1: MDCK II cells expressing PAPST1-GFP, 30 h of Doxo treatment. MDCK II PAPST1-GFP cells were grown to confluency, treated with Doxo for 30 h at the indicated concentrations and further incubated with 10 µg/mL Hoechst for 20 min prior to imaging. Laser strength was the same across all samples. A-C scale bar; 50 µm, D scale bar; 10 µm.

Some loss of cells was observed at the relatively high concentration of 5.0 µM Doxo, observable as a loss of cell layer confluency during visualization, but is not observable in these images. Figure 3.2.3.1 confirms our earlier results obtained with ceramide based marker, and showed that we can observe a dispersal of Golgi elements after treatment with both 2.0 µM and 5.0 µM Doxo. At higher magnification (Figure 3.2.3.1.D), it is evident that PAPST1-GFP becomes highly dispersed in the cytoplasm of the cells at the highest (5.0 µM) concentration of Doxo.

To reduce the risk of apoptosis and cell death (Section 3.3: Cell viability), the MDCK II PAPST1-GFP cell line was incubated with lower Doxo concentrations for a shorter period of time (6 h) in an attempt to identify the mildest Doxo treatment that would induce significant Golgi dispersal.

Figure 3.2.3.2 indicates that the Golgi apparatus may seem quite dispersed also in untreated samples, and it can be difficult to establish a low level of dispersal at moderate Doxo concentrations. The advantage of using PAPST1-GFP as the Golgi marker is a lower level of background fluorescence, when compared to BODIPY-TR-Ceramide-BSA.

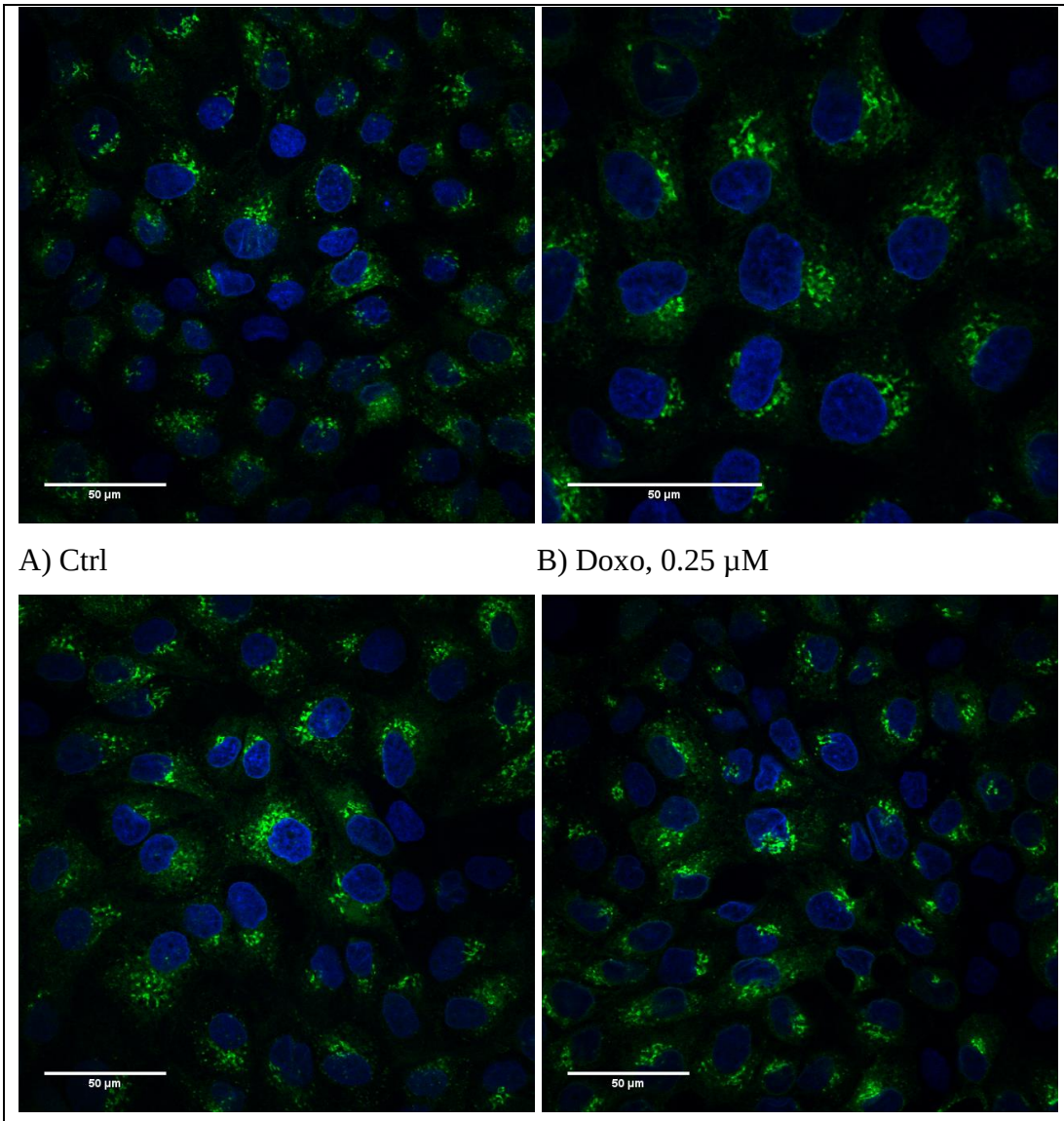

A) Ctrl B) Doxo, 0.25 µM

C) Doxo, 0.5 µM D) 0.75 µM

Figure 3.2.3.2: MDCK II PAPST1-GFP cells treated with sub-micromolar concentrations of Doxo for 6 h.

MDCK II PAPST1-GFP cells were grown to confluency, treated with Doxo for 6 h at the indicated concentrations and further incubated with 10 µg/mL Hoechst for 20 min prior to imaging. Laser strength was the same for all samples. Scale bar; 50 µm.

To investigate whether Hoechst treatment influenced the Golgi apparatus morphology or eventually visualization of the Golgi apparatus, an experiment was performed without addition of Hoechst towards the end of the experiment. Since treatment with 0.25 µM Doxo had not shown indication of Golgi dispersal, the incubations were performed in the presence or absence of 0.5 µm, 0.75 µm, 1.0 µM, and 2.0 µM Doxo. The two latter concentrations were below the concentration (3.0 µM) where some loss of cells had been observed.

In this experiment (Figure 3.2.3.3) we observed clear indications of Golgi dispersal which is most apparent in the basal area of the cell (Figure 3.2.3.3, comparing right panels). In a highly confluent layer of epithelial MDCK cells, there is not much cytoplasmic space available at the mid-nuclear level. Thus, it is sometimes easier to observe Golgi dispersal in the basal region of the cell, underneath the nucleus. A significant dispersal was observed already at sub-micromolar concentration and did not progress with higher Doxo concentrations (1.0 µM and 2.0 µM).

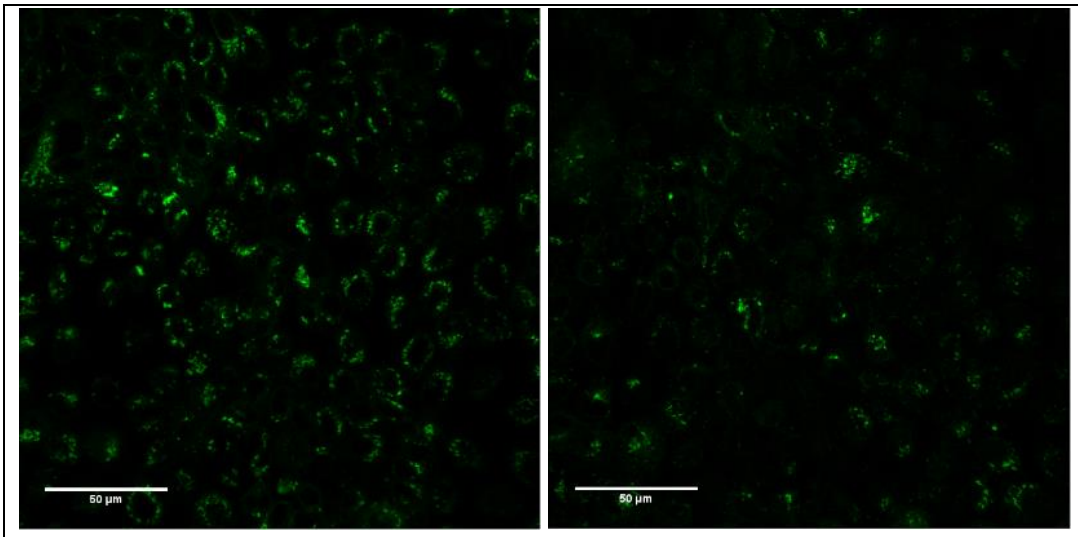

A) Ctrl: Middle plane Basal, lower plane

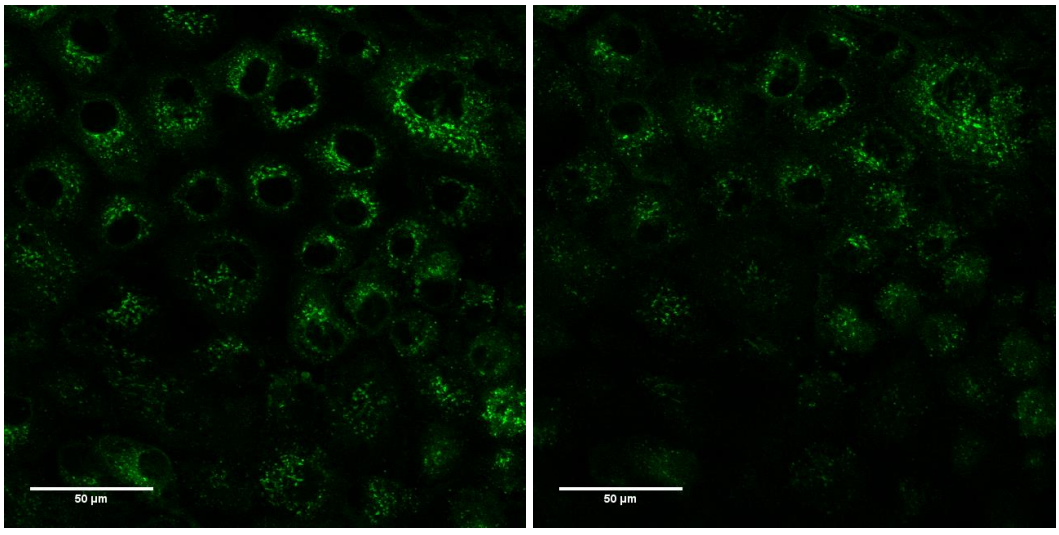

B) Doxo, 0.5 µM: Middle plane Basal, lower plane

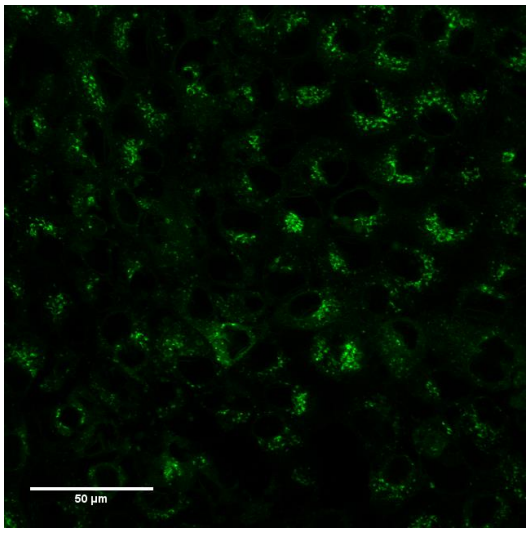

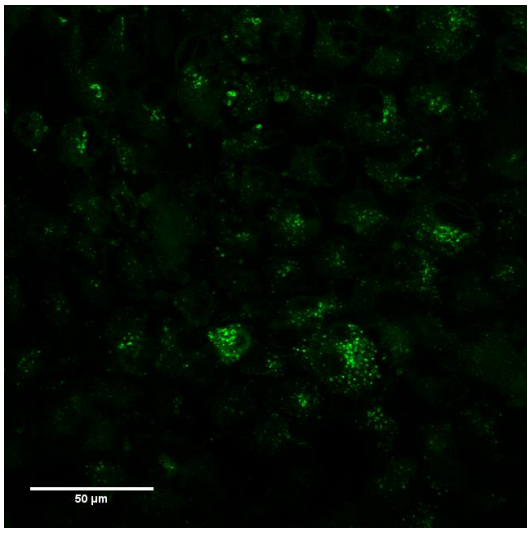

C) Doxo, 0.75 µM: Middle plane Basal, lower plane

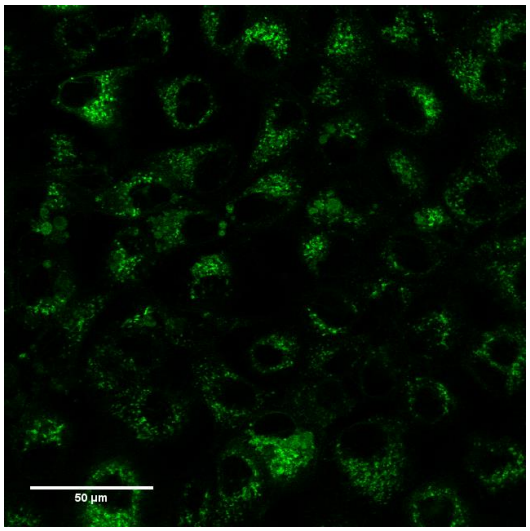

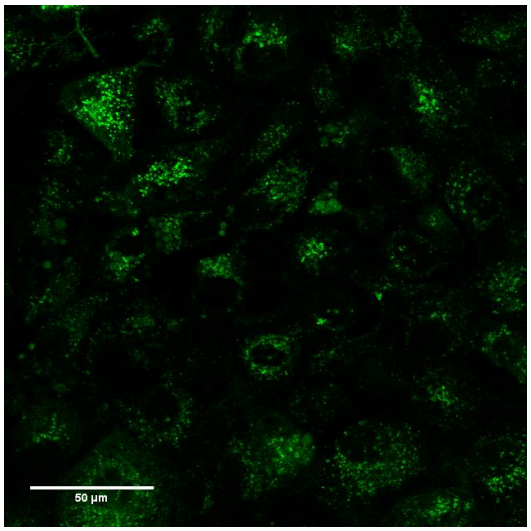

D) Doxo, 1.0 µM: Middle plane Basal, lower plane

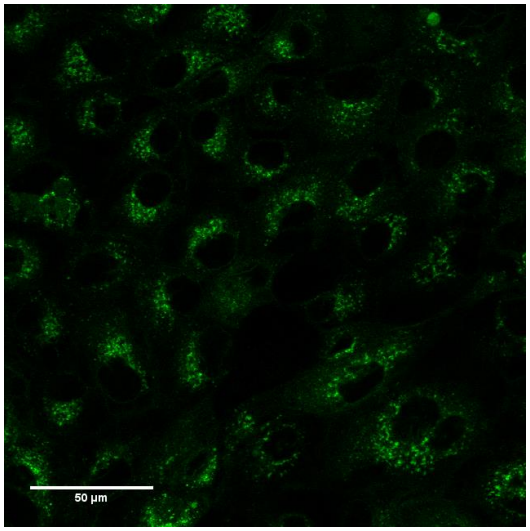

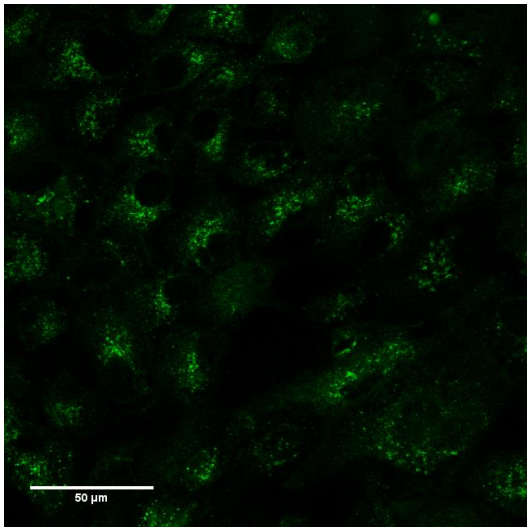

E) Doxo, 2.0 µM: Middle plane Basal, lower plane

Figure 3.2.3.3 MDCK II PAPST1-GFP cells treated with Doxo, no Hoechst.
MDCK II PAPST1-GFP cells were grown to confluency, then treated with Doxo for 6 h at the indicated concentrations. Laser strength was the same for all samples. Scale bar; 50 µm.

Previous experiments have shown some loss of cells at 3 to 5 µM Doxo, but primarily after 30 h of incubation. For the following analysis of Golgi apparatus function, it would be interesting to investigate the effect of higher concentrations (up to 5 µM) of Doxo after 6 h of incubation.

3.2.4 Time-lapse study of doxorubicin treated MDCK II PAPST1-GFP cells.

An alternative way of addressing the effect of Doxo on the morphology of the Golgi apparatus is to study the same cell population before and during drug treatment by time-lapse microscopy. Due to the potential problem of photo-bleaching during longer time-lapse experiments, 10 min intervals for recording images were chosen. The kalman filter and sequential imaging were used, but the kalman setting was 2 pictures, instead of the previously used 4 (Section 2.3.1: Live Imaging).

Because the microscope used did not have an autofocus feature, we lost our original focal plane between t = 0 min and t = 10 min. Between t = 10 min and t = 360 min we also had a gradual shift in the focal plane. This is why Figure 3.2.4.1.A represents a more basally localized plane with less of the Golgi apparatus present, compared to Figure 3.2.4.1.C, where we see more of the Golgi marker PAPST1-GFP. This is mostly not due to dispersal, but more due to a focus z-plane shift from the basal region of the cells towards the middle/apical. However, if we select individual cells to follow from t = 10 min to t = 360 min (Figure 3.2.4.1.D), we can observe some dispersal of the Golgi apparatus despite the change in focus.

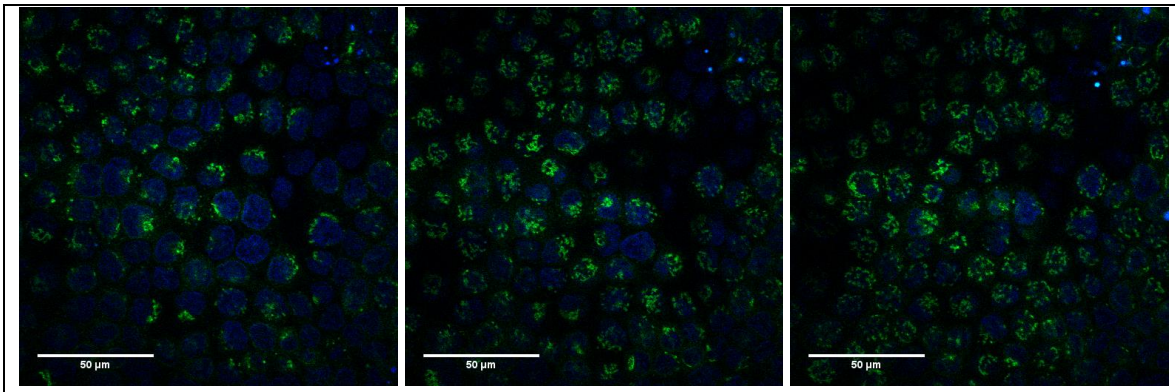

A) t = 10 min B) t = 180 min C) T = 360 min

Video: https://youtu.be/tx2hJ4u9Ua0

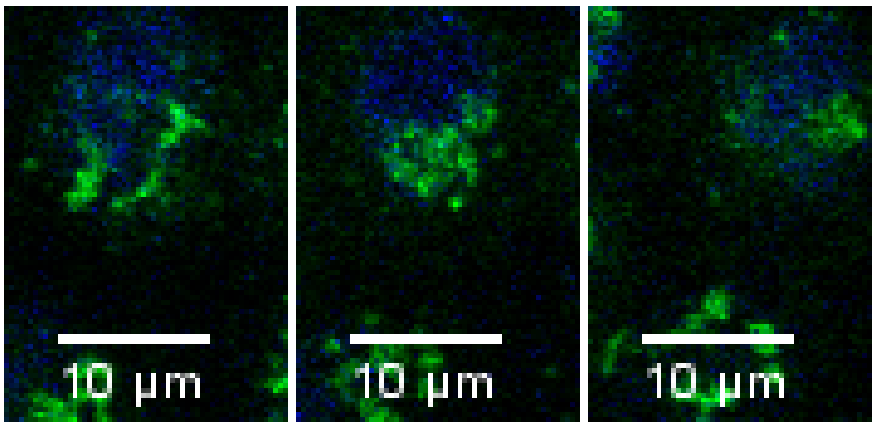

t = 10 min t = 180 min t = 360 min

D) Higher magnification of time-lapse images:

Figure 3.2.4.1: Time-lapse microscopy of MDCK II PAPST1-GFP cells treated with 0.75 µM Doxo.

MDCK II PAPST1-GFP cells were grown to confluency, incubated with 10 µg/mL Hoechst for 20 min, and then treated with Doxo for continuous visualization up to 6 h. The laser settings were the same for all time points and images were recorded every 10 min. A-C Scale bar; 50 µm, D Scale bar; 10 µm.

Due to the shift in z-plane during the time-lapse run and a modest effect of 0.75 µM Doxo on the morphology of the Golgi apparatus, the experiment was repeated with 2.0 µM Doxo. To try to counteract a shift in focal plane somewhat, the cells were allowed to accommodate for 15 min in the microscope hood before starting the recording. Otherwise, the experimental conditions were as in the first time-lapse experiment, recording images every 10 min.

Also in this experiment, a shift in the focal plane occurred already between t = 0 min and t = 10 min, which can be observed in the video link that is provided in Figure 3.2.4.2.E. However, we recorded z-stack images at t = 0 min and at the end of the experiment (t = 360). This made it possible to address changes in the same focal plane from t = 0 to t = 360 min. (Figure 3.2.4.2.C and Figure 3.2.4.2.D). Due to some photo-bleaching, most likely due to the extra z-stack images recorded, the signal is less strong at t = 360 min, but it is still evident that an intact Golgi structure becomes more dispersed towards the end of the incubation (Figure 3.2.4.2.D).

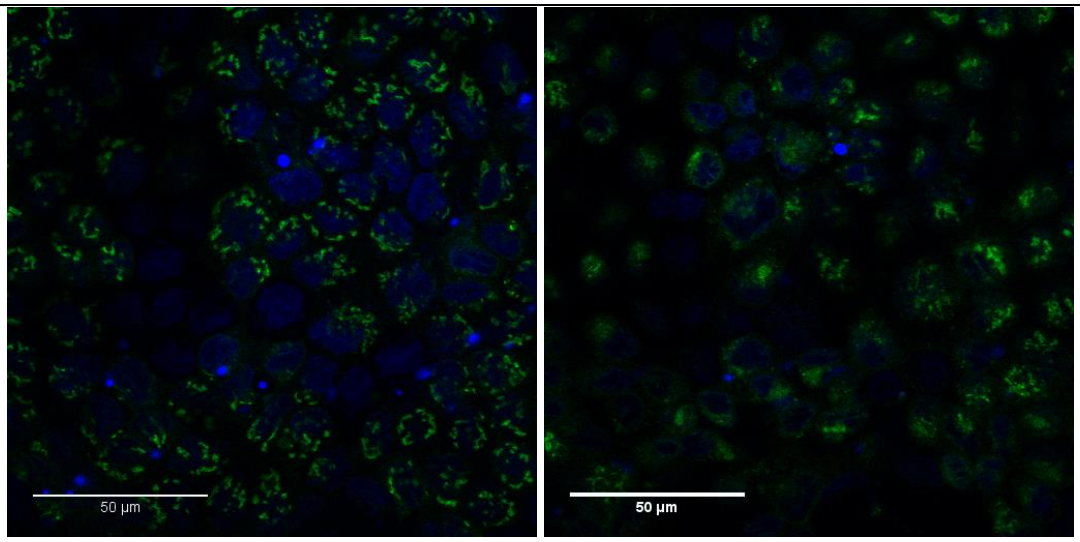

A) t = 0 min B) t = 360 min

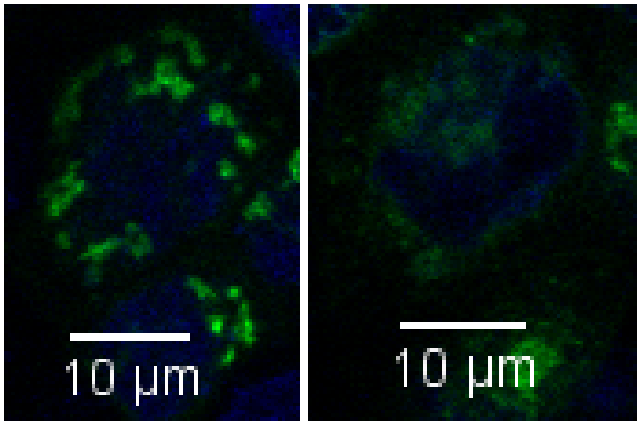

C) t = 0 min D) t = 360 min

Higher magnification from the same focal plane:

E) 6 h time-lapse: https://youtu.be/r00hJ8ckElA

Figure 3.2.4.2: Time-lapse microscopy of MDCK II PAPST1-GFP cells treated with 2.0 µM Doxo.

MDCK II PAPST1-GFP cells were grown to confluency, incubated with 10 µg/mL Hoechst for 20 min, and then treated with Doxo for continuous visualization up to 6 h. The laser settings were the same for all time points, and images were recorded every 10 min. A video is available for viewing the complete time-lapse for panel E. One stack of z-images was taken before the time-lapse experiment at t = 0 min and again after the end of the time-lapse

experiment at t = 360 min, which were used in A and B, respectively. A-B Scale bar; 50 µm, C-D Scale bar; 10 µm.

3.2.5 Camptothecin treatment of MDCK II PAPST1-GFP cells for visualization of the Golgi apparatus.

Induction of DNA damage in combination with studies of Golgi apparatus morphology in HeLa cells was studied by Faber-Katz et al. using both Doxo and CPT (Farber-Katz et al. 2014). The studies using Doxo in this work were therefore complemented with similar studies using CPT.

We find that CPT disperses the Golgi apparatus at 2.0 µM, which is most apparent in the image of the basal section (Figure 3.2.5.2.B). GFP excitation in the 5.0 µM sample was sparse. Only a few of the adhering cells were giving signal, and there were large gaps in cell layer.

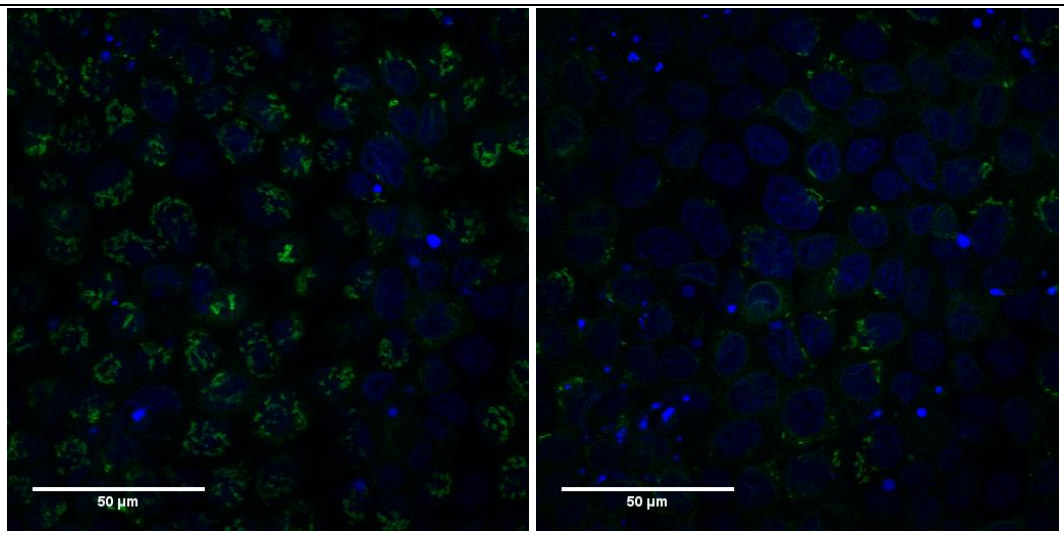

A) Ctrl: Middle plane Lower, basal plane

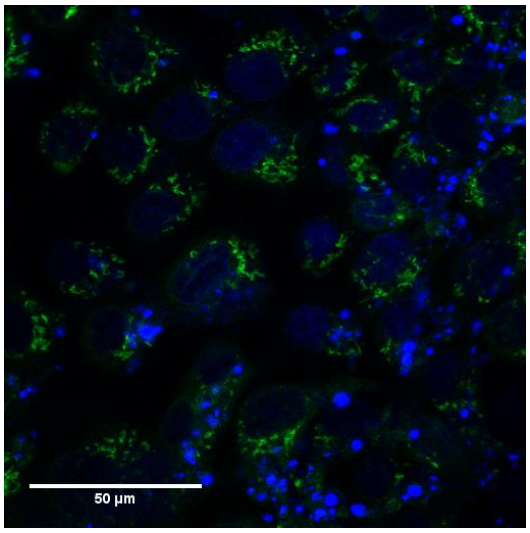

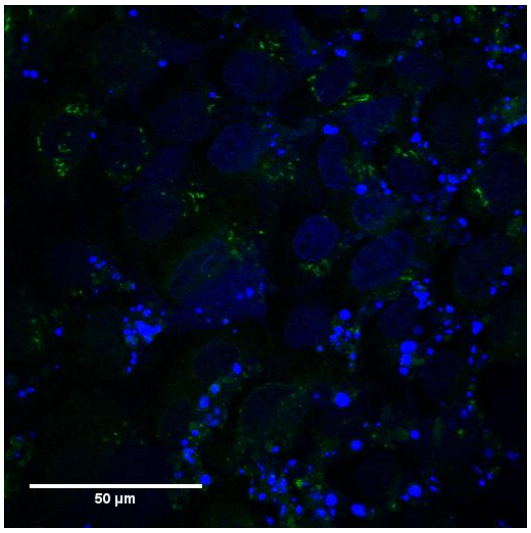

B) CPT, 2.0 µM: Middle plane Lower, basal plane

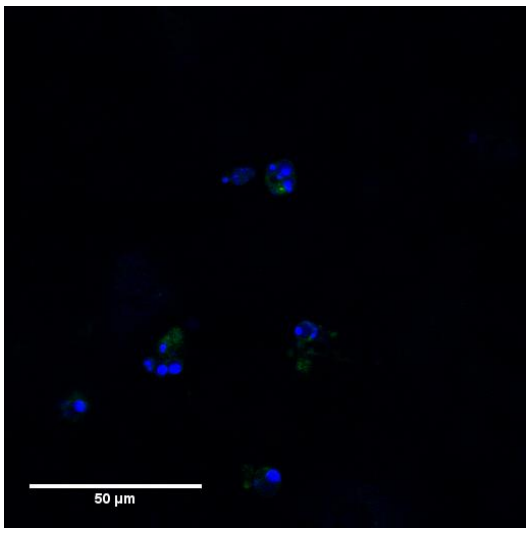

C) CPT, 5.0 µM: Middle plane

Figure 3.2.5.2: MDCK II PAPST1-GFP cells treated with CPT for 24 h.
MDCK II PAPST1-GFP cells were grown to confluency, treated with CPT for 24 h at the indicated concentrations and incubated with 10 µg/mL Hoechst for 20 min prior to imaging. Laser strength was the same for all samples. Scale bar: 50 µm.

A third experiment with incubation of MDCK II PAPST1-GFP cells in the presence of CPT (2.0 to 6.0 µM) was performed (Figure 3.2.5.3). We could observe dispersal of the Golgi apparatus in cells incubated in the presence of 4.0 µM CPT (Figure 3.2.5.3.C). All the CPT concentrations applied (2.0 to 6.0 µM) lead to Golgi dispersal towards the basal region of the cell. Little or no loss of cells from the monolayers could be observed during these incubations.

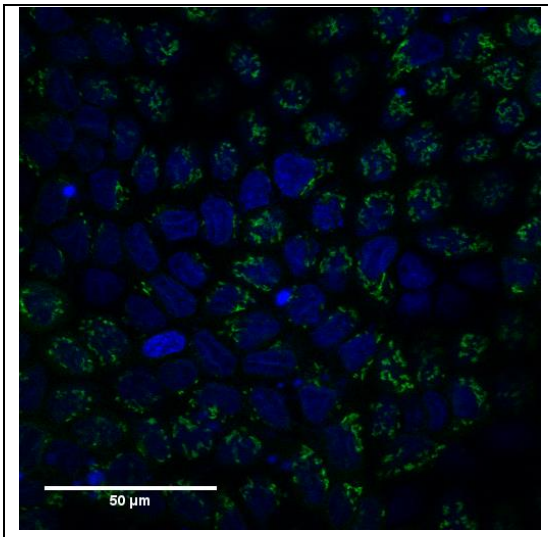

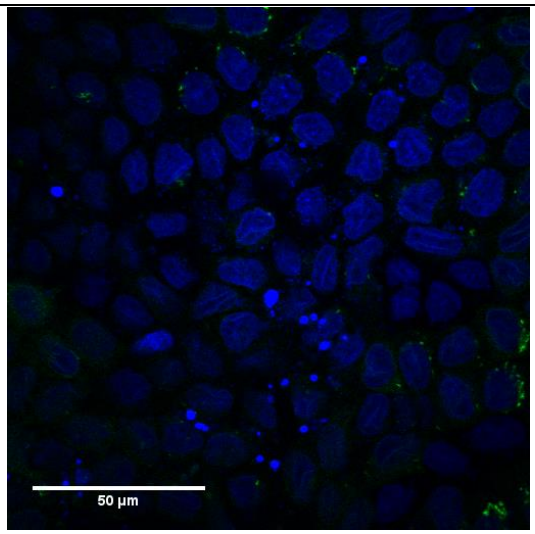

A) Ctrl: Middle plane Lower, basal plane

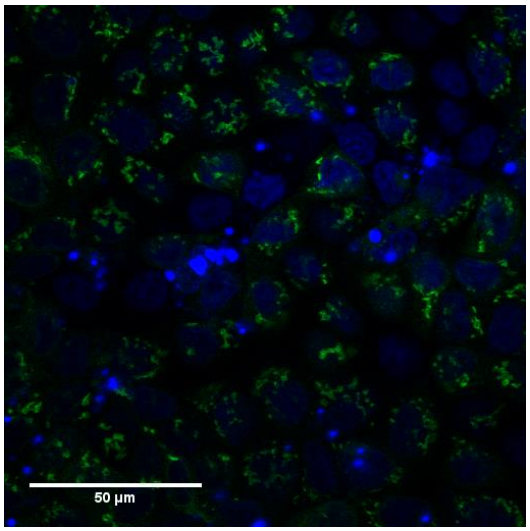

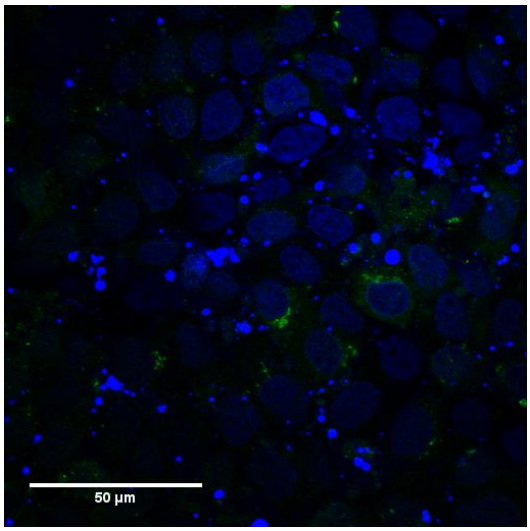

B) CPT, 2.0 µM: Middle plane Lower, basal plane

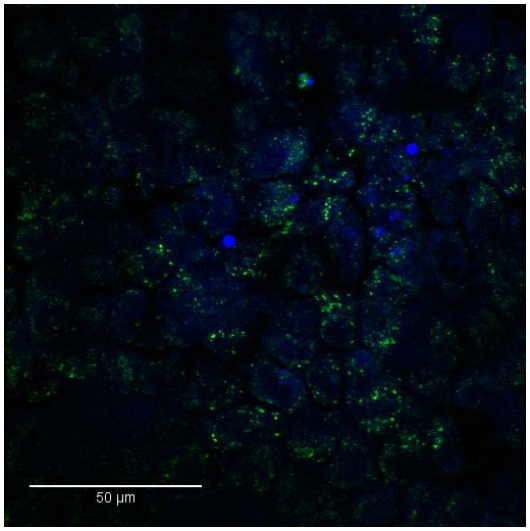

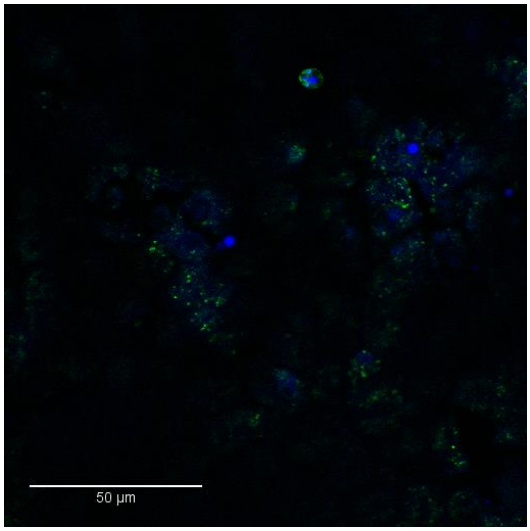

C) CPT, 4.0 µM: Middle plane Lower, basal plane

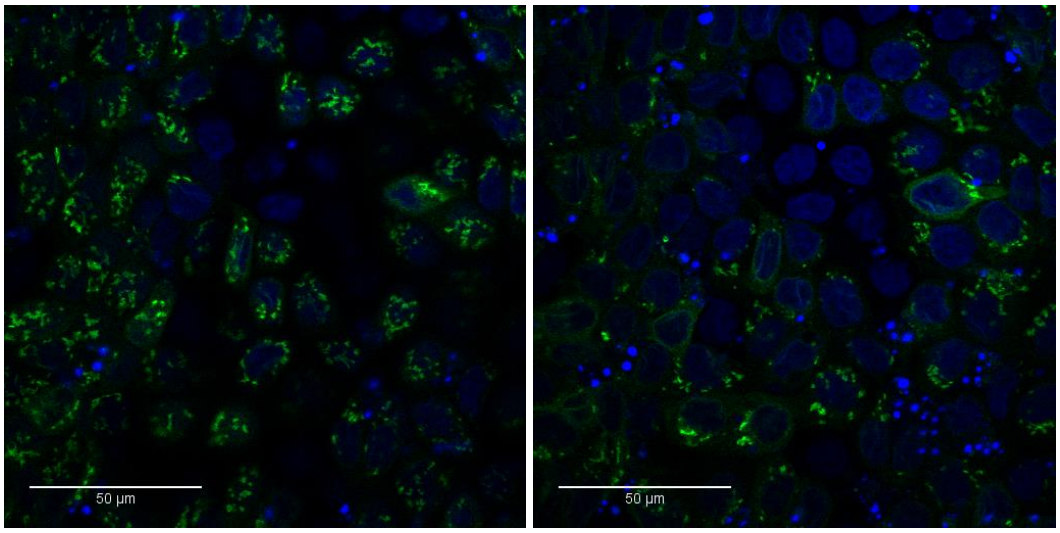

D) CPT, 6.0 µM: Middle plane Lower, basal plane

Figure 3.2.5.3: Incubation of MDCK II PAPST1-GFP cells in the presence of CPT, 24 h treatment.

MDCK II PAPST1-GFP cells were grown to confluency, treated with CPT for 24 h at the indicated concentrations and incubated further with 10 µg/mL Hoechst for 20 min prior to imaging. Laser strength was the same for all samples. Scale bar; 50 µm.

3.2.6 Establishing conditions for biochemical experiments

We wanted to perform biochemical experiments to address the effects of inducers of DNA damage, not only on the structure of the Golgi apparatus, but also on the function of the organelle system (Section 3.4: Effect of DNA damaging agents). The function of choice was the ability to perform synthesis and sorting of proteoglycans (PGs), monitored by investigating the incorporation of ^{35}S-sulphate into PGs and their subsequent secretion into the apical and the basolateral media of filter-grown polarized monolayers (Tveit et al. 2005; Dick et al. 2008; Grøndahl et al. 2009). Metabolic labeling of PGs with ^{35}S-sulphate may be performed over various time-spans, but to obtain sufficient material secreted for several types of analysis, incubation for 24 h is often used.

The biochemical studies should ideally be performed with experimental conditions similar to those giving a clear Golgi dispersal and little or no loss of cells from the monolayer. Experiments with CPT and Doxo in what seemed to be the optimal concentration range (4.0 µM or less CPT, and 0.5 µM to 2.0 µM Doxo). The incubation time was now set to 24 h to

comply with metabolic labeling conditions. For these experiments we used MDCK II PAPST1-GFP cells with a lower passage number.

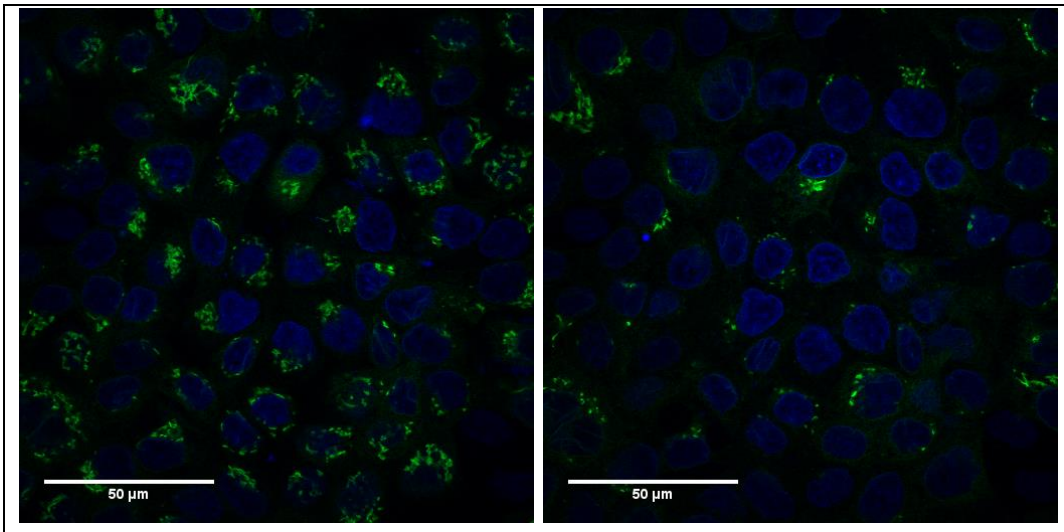

A) Ctrl: Middle plane Lower, basal plane

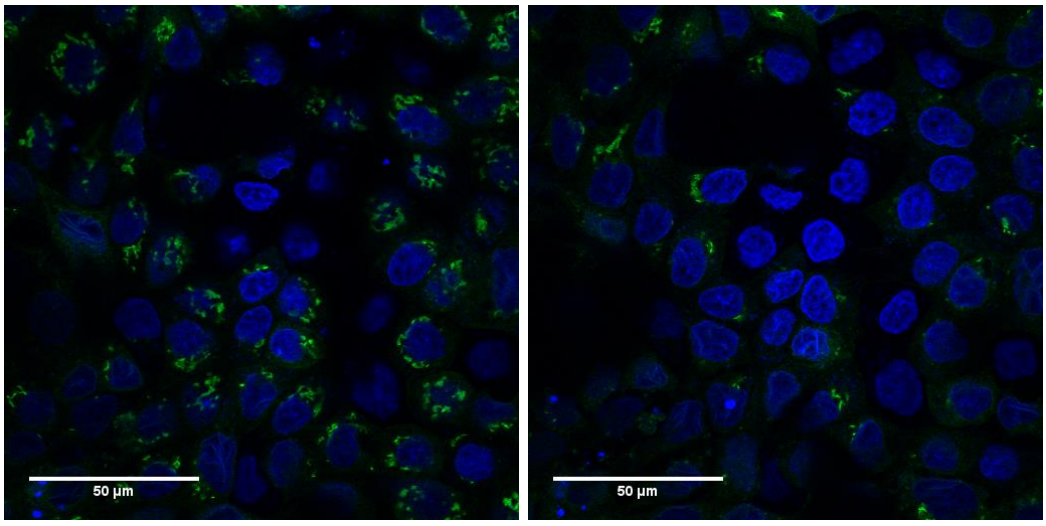

B) Doxo, 0.5 µM: Middle plane Lower, basal plane

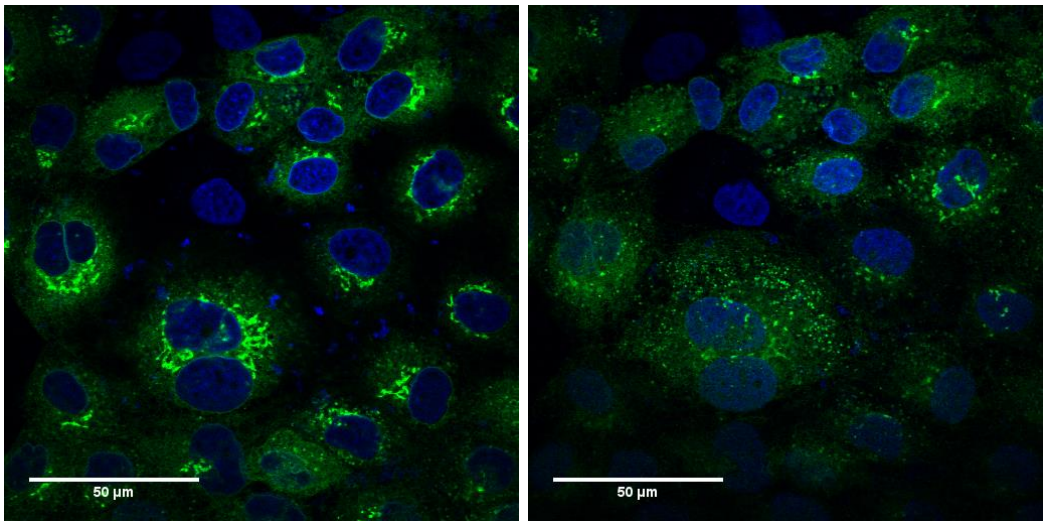

C) Doxo, 2.0 µM: Middle plane Lower, basal plane

Figure 3.2.6.1: Treatment of MDCK II PAPST1-GFP cells with Doxo, cells with low passage number.

MDCK II PAPST1-GFP cells were grown to confluency, treated with Doxo for 24 h at the indicated concentrations and further incubated with 10 µg/mL Hoechst for 20 min prior to imaging. Laser strength was the same for all samples. Scale bar: 50 µm.

Interestingly, the low passage cells showed a higher tendency to alter their Golgi morphology, especially when comparing cells treated with 2.0 µM Doxo in Figure 3.2.6.1.C with cells with higher passage number treated with the same concentration in Figure 3.2.6.2.C. After 24 h of treatment, a significant dispersal was observed (Figure 3.2.6.1.C), with PAPST1-GFP also present in the basal region of the cells.

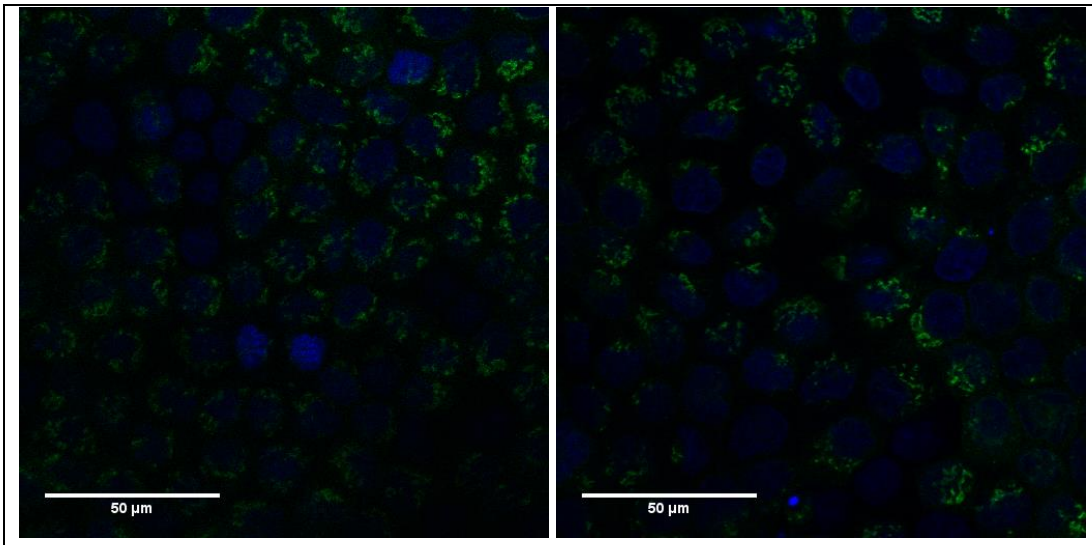

A) Ctrl B) Doxo, 0.5 µM

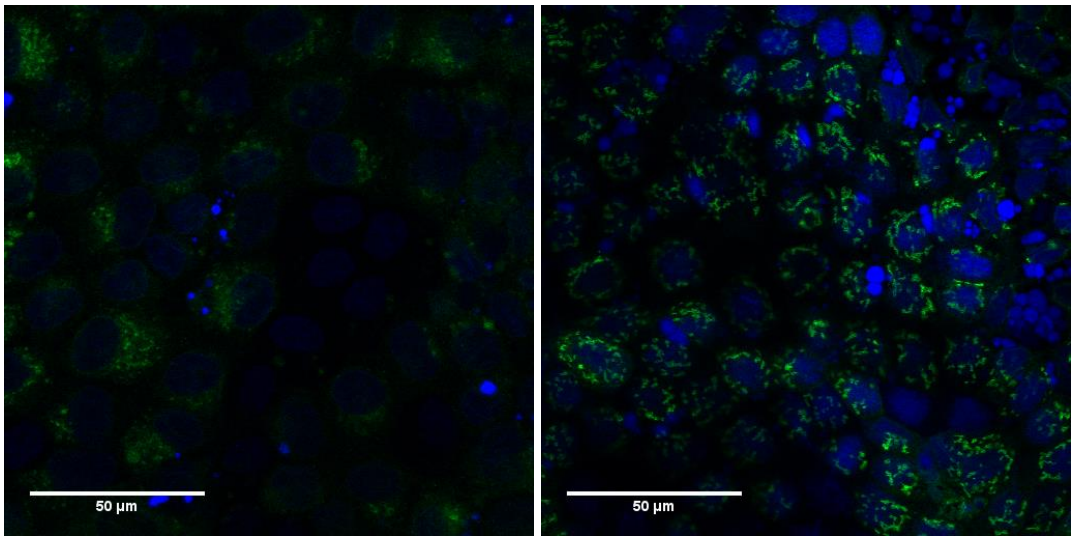

C) Doxo, 2.0 µM D) 4.0 µM CPT

Figure 3.2.6.2: Treatment of MDCK II PAPST1-GFP cells with Doxo, cells with high passage number.

MDCK II PAPST1-GFP cells were grown to confluency, treated with Doxo or CPT for 24 h at the indicated concentrations and further incubated with 10 µg/mL Hoechst for 20 min prior to imaging. Laser strength was the same for all samples. Scale bar; 50 µm.

3.2.7 3D-Modeling

The confocal microscope can record images at several xy-planes with sub-micrometer proximity. A confluent epithelium reaches a height of 10 µm or more (depending on seeding conditions). Several xy-planes comprise a z-stack which may be reconstructed into a 3D-image. For rendering the images in 3D, we use the software iMaris. This tool allows us also to perform further signal analysis. After producing modeling quality z-stacks, we were able to construct a 3D image from the recorded optical sections (Figure 3.2.7.1).

For incubations with 0.5 µM Doxo, we did observe some dispersal (Figure 3.2.7.1.B/3.2.6.1.B), but due to the background cut-off setting of iMaris for green fluorescence, it did not model the lower signals. This has an impact on the data in Table 3.2.7.1, where the Golgi area relative to the nuclear area is reduced in the presence of 0.5 µM Doxo in comparison to the control. Since strong signal areas were less frequent in the cells treated with 0.5 µM Doxo, with a wide dispersal of a weak signal, this is of course an indication of Golgi apparatus dispersal.

The cells in the sample treated with 2.0 µM Doxo (Figure 3.2.7.1.C/3.2.6.1.C) are relatively larger in size compared to the control cells. This is due to lesser cells, and could be an effect of a lower plating density, or an effect of the Doxo treatment, slowing the growth rate or inducing some detachment of cells. However, the background cut-off for these cells allowed a larger fraction of the Golgi membranes to be rendered in 3D, which is why a large spike in relative Golgi area is observed (Figure 3.2.7.2) compared to what is observed for cells treated with 0.5 µM Doxo. It is worth noting, when analyzing the 3D-images, that the green fluorescence area is generated by the program, and is not related to relative signal saturation.

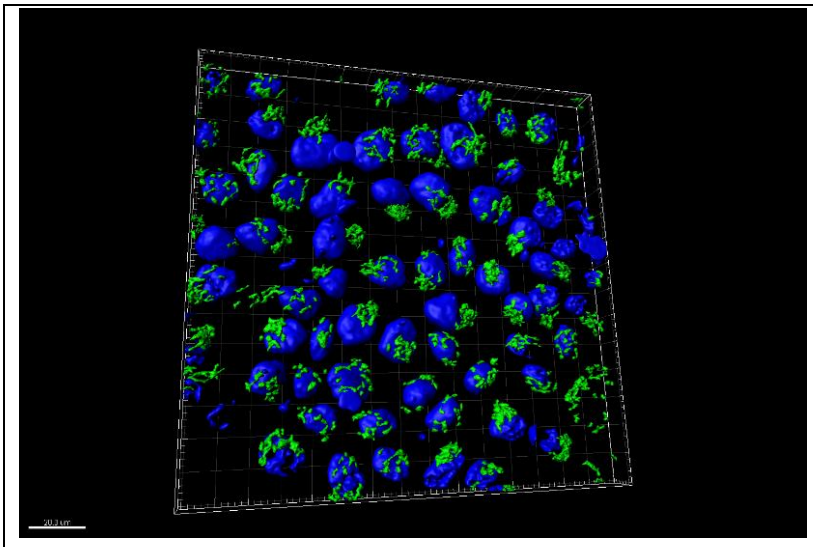

A) Ctrl

https://youtu.be/3K8gA3mt5p4

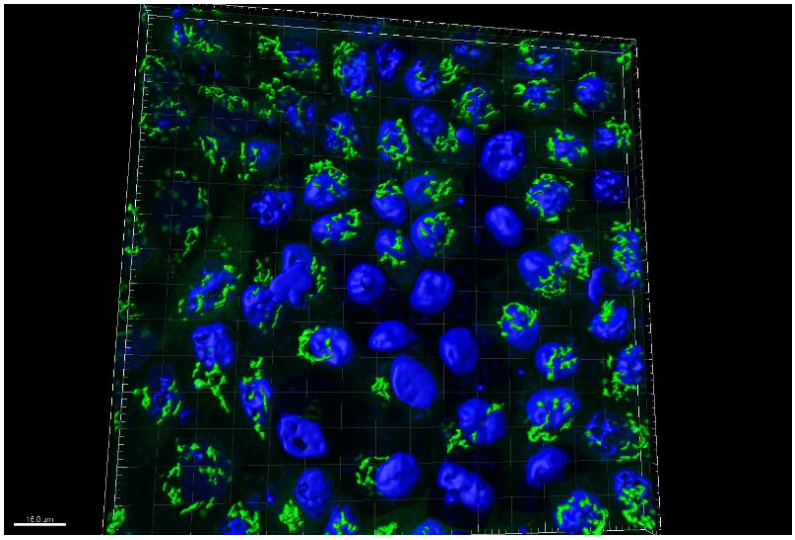

B) Doxo, 0.5 µM

https://youtu.be/uPBPCKgbUTE

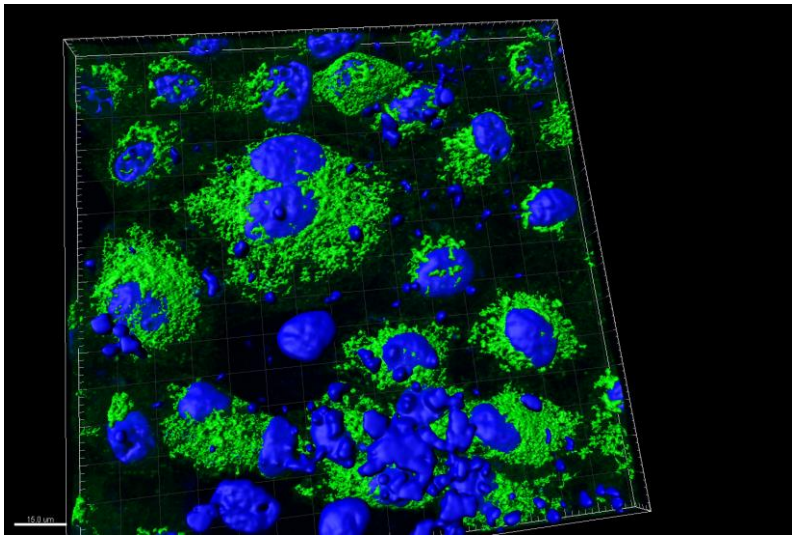

C) Doxo, 2.0 µM

https://youtu.be/LAJA1VGyfmU

Figure 3.2.7.1: 3D Modeling of Figure 3.2.6.1: Treatment of MDCK II PAPST1-GFP cells with Doxo, cells with low passage number.

Images rendered in iMaris. Cells used were low passage MDCK II PAPST1-GFP cells presented in Figure 3.2.6.1.

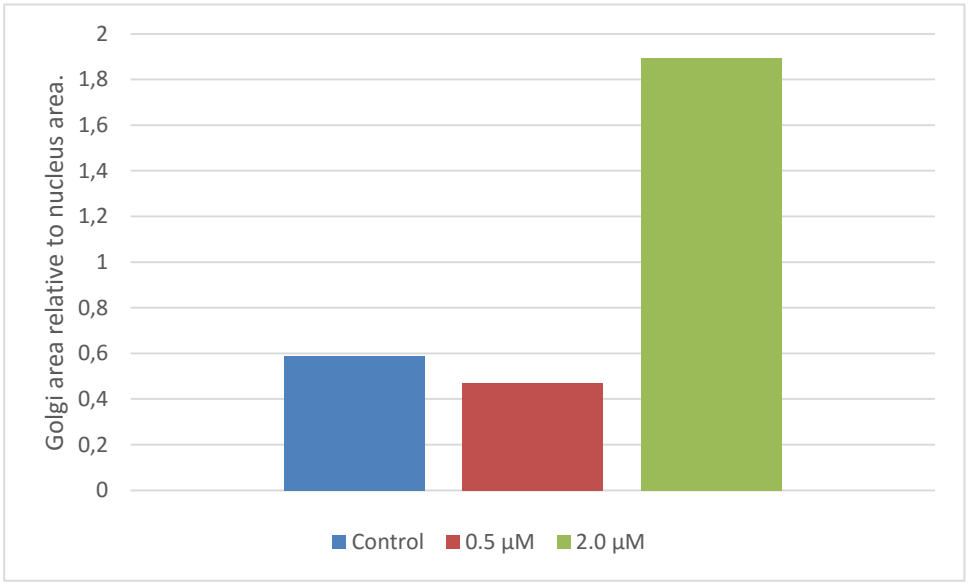

Figure 3.2.7.2: 3D modeled Golgi area relative to nucleus size.

Total nuclear signal area (Hoechst) was divided by the total number of detected nuclei in the

picture, giving an average size of each nucleus in the picture. Total Golgi signal area (PAPST1-GFP) was divided by the number of detected nuclei to give an average Golgi area per nucleus. Average Golgi area per nucleus was then divided by average size of each nucleus, to give the Golgi area relative to the nucleus size (Table 3.2.7.1).

The experiments have confirmed dispersal of the Golgi apparatus after 24 h treatment of MDCK II PAPST1-GFP cells with 2.0 µM – 6.0 µM CPT or 0.5 µM to 5.0 µM Doxo. The risk of losing cells from the monolayer upon treatment with 3.0 µM Doxo or more, indicates that a cell viability assay is required prior to the biochemical experiments.

3.3 Cell viability after incubation with DNA damage inducers

GOLPH3 is an oncogene that has been linked to the mTOR pathway (Scott et al. 2009) which has multiple metabolic roles, one of which is connected to delivery of cell survival signals (Laplante & Sabatini 2009). Following this, Farber-Katz, et al. showed in their 2014 article (Farber-Katz et al. 2014) that treatment of HeLa cells with doxorubicin (Doxo) led to an increase in apoptotic cell death. What we have observed is that under conditions of higher concentrations of Doxo or Camptothecin (CPT), there is a loss of cell layer confluency in the microscope. We were therefore interested in determining how many viable cells we have after incubation of MDCK II cells with DNA damaging agents, which we can use to gauge the optimal dosage for our proteoglycan analysis. We tested two cell viability assays, Propidium iodide stain (PI-stain) and Trypan blue stain.

3.3.1 Propidium iodide stain

What we observed in the first trial, was that combining Hoechst with a Golgi signal caused a signal overflow of the Hoechst stain, leading to an increase in signal noise for the initial run, giving a clear positive signal in the control cells (Figure 3.3.1.A, upper left panel). Despite this, when the cells were treated with increasing amount of Doxo, there was a larger amount of concentrated signal ‘dots’ dispersed in and around the cytosol (Figure 3.3.1D/3.3.1F). This indicated that there was indeed a loss of viability at higher concentrations of the DNA damaging agents.

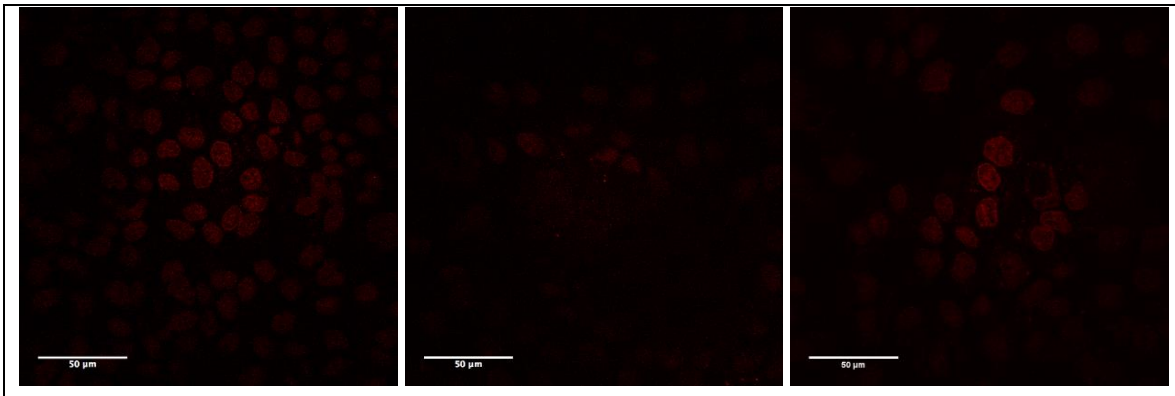

A) Ctrl: B) Doxo, 0.1 µM C) Doxo, 0.5 µM

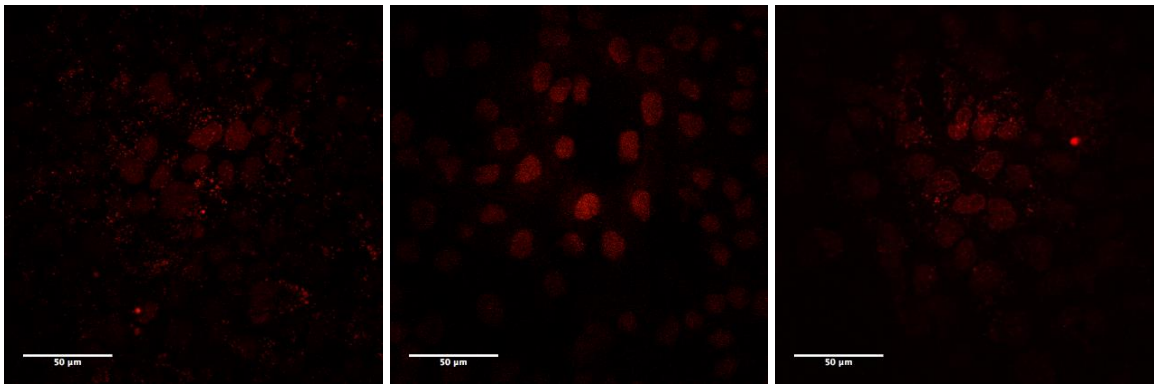

D) Doxo, 1.0 µM E) Doxo, 3.0 µM F) Doxo, 5.0 µM

Figure 3.3.1.1: **MDCK II cells treated with Doxo at increasing concentration, PI stain with Hoechst present.**

MDCK II cells were grown to confluency in 35 mm glass bottom dishes. They were then incubated with Doxo for 6 h at the listed concentrations, followed by a 60 min treatment with PI-stain and then treated 30 min with Hoechst. Scale bar; 50 µm.

Following this, it seemed apparent that using Hoechst was not needed and also caused unnecessary signal bleed through, therefore we did a second run without the Hoechst dye present (Figure 3.3.2).

Through visualization of Golgi dispersal induced by DNA damage, we have observed a good dispersal of the Golgi apparatus at 0.75 µM of Doxo. We would therefore apply concentration in the subsequent experiments, and wanted to test the cell viability at this concentration. We were also interested in addressing cell viability at a slightly higher concentration, like 1.0 µM Doxo. This resulted in that we actually had more PI signal at the 0.75 µM (Figure3.3.2.B) concentration than at 1.0 µM (Figure 3.3.2.C).

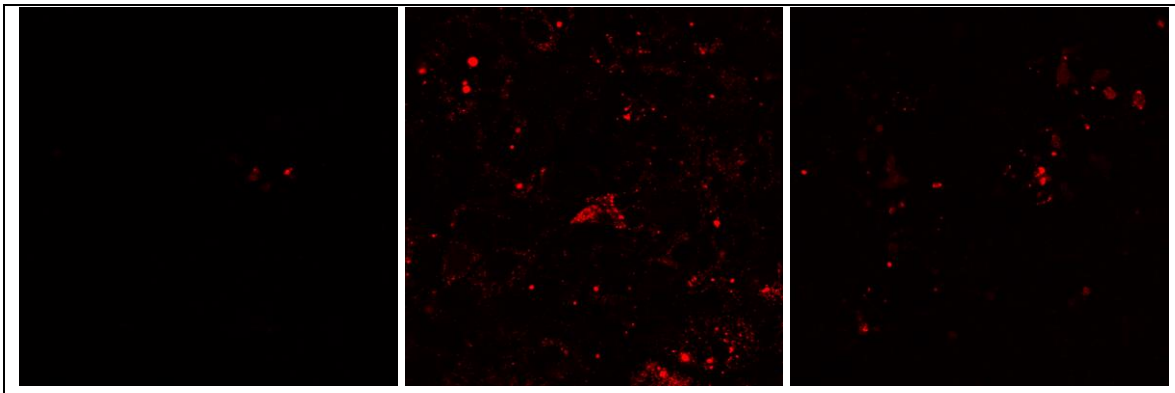

A) Ctrl B) Doxo, 0.75 µM C) Doxo, 1.0 µM

Figure 3.3.1.2: **MDCK II cells treated with Doxo, PI-stain with no Hoechst.**
MDCK II cells were grown to confluency in 35 mm glass bottom dishes. They were then incubated with Doxo for 6 h at the indicated concentrations, followed by a 60 min treatment with PI-stain. Scale bar; 50 µm.

3.3.2 Trypan blue cell viability assay

Due to the inconsistency with the PI stain, we decided to compare the results with a Trypan blue cell viability assay. Certain samples were analyzed more than once, and an average was generated of these before being plotted (Figure 3.3.2/3.3.3).

Incubation of MDCK II cells with concentrations below or equal to 5.0 µM Doxo for 24 h did not cause a significant loss in viability (Figure 3.3.2.A). Since we noticed some decrease in cell count upon treatment with CPT, we also added a graph showing the total amount of cells counted in Doxo treated cells compared to control (Figure 3.3.2.A). If the dead cells (or the living cells for that matter) were not firmly attached to the dish when they are being prepared for Trypan blue stain, they would be removed during the subsequent washing steps. This would also be noticeable in Figure 3.3.2.1 when looking at the total number of cells. In the case of Doxo treatment, we did not find any reduction in the total cell number.

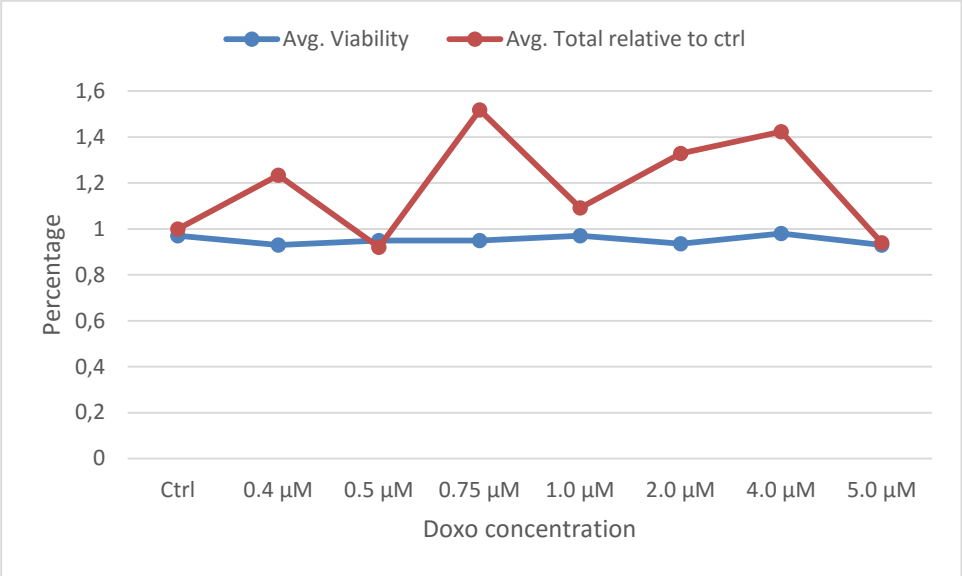

Figure 3.3.2.1: MDCK II PAPST1-GFP cells treated with Doxo, subjected to Trypan blue stain (Table 3.3.2). Viability and total cell number relative to control of MDCK II PAPST1-GFP cells after 24 h treatment with the indicated Doxo concentration.

CPT treatment did not reduce the viability dramatically for incubations at 6 µM or less, maintaining at least 90 % viability (Figure 3.3.2.2). However, the total number of cells declined for incubations with more than 4.0 µM CPT, indicating that cells detach at higher concentrations. Therefore, in further experiments, 4.0 µM CPT should be the highest concentration.

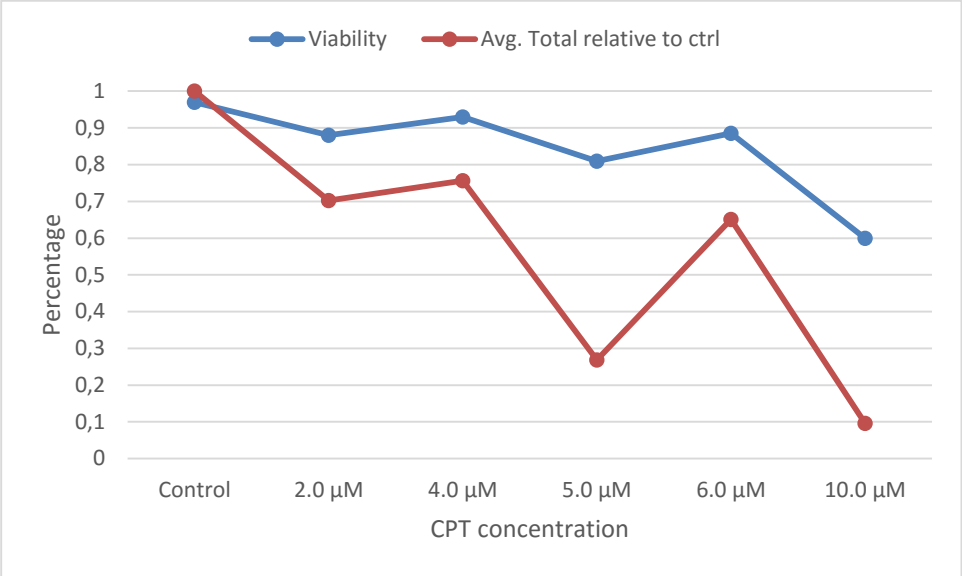

Figure 3.3.2.2: MDCK IIPAPST1 cells treated with CPT, subjected to Trypan blue stain (Table 3.3.4).

Viability and total cell number relative to control of MDCK II PAPST1-GFP cells after 24 h treatment of the indicated concentrations of CPT.

The viability studies suggest that 4.0 µM CPT will be the highest concentration suitable for studies of PG synthesis and sorting, and that concentrations of up to 5.0 µM Doxo also allow most of the cells to survive (Figure 3.3.2.2). However, occasionally, some loss of cell layer confluency was observed at Doxo concentrations between 3.0 and 5.0 µM. Therefore, 2.0 µM Doxo was the highest concentration used in studies of PG synthesis and sorting.

3.4 The effect of DNA damaging agents on proteoglycan synthesis and sorting.

3.4.1 The effect of Camptothecin on synthesis and secretion of ^{35}S-sulphate labeled macromolecules

Treatment of MDCK cells with inducers of DNA damage led to a significant change in the Golgi apparatus morphology (Figure 3.2.7.2). We therefore wanted to investigate whether these changes also had consequences for some of the functions of the Golgi apparatus. To this end, we metabolically labeled polarized, filter-grown epithelial cells with ^{35}S-sulphate to address proteoglycan (PG) sorting and secretion in the apical and basolateral direction. The initial experiments were carried out by using Camptothecin (CPT) as the inducer of DNA damage. We chose to test two cell lines, regular MDCK II cells and MDCK II Serglycin-GFP cells, expressing Serglycin with a C-terminal GFP tag, as Serglycin-GFP could be used in studies of synthesis and sorting of one individual PG molecule in addition to studies of the bulk of PGs secreted.

The experiment was conducted as described in the methods chapter (Section 2.2: Biochemical analysis of proteoglycans). The cells were preincubated with 2.0 µM CPT for 4 h before addition of ^{35}S-sulphate to the medium, followed by a 20 h labeling period in the absence or presence of CPT.

At the end of the labeling period, apical media, basolateral media, and cell lysates were harvested. Macromolecules were separated from unincorporated ^{35}S-sulphate by gel filtration on Sephadex G-50 fine columns and aliquots were subjected to scintillation counting (Figure 3.4.1.1).

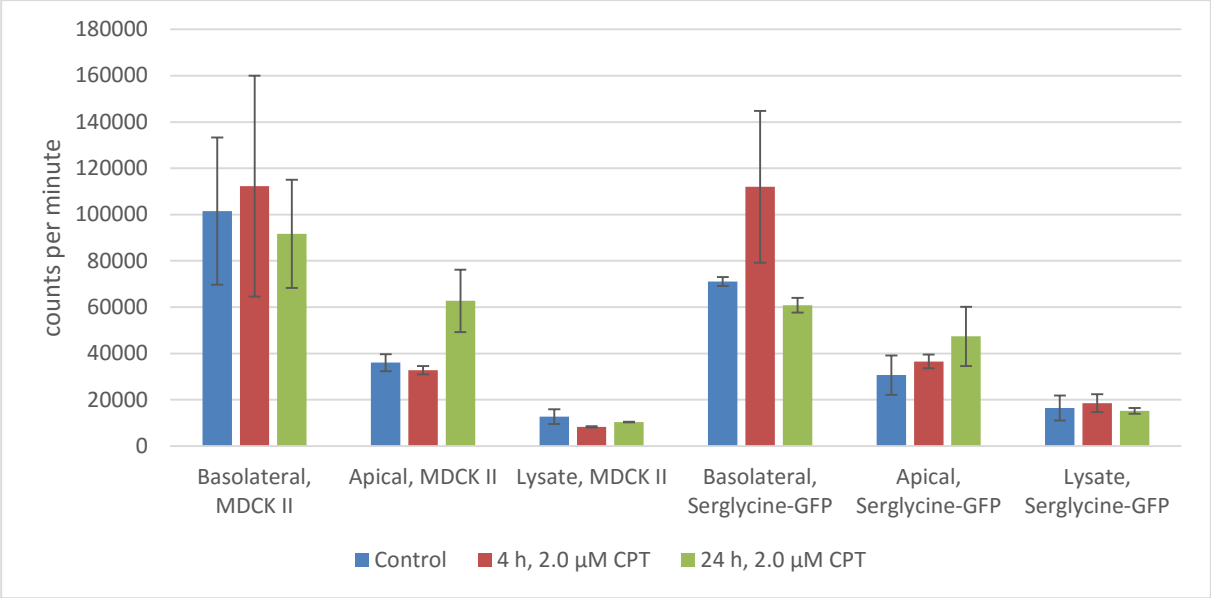

Figure 3.4.1.1: Incorporation ^{35}S-sulphate into macromolecules by MDCK II cells and MDCK II Serglycin-GFP cells treated or not with 2.0 µM CPT for 4 h and 24 h. Secretion of ^{35}S-sulphate labeled macromolecules in the absence (control) or presence of 2.0 µM CPT. MDCK II cells (MDCK II) and MDCK II Serglycin-GFP cells (Serglycin-GFP) were incubated (4 h and 24 h) or not (Control) for 4 h, before addition of 0.2 mCi/ml of ^{35}S-sulphate to the medium and further incubation in the absence (Control and 4 h) and presence (24 h) of CPT. Labeled macromolecules secreted to the apical or basolateral media or remaining in the cell fractions were isolated by Sephadex G-50 Fine and representative aliquots were analyzed by scintillation counting. Bars show average of 2 parallel samples. Error bars represent the standard error multiplied by 2. (Table 3.4.1.1)

In the untreated fractions (Control), the major amount of labeled macromolecules is secreted to the basolateral media, a lesser amount is secreted apically, and a minor amount is retained in the cell fraction (Figure 3.4.1.1). This distribution is observed for both MDCK II cells and MDCK II Serglycin-GFP cells. Due to the low sample size, variations between these two cell lines could not be established to be significant.

There is an increase in the average of basolaterally secreted macromolecules upon CPT treatment for 4 h, but the variation in the parallels and the low number of experiments means that this cannot be said to be significant (Figure 3.4.1.1). Basolaterally, 24 h treated cells

secreted less labeled macromolecules compared to the control, possibly a significant reduction for the MDCK II Serglycin-GFP samples. The apical medium showed an increase in the average amount of secreted macromolecules after 24 h of CPT treatment, when compared to the control (Figure 3.4.1.1). However, the results in Figure 3.4.1.1 are uncertain due to the low number of experiments and the large variation in the parallels.

The MDCK II Serglycin-GFP samples were subjected to SDS-PAGE. Metabolic label with ^{35}S-sulphate were mainly incorporated into PGs. Due to modification with GAG chains, these are often large in size, and will not migrate far into the gel.

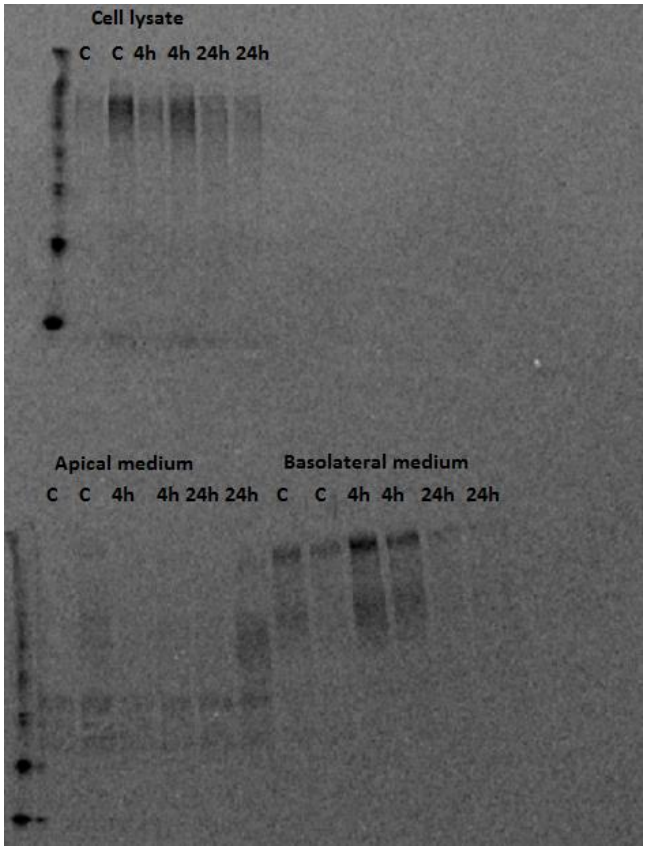

Figure 3.4.1.2: MDCK II Serglycin-GFP cells treated with CPT and metabolically labeled with ^{35}S-sulphate.

MDCK II SG-GFP cells were grown on filters to confluency (96 h). Two samples were left untreated (C), and two samples were treated for 4 h with 2.0 μM CPT (4h). The last two samples were treated for 4 h with 2.0 μM CPT followed by an additional 20 h with 2.0 μM CPT (24h). Metabolic labeling was performed for all samples for 20 h. Labeled macromolecules secreted to the apical or basolateral media or remaining in the cell fractions

were isolated by Sephadex G-50 Fine. SDS-PAGE was then performed. Bands show secreted and cellular macromolecules that have been metabolically labeled with ^{35}S-sulphate.

From the SDS-PAGE (Figure 3.4.1.2), we observed that the apical samples have low signal strength, with some variation between the parallels. Also the cell lysate samples have some variation between the parallels, including in the control samples. The basolateral samples have bands stronger than untreated (control) samples after 4 h of treatment, but bands with less signal than untreated cells at 24 h (Figure 3.4.1.3.B). The variation between 4 h and 24 h treated basolateral fractions could possibly indicate a concentration and/or time dependent change in secretion.

3.4.2 The effect of doxorubicin on synthesis and secretion of ^{35}S-sulphate labeled macromolecules by MDCK II PAPST1-GFP cells

Doxorubicin (Doxo) was employed in a second trial to investigate effects on polarized PG synthesis and secretion in epithelial cells. For this experiment, we use another sub-cell line of MDCK II cells expressing PAPST1-GFP. Due to the PAPST1-GFP cells expressing increased amounts of the PAPST1 protein, these cells exhibit higher levels of sulphation of apically sorted chondroitin sulphate (CS) (Dick et al. 2008). We also used this cell line for the majority of the Golgi apparatus imaging experiments in Section 3.2, and for cell death assays in Section 3.3, allowing us to compare results in this section with those presented in earlier sections.

To study the effects of Doxo on sorting of labeled macromolecules, the cells were treated with 0.25 µM Doxo, 0.5 µM Doxo, and 0.75 µM Doxo. 0.25 µM Doxo had previously not been observed to induce Golgi dispersal in MDCK II PAPST1-GFP cells, but we were interested to investigate whether this concentration could still affect PG sorting. We increased our initial incubation time with Doxo to 6 h, for which we had previously observed the Golgi apparatus to be dispersed (Section 3.2: Incubating with DNA damaging agents). Subsequently, we initiated metabolic labeling for 18 h with ^{35}S-sulphate in the continued presence of Doxo. This combines to a total 24 h Doxo treatment time.

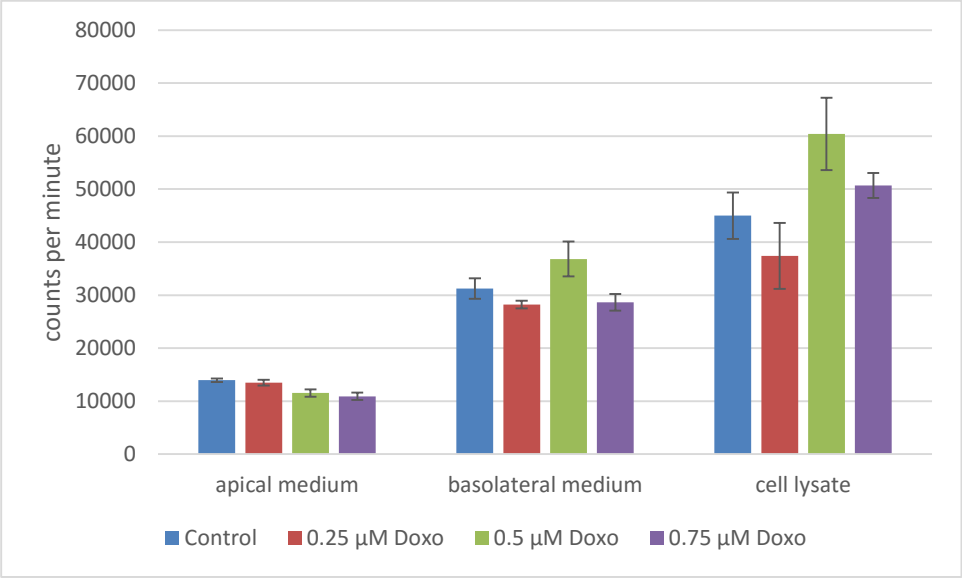

Figure: 3.4.2.1: Synthesis and secretion of ^{35}S-sulphate labeled macromolecules by MDCK II PAPST1-GFP cells treated with 0.25 µM, 0.5 µM or 0.75 µM Doxo (Table 3.4.2.1).

Secretion of ^{35}S-sulphate labeled macromolecules in the absence (Control) or presence of 0.25 µM, 0.5 µM, or 0.75 µM Doxo. MDCK II PAPST1-GFP cells were grown on filters to confluency (96 h). The cells were incubated for 6 h before addition of 0.2 mCi/ml of ^{35}S-sulphate to the medium and further incubation in the presence (24 h total) of Doxo. Labeled macromolecules secreted to the apical and basolateral media or remaining in the cell fractions were isolated by Sephadex G-50 Fine and representative aliquots were analyzed by scintillation counting. Bars show average scintillation counts of 3 (2 of 0.75 µM, apical medium) parallel samples. Error bars represent the standard error multiplied by 2. (Table 3.4.2.1).

Upon Doxo treatment, there was a gradual decline in the apical secretion of ^{35}S-sulphate labeled macromolecules (Figure 3.4.3.1/Table 3.4.3.1). For the basolateral medium, we could not observe a corresponding decline in the secretion of sulphated macromolecules, but rather a possible increase (not necessarily significant) for the samples treated with 0.5 µM Doxo, which was also observed for the cell lysates (Figure 3.4.2.1). The samples were further analyzed by SDS-PAGE.

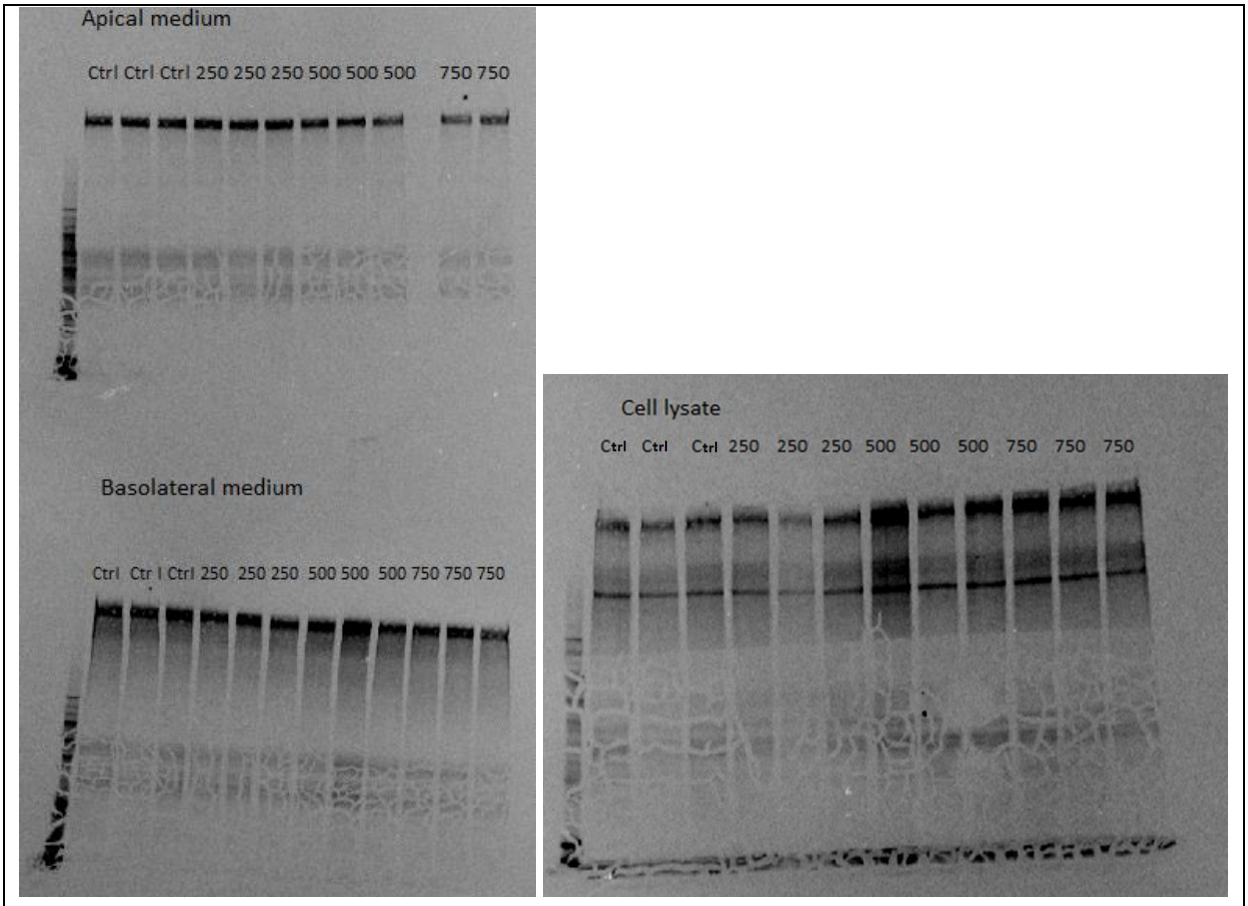

A) apical and basolateral medium B) Cell lysates

Figure 3.4.2.2: SDS-PAGE of samples from MDCK II PAPST1-GFP cells treated with 0.25 µM, 0.5 µM or 0.75 µM Doxo.

Secretion of ^{35}S-sulphate labeled macromolecules in the absence (Ctrl) or presence of 0.25 µM (250), 0.5 µM (500), or 0.75 µM Doxo (750). MDCK II PAPST1-GFP cells were grown on filters to confluency (96 h). The cells were then incubated for 6 h before addition of 0.2 mCi/ml of ^{35}S-sulphate to the medium and further incubation in the presence (24 h total) of Doxo. Labeled macromolecules secreted to the apical or basolateral media or remaining in the cell fractions were isolated by Sephadex G-50 Fine. SDS-PAGE was then performed. Bands show secreted macromolecules that have been metabolically labeled with ^{35}S-sulphate.

We observed some cracking towards the bottom of the SDS-PAGE gels, due to insufficient drying (Figure 3.4.2.2), the PGs, however, are mainly located at the top of the gel. The apical gel showed a possible reduction in signal at 0.75 µM, which could also be the case for the basolateral samples. The lysate gel has two bands of interest in each sample, an upper band and one further into the gel. The upper band increases in signal density with increased Doxo concentration, while the lower band seems to remain unchanged (Figure 3.4.2.2). Further

quantification of the gels was performed using ImageQuant TL.

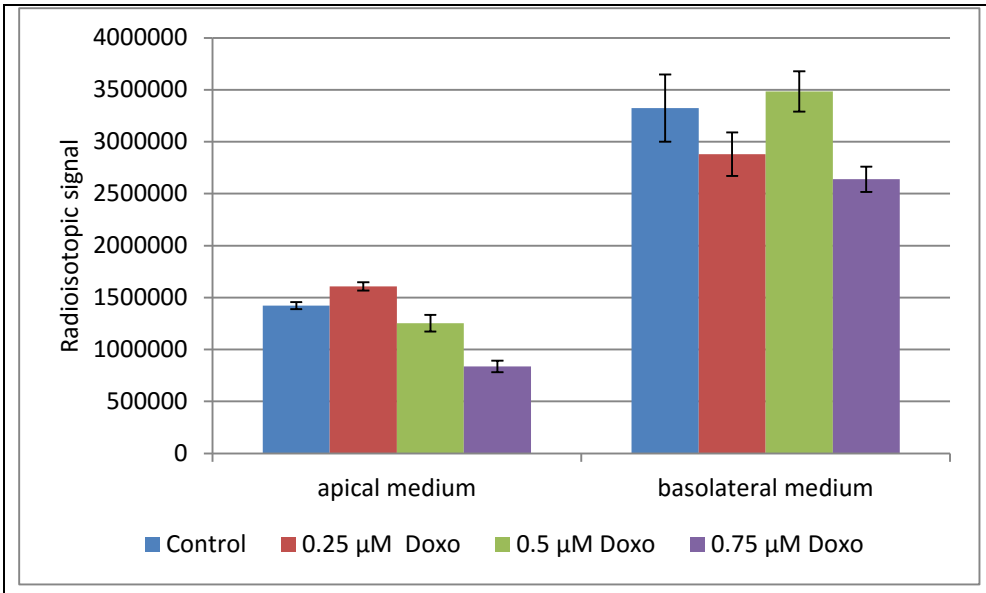

Figure 3.4.2.3: Quantification of SDS-PAGE gels of ^{35}S-sulphate labeled macromolecules synthesized by MDCK II PAPST1-GFP cells treated with 0.25 µM, 0.5 µM or 0.75 µM Doxo. Apical and basolateral media (Table 3.4.2.3).

The chart was created using numerical values from Appendix Table 3.4.2.3. These numbers represent the average area and strength of each upper band in the apical and basolateral gels from Figure 3.4.2.2, as generated using ImageQuant TL. This graph is representative for changes in apically and basolaterally secreted macromolecules after treatment with 0.25 µM, 0.5 µM or 0.75 µM Doxo. The Y-Axis has arbitrary units, representing quantitation by ImageQuant of radioisotopic signals detected by phosphorimager screens scanned in a Typhoon 9400 FLA laser scanner. Error bars represent the standard error multiplied by 2 (Table 3.4.2.3).

After analysis of the apical and basolateral medium samples (Figure 3.4.2.3), we observed a reduction in signal strength of the upper band for the apical samples for cells treated with 0.50 µM and 0.75 µM, when Doxo compared to untreated (Control). At 0.25 µM Doxo we observed an increase in signal strength, which could be an indication of a concentration dependent change in apical secretion (Figure 3.4.2.3). For the basolateral samples, there is more variation in the signals from the Doxo treated-samples (Figure 3.4.2.3). It is not possible to conclude whether there has been a significant change in PG secretion to the basolateral medium during Doxo treatment.

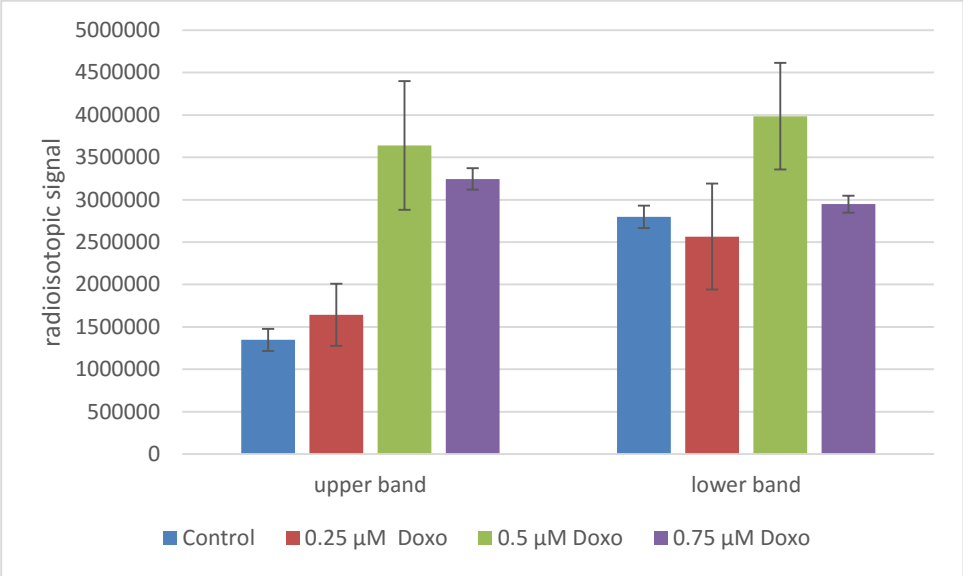

The Y-Axis has arbitrary units, represents quantitation by ImageQuant of radioisotopic signals detected by phosphorimager screens as scanned in a Typhoon 9400 FLA laser scanner.

Figure 3.4.2.4 SDS-PAGE of ^{35}S-labeled macromolecules synthesized by MDCK II PAPST1-GFP cells treated with 0.25 µM, 0.5 µM or 0.75 µM Doxo, 2 bands in cell lysate. (Table 3.4.2.3).

The chart presents numerical values from Table 3.4.2.3. These numbers represent the average area and strength of each upper and lower bands in the gel with the lysate samples (Figure 3.4.2.2), as generated using ImageQuant TL. This graph is representative for changes in macromolecules retained in the cell lysate after treatment (or not) with 0.25 µM, 0.5 µM or 0.75 µM Doxo. Error bars represent the standard error multiplied by 2 (Table 3.4.2.3).

There was an increase in the upper band signal strength after treatment with 0.5 µM and 0.75 µM Doxo (Figure 3.4.2.4). The 0.25 µM sample increase is not as noticeable, and the error bar has overlap with the untreated (Control) sample. The middle band does not have a clear indication of any change in signal strength after treatment with Doxo.

3.4.3 The effect of doxorubicin and Camptothecin on synthesis and secretion of ^{35}S-sulphate labeled macromolecules in MDCK II PAPST1-GFP cells

Due to variations between parallels and relatively large error bars (due to few samples) between average concentrations, it was decided to do a third ^{35}S-sulphate labeling experiment.

For this experiment we used both CPT and Doxo. We had earlier deduced (Section 3.3: Cell viability) that we could incubate MDCK II PAPST1-GFP cells for 24 h in the presence of 4.0 µM Doxo and still retain > 90 % viability. We have also concluded that MDCK II PAPST1-GFP cells can be incubated for 24 h with 2.0 µM Doxo and retain > 90 % viability. This would be the upper limit concentrations of what we could use. We also decided to incubate in the presence of 0.5 µM Doxo, due to earlier Doxo experiments showing high variation between parallels at this concentration. 0.5 µM also represents the lowest concentration where we have observed a change in Golgi structure (Section 3.2: Incubation with DNA damaging agents).

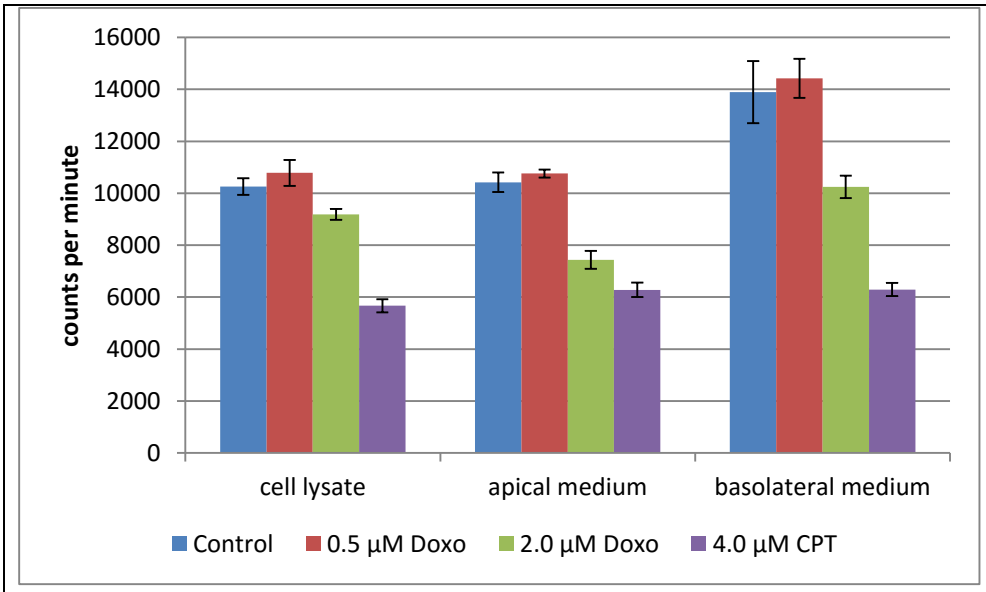

Figure: 3.4.3.1: Scintillation count of samples from MDCK II PAPST1-GFP cells treated with 0.5 µM or 2.0 µM of Doxo, or 4.0 µM CPT (Table 3.4.3.1).
Secretion of ^{35}S-sulphate labeled macromolecules in the absence (Control) or presence of 0.5 µM Doxo, 2.0 µM Doxo, or 4.0 µM CPT. MDCK II PAPST1-GFP cells were grown on filters to full confluency (96 h). The cells were incubated for 6 h before addition of 0.2 mCi/ml of ^{35}S-sulphate to the medium and further incubation in the presence (24 h total) of Doxo or CPT. Labeled macromolecules secreted to the apical or basolateral media, or remaining in the cell fractions were isolated by Sephadex G-50 Fine and representative aliquots were analyzed by scintillation counting. Bars show average scintillation counts of 3 (2 of 0.5 µM Doxo) parallel samples. Error bars represent the standard error multiplied by 2 (Table 3.4.2.1).

What we could observe from the scintillation counting (Figure 3.4.3.1), was a significant reduction of the signal in samples treated with 4.0 µM CPT and 2.0 µM Doxo in the cell

lysates, the apical medium and the basolateral medium in comparison to the untreated (Control) samples. Further analysis was done by SDS-PAGE.

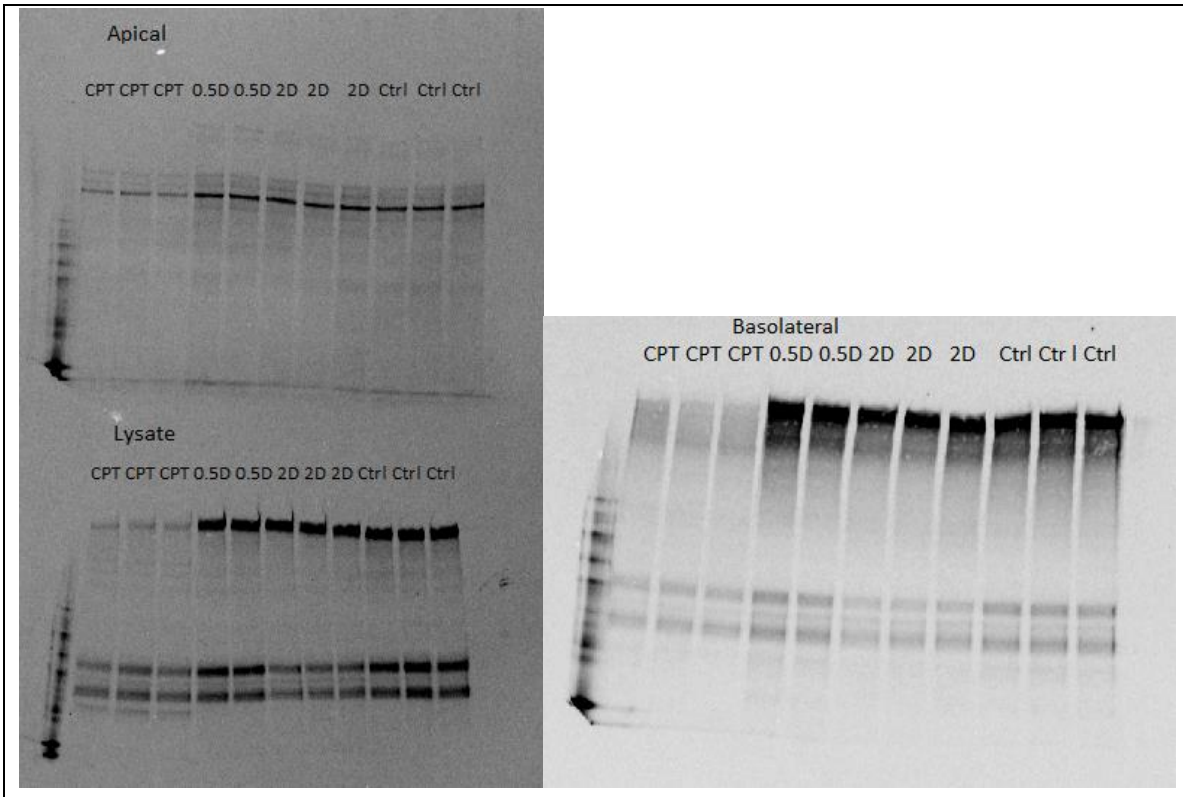

A) Apical media and cell lysates B) basolateral media

Figure 3.4.3.2: SDS-PAGE of samples from MDCK II PAPST1-GFP cells treated with 0.5 µM or 2.0 µM Doxo, or 4.0 µM CPT.

Secretion of ^{35}S-sulphate labeled macromolecules in the absence (Ctrl) or presence of 0.5 µM Doxo (0.5D), 2.0 µM Doxo (2D), or 4.0 µM CPT (CPT). MDCK II PAPST1-GFP cells were grown on filters to confluency (96 h). The cells were then incubated for 6 h before addition of 0.2 mCi/ml of ^{35}S-sulphate to the medium and further incubation in the absence, or presence, (24 h total) of Doxo. Labeled macromolecules secreted to the apical or basolateral media or remaining in the cell fractions were isolated by Sephadex G-50 Fine. SDS-PAGE was then performed. Bands show macromolecules that have been metabolically labeled with ^{35}S-sulphate.

As was observed for the scintillation counts, there was a significant reduction in ^{35}S-labeled macromolecules in the cell lysate (Figure 3.4.3.2.B). There was a lesser separation of the upper and lower bands in the cell lysate samples.

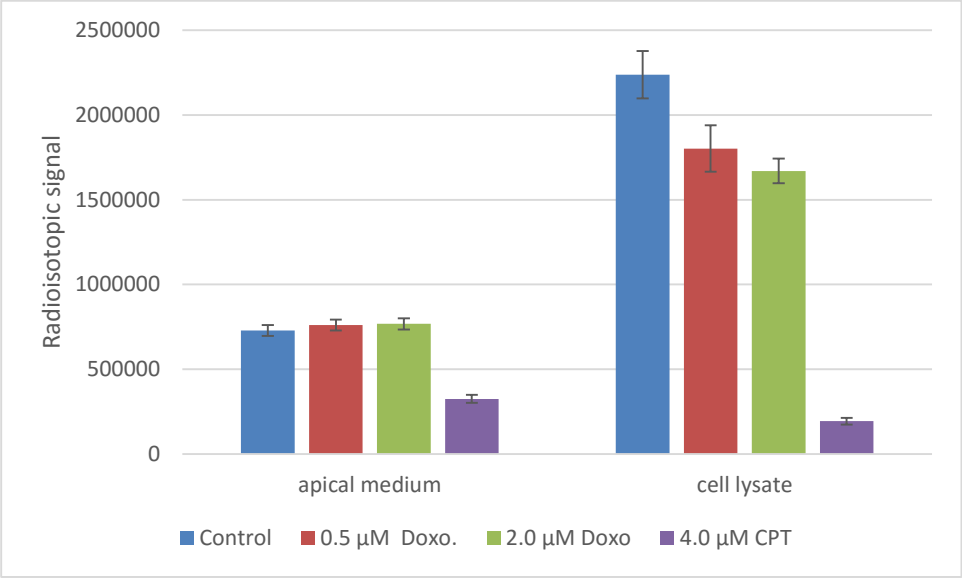

A) Apical medium and lysate.

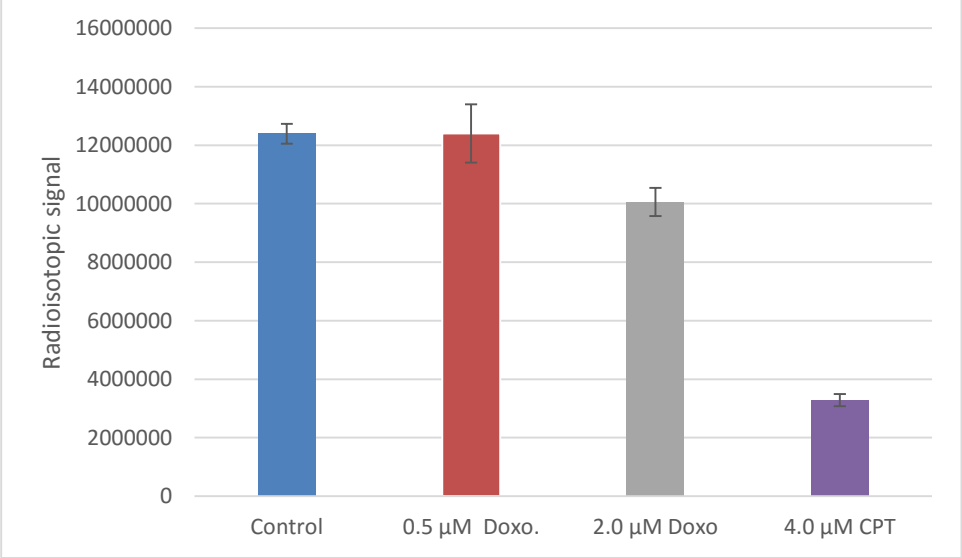

B) Basolateral medium

Figure 3.4.3.3: SDS-PAGE of samples from MDCK II PAPST1-GFP cells treated with 0.5 µM and 2.0 µM of Doxo, and 4.0 µM CPT (Table 3.4.3.2).

A) The chart presents numerical values from Appendix Table 3.4.3.2. These numbers represent the average area and strength of each top and middle band in the apical medium and cell lysate samples from Figure 3.4.3.2.A, as generated using ImageQuant TL. This graph describes the labeled macromolecules in the SDS-PAGE gels with samples of apical medium and cell lysates after treatment (or not) with 0.5 µM Doxo, 2.0 µM Doxo, or 4.0 µM CPT. The Y-Axis has arbitrary units, represents quantitation by ImageQuant of radioisotopic

signals detected by phosphorimager screens as scanned in a Typhoon 9400 FLA laser scanner. Error bars represent the standard error multiplied by 2 (Table 3.4.3.2).

B) The chart was created using numerical values from Appendix Table 3.4.3.2. These numbers represent the average area and strength of each upper and lower band in the basolateral medium samples in Figure 3.4.3.2.B, generated using ImageQuant TL. This graph is shows the labeled macromolecules in the SDS-PAGE gels with samples of basolateral medium after treatment (or not) with 0.5 µM Doxo, 2.0 µM Doxo, or 4.0 µM CPT. The Y-Axis has arbitrary units, represents quantitation by ImageQuant of radioisotopic signals detected by phosphorimager screens as scanned in a Typhoon 9400 FLA laser scanner. Error bars represent the standard error multiplied by 2. (Table 3.4.3.2)

In accordance with the data obtained for ^{35}S-labeled macromolecules (Figure 3.4.3.1) SDS-PAGE also indicated a reduction in ^{35}S-labeled macromolecules in the apical and basolateral media after incubation with 4.0 µM Doxo (Figure 3.4.3.3). The 4.0 µM CPT treatment had a more significant effect than earlier treatments by Doxo. Opposed to the preceding experiment (Figure 3.4.2.3), we had no reduction in ^{35}S-labeled macromolecules secreted apically in the Doxo treated samples this time (Figure 3.4.3.3).

The lysate samples were more difficult to compare to the previous experiment with Doxo, since the two (upper and lower) bands were less separated in this experiment Figure 3.4.3.3.A: cell lysate compared to Figure 3.4.2.4). Of note is also that the Doxo concentrations used are different.

4 Discussion

4.1 DNA damage induced morphological changes in the Golgi apparatus structure in MDCK II cells

The aim of this study was to induce DNA damage and visualize the effect on the morphology of the Golgi apparatus, and to analyze the effect on PG sorting and secretion in polarized epithelial cells.

The Golgi apparatus in an MDCK cell grown under optimal growth conditions should form a tight monolayer with each cell having a columnar shape, with the Golgi apparatus forming a ribbon-like structure located in the apical region, above the nucleus (Bacallao et al. 1989). In our visualization experiments this was similarly observed, where optical planes towards the basolateral side of columnar epithelial cells, below the nucleus, had little Golgi-specific signal. However, in our visualization experiments the cells were grown on glass bottom dishes, which are not as optimal for growing a tight cell layer as the filters used in Bacallao et al.'s experiments (Bacallao et al. 1989). Thus, the cell layer is not as tight, and the cells themselves are not as columnar as they would be when grown on filter. For this reason, in our images the Golgi apparatus is not located to the same degree towards the apical side, and is located more towards the side of the nucleus in the middle plane. Nucleus size and position was visualized using the Hoechst stain. From this area of the cell, the Golgi marker is naturally absent. When a DNA inducing agent was added, an x-, y- and z-plane dispersal was induced. Areas of the cell cytoplasm that previously had no Golgi signal present, now show a less concentrated and dispersed signal.

In this thesis we worked with DNA damaging agents that have been reported to increase cell death due to apoptosis (Liu et al. 2000; Morris & Geller 1996; Tacar, Sriamornsak & Crispin R. Dass 2013; Eom et al. 2005). It has also been observed that changes in Golgi morphology can occur as a result of apoptosis (Qian & Yang 2009; Chiu et al. 2002; Jung et al. 2006; Lane et al. 2002; Mancini et al. 2000). So the changes to Golgi morphology seen in this thesis could be wholly or partially a result of apoptosis. However, it has been shown that treatment with an anti-apoptotic drug reduced the number of apoptotic cells after treatment with CPT, but without causing a reduction in Golgi dispersal (Farber-Katz et al. 2014). This indicates that the Golgi dispersal from DNA damage is not linked to the dispersal from apoptosis.

Fragmentation and dispersal of the Golgi apparatus can occur in other situations as well. For example, treatment with the microtubule depolymerizing agent nocodazole creates a situation where the Golgi disperses and locates to specific ER exit sites where the stacks regenerate and most Golgi function is restored (Iida & Shibata 1991; Cole et al. 1996). This sets a precedent of Golgi function being intact despite morphological changes. However, microtubule depolymerized dispersal of the Golgi apparatus is unlike the GOLPH3/MYO18A/F-actin pathway in that the fragmentation in this pathway is random, the Golgi apparatus completely disperses through the cytoplasm, and does not specifically localize to peripheral sites in the cell.

Another example is during mitosis, where the Golgi apparatus disperses through the activation of a MEK1/ERK-signaling cascade (Wei & Seeman 2009). This does not employ the same mechanisms as DNA damage induced Golgi dispersal, as cell-cycle arrest in CPT treated cells are observed to occur in G1 or early S phase, and the dispersal of the Golgi apparatus is noticeable after cell proliferation as recovered (Farber-Katz et al. 2014).

In future experiments it could be interesting to perform 3D modeling with several z-stacks from the same sample and process these through iMaris, in combination with a time-lapse experiment, utilizing the lower passage MDCK II PAPST1-GFP cells due to their sensitivity to DNA damage. This would allow us to produce a 3D model of Golgi dispersal as it happens in individual cells. To reduce the effects of photo-bleaching, the interval between z-stack scanning would have to be set significantly higher than what was done in the time-lapse experiment in this thesis. Such experiments could yield better dispersal data through iMaris, as long as complications like cell death does not compromise the experiment.

4.2 Cell viability assays

While doing initial imaging experiments to investigate possible Golgi apparatus dispersal, it was discovered that high concentrations of Doxo and CPT would cause a loss of cell layer confluency in the 35 mm MatTek glass bottom dishes. Earlier findings have also observed apoptosis mediated cell death through treatment with both CPT (e.g. Liu et al. 2000; Morris & Geller 1996) and Doxo (e.g. Tacar, Sriamornsak & Crispin R. Dass 2013; Eom et al. 2005). This led us to investigate the viability of cells treated with DNA damaging agents. The activation of the GOLPH3/MYO18A/F-actin pathway triggered by such agents should protect

against activation of apoptosis and increase cell survival (Farber-Katz et al. 2014), but it has also been reported that both CPT and Doxo have cytotoxic properties beyond damage to DNA (Liu et al. 2000; Tacar, Sriamornsak & Crispin R Dass 2013; Farber-Katz et al. 2014). For this reason, it is difficult to say whether any cell death observed has a single cause.

What was interesting was that MDCK II cells treated with Doxo frequently showed loss of cell layer confluency when treated with more than 3 μM Doxo during visualization experiments (mentioned in Section 3.2: Incubation with DNA damaging agents), but the Trypan blue exclusion assays showed at least 90 % viability after incubation in the presence of 5 μM Doxo or less (Section 3.3.2: Trypan blue viability assay), without any significant reduction in total cell number due to loss of cell adhesion. Incubation with CPT showed a significant decline in total cell numbers compared to control at concentrations higher than 4 μM, indicating reduced cell adhesion as well as possible cell death. This is important, because a consequence of a high viability loss, or a reduction in cell number, results in a reduction in the total synthesis of PGs in a culture system.

4.3 Metabolic ^{35}S-labeling of PGs

A major aim of this thesis was to investigate to what extent a dispersed Golgi apparatus was functionally affected. One major function of the Golgi apparatus in mammalian cells is the synthesis and secretion of PGs. As discussed in the introduction, there are still areas of Golgi function that are unknown, leading to several models for how the organelle operates. It was hoped that we could expand our understanding of the Golgi apparatus by addressing how the Golgi functions like synthesis, sorting, and secretion of PGs are affected when the organelle system is in a dispersed state. If normal Golgi functions is retained it could operate with or without a reduction in efficiency. Glycosylation mechanisms could be performed as normal, or there could be possible changes to the glycosylation patterns. GAG composition could change, as well as the length, type and sulphation patterns of the individual GAGs. There could be a change in polarized sorting in epithelial cells, and these changes could be connected to certain morphological changes in the Golgi apparatus.

The labeling experiments we performed showed us that the Golgi apparatus appears to have retained some function post-death. We still found sulphated PGs secreted to the apical and basolateral media. We did not, however, see any major change in the sorting and secretion of

PGs between apical and basolateral media. In experiment 3.4.2 we observed a reduction in apical and basolateral sorted PGs (Figure 3.4.2.3), but a potential increase in PGs in the cell fraction (Figure 3.4.2.4). This could be an indication of an increase in the time lag between synthesis and secretion of PGs. In the final experiment (Section 3.4.3: Effect of doxorubicin synthesis and sorting) we were able to observe a reduction in sulphated PGs in the cell lysate and both apical and basolateral media when the cells were treated with 4.0 μM CPT (Figure 3.4.3.3). We also observed a reduction of sulphated PGs in lysates and basolateral medium samples from cells treated with 2.0 μM Doxo, but not in the apical medium samples.

Due to the large reduction of ^{35}S-labeled macromolecules in the cell lysate and in the apical and basolateral media after incubation with 4.0 μM CPT, there is a good possibility that this is a result of loss of cell adhesion and/or cell death. However, our cell viability assays (Section 3.3: Cell viability) and microscope visualization (Section 3.2: Incubation with DNA damaging agents) indicated that this was not the case. Due to the low number of experiments performed, it is difficult to conclude, and the viability criteria need to be established firmly. Especially considering that in one experiment, treatment of cells with 2.0 μM Doxo gives no significant reduction in apical secretion of PGs as observed by SDS-PAGE analysis (Figure 3.4.3.3), while another experiment shows a significant reduction in apically secreted PGs after SDS-PAGE for cells treated with 0.75 μM Doxo (Figure 3.4.2.3). In conclusion, there seems to be a reduction in the synthesis of ^{35}S-sulphate labeled macromolecules upon Doxo treatment, but the concentration dependence needs to be addressed further.

Additional experiments could be performed to investigate whether there is a variation in the change of modification pattern and synthesis levels for individual PGs that are being secreted or remain in the cell fraction. It could be interesting to analyze if the sorting of PGs rich in CS or HS are affected similarly post Golgi dispersal. It could also be of interest to analyze the PG sulphation patterns in cells with a dispersed Golgi apparatus. More metabolic labeling experiments could be performed to better quantify the reduction in PG secretion to strengthen the data obtained, and to investigate whether the reduction is similar for both apical and basolateral secretion of CS- and HSPGs. Considering there are also secretory Golgi apparatus bypass routes described for MDCK cells (Tveit et al. 2009; Prydz et al. 2013). It could also be worth labeling the cells with ^{35}S-cysteine/methionine to detect changes in overall protein synthesis and secretion after Golgi dispersal by Doxo or CPT.

Incubation of MDCK cells with Brefeldin A (BFA), which in most cell types causes a disassembly of the Golgi complex by preventing COPI vesicles to bind to Golgi membranes by inhibition of ARF1 (Fujiwara et al. 1988; Alvarez & Sztul 1999; Orci et al. 1991; Donaldson et al. 1992), have shown that treatment of the more BFA-resistant MDCK cells with high concentrations of BFA causes a retardation of secreted proteins, particularly in the apical direction, and an accumulation in the ER and ERGIC, giving a more dispersed distribution of molecules that normally enter the Golgi apparatus (Tveit et al. 2009). This could be similar to what was observed in this thesis in section 3.4.2, and might warrant further investigation in the future.

It has also been observed that the transport retardation of secreted proteins is BFA concentration dependent in MDCK cells. At low concentrations (2 µg/mL) only apical transport is affected, while basolateral transport is only affected at higher concentration (5 µg/mL and above) (Tveit et al. 2009). It is possible that PG synthesis and sorting after dispersal of the Golgi complex due to DNA damage induction could be concentration dependent in a similar manner. We observed some variations in concentration which could be attributed to this, with a small increase in basolaterally secreted macromolecules at 0.5 µM Doxo but a reduction at 0.75 µM Doxo (Figure 3.4.2.3). However, we would need to do more experiments at these concentrations to establish the result as significant, especially since this was not reproduced in the last experiment (Figure 3.4.3.2).

It has also been shown that in the case of apical secretory transport of Serglycin-GFP that bypasses the Golgi apparatus, that these protein cores were secreted without Golgi modifications, with a lower molecular mass. Since these protein cores lack sulphate labeling, it was not possible to establish whether we have an increase in secretion of unmodified proteins, and this could be worth investigating in the future.

4.4 Golgi morphology changes in cancer development and GOLPH3

As stated in the introduction, changes in the Golgi apparatus structure and internal environment have been observed in cancer cells (Kellokumpu et al. 2002; Li & Wang 1989; Schulenberg et al. 2003). Further, altered glycosylation in cancer cells is prolific and possibly

universal (Gao et al. 2012), warranting further investigations into how tumor cells change their glycosylation patterns, both as studies of how this affects cell survival, but also for developing novel screening methods for certain cancers (Dabelsteen 1996). These alterations could change antigenicity (Peracaula et al. 2003; Bresalier et al. 1996; Burke et al. 2006; Garbar et al. 2008; Tabarés et al. 2006), which could aid cancer cells in avoiding immune system surveillance. Glycans are further involved in tumor cell processes like cell signaling, tumor cell dissociation and invasion, cell–matrix interactions, tumor angiogenesis, and metastasis (Pinho & Reis 2015).

It would be of interest to investigate whether the changes in Golgi morphology due to incubation with DNA damage inducers observed in this thesis, share similarities with changes in the Golgi morphology and proteoglycan synthesis and cell surface transport observed in cancer cells (Salanti et al. 2015). Visually, the morphological changes to the cancer cells are very similar to pH dependent dispersal of the Golgi apparatus, where in both cases the Golgi apparatus can be relatively well dispersed through the cytoplasm of the whole cell (Kellokumpu et al. 2002). Since it has been shown that GOLPH3 is an oncogene that when overexpressed is associated with poor clinical outcome in several cancer types (Hu et al. 2013; Hua et al. 2012; Kunigou et al. 2011; Li et al. 2012), and overexpression of GOLPH3 leads to Golgi dispersal (Ng et al. 2013), more research is required to investigate why dispersal of the Golgi apparatus is the cellular response to chemically induced DNA damage.

List of references

Alvarez, C. & Sztul, E.S., 1999. Brefeldin A (BFA) disrupts the organization of the microtubule and the actin cytoskeletons. *European journal of cell biology*, 78(1), pp.1–14.

Bacallao, R. et al., 1989. The subcellular organization of Madin-Darby canine kidney cells during the formation of a polarized epithelium. *The Journal of cell biology*, 109(6), pp.2817–32.

Bannykh, S.I., Rowe, T. & Balch, W.E., 1996. The organization of endoplasmic reticulum export complexes. *The Journal of cell biology*, 135(1), pp.19–35.

Bresalier, R.S. et al., 1996. Enhanced sialylation of mucin-associated carbohydrate structures in human colon cancer metastasis. *Gastroenterology*, 110(5), pp.1354–67.

Brown, P.S. et al., 2000. Definition of distinct compartments in polarized Madin-Darby canine kidney (MDCK) cells for membrane-volume sorting, polarized sorting and apical recycling. *Traffic*, 1(2), pp.124–40.

Burke, P.A. et al., 2006. Characterization of MUC1 glycoprotein on prostate cancer for selection of targeting molecules. *International journal of oncology*, 29(1), pp.49–55.

Chiu, R. et al., 2002. A caspase cleavage fragment of p115 induces fragmentation of the Golgi apparatus and apoptosis. *The Journal of cell biology*, 159(4), pp.637–48.

Cole, N.B. et al., 1996. Golgi dispersal during microtubule disruption: regeneration of Golgi stacks at peripheral endoplasmic reticulum exit sites. *Molecular biology of the cell*, 7(4), pp.631–50.

Dabelsteen, E., 1996. Cell surface carbohydrates as prognostic markers in human carcinomas. *The Journal of pathology*, 179(4), pp.358–69.

Dick, G. et al., 2015. PAPST1 regulates sulfation of heparan sulfate proteoglycans in epithelial MDCK II cells. *Glycobiology*, 25(1), pp.30–41.

Dick, G., Grondahl, F. & Prydz, K., 2008. Overexpression of the 3'-Phosphoadenosine 5'-Phosphosulfate (PAPS) Transporter 1 Increases Sulfation of Chondroitin Sulfate in the Apical Pathway of MDCK II Cells. *Glycobiology*, 18(1), pp.53–65.

Dippold, H.C. et al., 2009. GOLPH3 bridges phosphatidylinositol-4- phosphate and actomyosin to stretch and shape the Golgi to promote budding. *Cell*, 139(2), pp.337–51.

Donaldson, J.G. et al., 1992. ADP-ribosylation factor, a small GTP-binding protein, is required for binding of the coatomer protein beta-COP to Golgi membranes. *Proceedings of the national academy of sciences of the United States of America*, 89(14), pp.6408–12.

Eom, Y.-W. et al., 2005. Two distinct modes of cell death induced by doxorubicin: apoptosis and cell death through mitotic catastrophe accompanied by senescence-like phenotype. *Oncogene*, 24(30), pp.4765–77.

Farber-Katz, S.E. et al., 2014. DNA Damage Triggers Golgi Dispersal via DNA-PK and GOLPH3. *Cell*, 156(3), pp.413–427.

Fujiwara, T. et al., 1988. Brefeldin A causes disassembly of the Golgi complex and accumulation of secretory proteins in the endoplasmic reticulum. *The Journal of biological chemistry*, 263(34), pp.18545–52.

Futter, C.E. et al., 1995. Newly synthesized transferrin receptors can be detected in the endosome before they appear on the cell surface. *The Journal of biological chemistry*, 270(18), pp.10999–1003.

Gao, Y. et al., 2012. Glycosylation potential of human prostate cancer cell lines. *Glycoconjugate journal*, 29(7), pp.525–37.

Garbar, C., Mascaux, C. & Wespes, E., 2008. Expression of MUC1 and sialyl-Tn in benign prostatic glands, high-grade prostate intraepithelial neoplasia and malignant prostatic glands: a preliminary study. *Analytical and quantitative cytology and histology / the international academy of cytology [and] american society of cytology*, 30(2), pp.71–7.

Garcia-Gonzalo, F.R. & Reiter, J.F., 2012. Scoring a backstage pass: mechanisms of ciliogenesis and ciliary access. *The Journal of cell biology*, 197(6), pp.697–709.

Glick, B.S. & Luini, A., 2011. Models for Golgi traffic: a critical assessment. *Cold spring harbor perspectives in biology*, 3(11), p.a005215.

Grøndahl, F., Tveit, H. & Prydz, K., 2009. Neutralization of endomembrane compartments in epithelial MDCK cells affects proteoglycan synthesis in the apical secretory pathway. *Biochemical journal*, 418(3), pp.517–528.

Herzlinger, D.A., Easton, T.G. & Ojakian, G.K., 1982. The MDCK epithelial cell line expresses a cell surface antigen of the kidney distal tubule. *The Journal of cell biology*, 93(2), pp.269–77.

Hu, B.-S. et al., 2013. Overexpression of GOLPH3 is associated with poor clinical outcome in gastric cancer. *Tumor biology*, 34(1), pp.515–520.

Hua, X. et al., 2012. Increased expression of Golgi phosphoprotein-3 is associated with tumor aggressiveness and poor prognosis of prostate cancer. *Diagnostic pathology*, 7, p.127.

Iida, H. & Shibata, Y., 1991. Functional Golgi units in microtubule-disrupted cultured atrial myocytes. *The journal of histochemistry and cytochemistry*, 39(10), pp.1349–55.

Jung, E.J. et al., 2006. Myosin VI is a mediator of the p53-dependent cell survival pathway. *Molecular and cellular biology*, 26(6), pp.2175–86.

Kellokumpu, S., Sormunen, R. & Kellokumpu, I., 2002. Abnormal glycosylation and altered Golgi structure in colorectal cancer: dependence on intra-Golgi pH. *FEBS Letters*, 516(1-3), pp.217–224.

Kolset, S.O., Vuong, T.T. & Prydz, K., 1999. Apical secretion of chondroitin sulphate in polarized Madin-Darby canine kidney (MDCK) cells. *Journal of cell science*, 112, pp.1797–801.

Kunigou, O. et al., 2011. Role of GOLPH3 and GOLPH3L in the proliferation of human rhabdomyosarcoma. *Oncology reports*, 26(5), pp.1337–42.

Lane, J.D. et al., 2002. Caspase-mediated cleavage of the stacking protein GRASP65 is required for Golgi fragmentation during apoptosis. *The Journal of cell biology*, 156(3), pp.495–509.

Laplante, M. & Sabatini, D.M., 2009. mTOR signaling at a glance. *Journal of cell science*, 122, pp.3589–94.

Lavieu, G., Zheng, H. & Rothman, J.E., 2013. Stapled Golgi cisternae remain in place as cargo passes through the stack. *eLife*, 2, p.e00558.

Li, H. et al., 2012. GOLPH3 overexpression correlates with tumor progression and poor prognosis in patients with clinically N0 oral tongue cancer. *Journal of translational medicine*, 10, p.168.

Li, Q.F. & Wang, D.Y., 1989. [Changes of Golgi complex during the induced differentiation of human gastric adenocarcinoma cells in vitro]. *Shi yan sheng wu xue bao*, 22(1), pp.87–97.

Lin, W.-L. et al., 2015. Lewisy promotes migration of oral cancer cells by glycosylation of epidermal growth factor receptor. *PloS one*, 10(3), p.e0120162.

Liu, L.F. et al., 2000. Mechanism of action of camptothecin. *Annals of the New York academy of sciences*, 922, pp.1–10.

Mancini, M. et al., 2000. Caspase-2 is localized at the Golgi complex and cleaves golgin-160 during apoptosis. *The Journal of cell biology*, 149(3), pp.603–12.

Mertens, G. et al., 1996. Heparan sulfate expression in polarized epithelial cells: the apical sorting of glypican (GPI-anchored proteoglycan) is inversely related to its heparan sulfate content. *The Journal of cell biology*, 132(3), pp.487–97.

Mogelsvang, S. et al., 2004. Predicting Function from Structure: 3D Structure Studies of the Mammalian Golgi Complex. *Traffic*, 5(5), pp.338–345.

Morris, E.J. & Geller, H.M., 1996. Induction of neuronal apoptosis by camptothecin, an inhibitor of DNA topoisomerase-I: evidence for cell cycle-independent toxicity. *The Journal of cell biology*, 134(3), pp.757–70.

Morsomme, P., Prescianotto-Baschong, C. & Riezman, H., 2003. The ER v-SNAREs are required for GPI-anchored protein sorting from other secretory proteins upon exit from the ER. *The Journal of cell biology*, 162(3), pp.403–12.

Muñiz, M. & Riezman, H., 2000. Intracellular transport of GPI-anchored proteins. *The EMBO journal*, 19(1), pp.10–5.

Ng, M.M. et al., 2013. GOLPH3L antagonizes GOLPH3 to determine Golgi morphology. *Molecular biology of the cell*, 24(6), pp.796–808.

Orci, L. et al., 2000. Anterograde flow of cargo across the golgi stack potentially mediated via bidirectional "percolating" COPI vesicles. *Proceedings of the national academy of sciences of the United States of America*, 97(19), pp.10400–5.

Orci, L. et al., 1991. Brefeldin A, a drug that blocks secretion, prevents the assembly of non-clathrin-coated buds on Golgi cisternae. *Cell*, 64(6), pp.1183–95.

Peracaula, R. et al., 2003. Altered glycosylation pattern allows the distinction between prostate-specific antigen (PSA) from normal and tumor origins. *Glycobiology*, 13(6), pp.457–70.

Pfeffer, S.R., 2010. How the Golgi works: A cisternal progenitor model. *Proceedings of the national academy of sciences of the United States of America*, 107(46), pp.19614–19618.

Pinho, S.S. & Reis, C.A., 2015. Glycosylation in cancer: mechanisms and clinical implications. *Nature*, 15(9), pp.540–555.

Prydz, K. et al., 2013. Arrivals and departures at the plasma membrane: direct and indirect transport routes. *Cell and tissue research*, 352(1), pp.5–20.

Prydz, K. & Dalen, K.T., 2000. Synthesis and sorting of proteoglycans. *Journal of cell science*, 113, pp.193–205.

Prydz, K., Dick, G. & Tveit, H., 2008. How Many Ways Through the Golgi Maze? *Traffic*, 9(3), pp.299–304.

Przybylo, M. et al., 2002. Different glycosylation of cadherins from human bladder non-malignant and cancer cell lines. *Cancer cell international*, 2, p.6.

Qian, H. & Yang, Y., 2009. Alterations of cellular organelles in human liver-derived hepatoma G2 cells induced by adriamycin. *Anti-cancer drugs*, 20(9), pp.779–86.

Rossi, S., 2013. *Australian medicines handbook (2013 ed.)*

Salanti, A. et al., 2015. Targeting Human Cancer by a Glycosaminoglycan Binding Malaria Protein. *Cancer cell*, 28(4), pp.500–514.

Sannerud, R. et al., 2006. Rab1 defines a novel pathway connecting the pre-Golgi intermediate compartment with the cell periphery. *Molecular biology of the cell*, 17(4), pp.1514–26.

Saraste, J. & Kuismanen, E., 1984. Pre- and post-Golgi vacuoles operate in the transport of Semliki Forest virus membrane glycoproteins to the cell surface. *Cell*, 38(2), pp.535–49.

Sarnataro, D. et al., 2004. PrP(C) association with lipid rafts in the early secretory pathway stabilizes its cellular conformation. *Molecular biology of the cell*, 15(9), pp.4031–42.

Schulenberg, B., Beechem, J.M. & Patton, W.F., 2003. Mapping glycosylation changes related to cancer using the Multiplexed Proteomics technology: a protein differential display approach. *Journal of chromatography B*, 793(1), pp.127–139.

Schweizer, A. et al., 1991. The isolated ER-Golgi intermediate compartment exhibits properties that are different from ER and cis-Golgi. *The Journal of cell biology*, 113(1), pp.45–54.

Scott, K.L. et al., 2009. GOLPH3 modulates mTOR signalling and rapamycin sensitivity in cancer. *Nature*, 459(7250), pp.1085–90.

Sheff, D.R. et al., 1999. The receptor recycling pathway contains two distinct populations of early endosomes with different sorting functions. *The Journal of cell biology*, 145(1), pp.123–39.

Simons K, Wandinger-Ness A., 1990. Polarized sorting in epithelia. *Cell*, pp.62:207–210.

Slimane, T.A. et al., 2000. Apical secretion and sialylation of soluble dipeptidyl peptidase IV are two related events. *Experimental cell research*, 258(1), pp.184–94.

Stoops, E.H. & Caplan, M.J., 2014. Trafficking to the Apical and Basolateral Membranes in Polarized Epithelial Cells. *Journal of the american society of nephrology*, 25(7), pp.1375–1386.

Stornaiuolo, M. et al., 2003. KDEL and KKXX retrieval signals appended to the same reporter protein determine different trafficking between endoplasmic reticulum, intermediate compartment, and Golgi complex. *Molecular biology of the cell*, 14(3), pp.889–902.

Svennevig, K., Prydz, K. & Kolset, S.O., 1995. Proteoglycans in polarized epithelial Madin-Darby canine kidney cells. *The biochemical journal*, 311, pp.881–8.

Tabarés, G. et al., 2006. Different glycan structures in prostate-specific antigen from prostate cancer sera in relation to seminal plasma PSA. *Glycobiology*, 16(2), pp.132–45.

Tacar, O., Sriamornsak, P. & Dass, C.R., 2013. Doxorubicin: An update on anticancer molecular action, toxicity and novel drug delivery systems. *Journal of pharmacy and pharmacology*, 65(2), pp.157–170.

Tveit, H. et al., 2005. A Proteoglycan Undergoes Different Modifications en Route to the Apical and Basolateral Surfaces of Madin-Darby Canine Kidney Cells. *Journal of biological chemistry*, 280(33), pp.29596–29603.

Tveit, H. et al., 2009. A Secretory Golgi Bypass Route to the Apical Surface Domain of Epithelial MDCK Cells. *Traffic*, 10(11), pp.1685–1695.

Walter, P. & Johnson, A.E., 1994. Signal Sequence Recognition and Protein Targeting to the Endoplasmic Reticulum Membrane. *Annual review of cell biology*, 10(1), pp.87–119.

Wei, J.-H. & Seemann, J., 2009. Mitotic division of the mammalian Golgi apparatus. *Seminars in cell & developmental biology*, 20(7), pp. 810-816.

Wei, J.-H. & Seemann, J., 2010. Unraveling the Golgi ribbon. *Traffic*, 11(11), pp.1391–400.

Appendix 1: Materials and reagents

Radioactive isotopes	Manufacturer	Cat. No
[^{35}S] Sulphuric acid	Hartmann Analytic	S-RA-1

Disposable equipment	Manufacturer
10 mL syringe	BD
15 mL tubes	Sarstedt
50 mL tubes	Sarstedt
6 well culture plate	Costar
Criterion XT Precast Gel 4 - 12 % Bis - Tris	BioRad
Cryogenic vial	Corning
Microfuge tube	Sarstedt
Sterile 5, 10 and 25 mL pipettes	Sarstedt
Ultra clear centrifuge tubes	Beckman
Nunc EasyFlask 75 cm2	Thermo Scientific
35 mm glass bottom dishes	MatTek

Equipment	Manufacturer
Autoclave SS -325	TOMY
Cell incubator	
Centrifuge 5415R	Eppendorf
Centrifuge GS-15R	Beckman
Minispin	Eppendorf
Confocal laser scanning microscope FLUOVIEW FV1000	Olympus
Liquid scintillation analyzer 1900 TR	Packard
pH meter 420	Thermo
Typhoon 9400 Variable Mode Imager	GE Healthcare
Gel electrophoresis chamber	VWR
PowerPac basic power supply	BIO-RAD

Reagents	Manufacturer	Cat. No
DMEM 4.5 g/L glucose w/ L-glutamine	Lonza	BE12-604F/12
DMEM Opti-MEM (1X)	Gibco	11058-021
DMEM RPMI 1640 medium	Gibco	041-90985 M
Penicillin-Streptomycin	Lonza	17-602

Trypsin-EDTA	Gibco	25300-104
Amplify	GE Healthcare	NAMP100
XT-MOPS running buffer	BioRad	161-0788
XT reducing agent	BioRad	161-0792
XT sample buffer	BioRad	161-0791
Protein molecular weight marker [methyl - 14 C] methylated	Perkin Elmer	81101 UC
Sephadex G-50 Fine	GE Healthcare	17-0042-01
Camptothecin	Sigma-Aldrich	C911
Doxorubicin hydrochloride	Sigma-Aldrich	D4583
Dimethylsulfoxide	Duchefa	D1370 0250
Ultima Gold XR	PerkinElmer	6013119

Molecular markers and stains	Manufacturer	Cat. No.
CellLight Golgi-RFP	ThermoFisher	C10593
Hoechst 33258	ThermoFisher	31716W
Propidium iodide	ThermoFisher	P3566
BODIPY® TR Ceramide complexed to BSA	ThermoFisher	B-34400
Trypan blue stain	ThermoFisher	T10282

Software	Manufacturer	Link:
ImageQuant TL	GE Healthcare	tinyurl.com/ogptvbh
iMaris	BITPLANE	tinyurl.com/p9f9j66

Appendix 2: Results data

Section 3.2: Incubation with DNA damaging agents and changes in the Golgi apparatus morphology

Table 3.2.7.1: Golgi apparatus and nuclear areas (µm^2) derived from 3D images.

	Control	0.5 µM	2 µM
Nuclear area (µm^2)	25353	19473	18397
Nuclear count	82	80	84
Avg. nuclear area (µm^2)	309,1829	243,4125	219,0119
Golgi area (µm^2)	14951	9173,73	34822,45
Golgi area nuclear average (µm^2)	182,3293	114,6716	414,553
Golgi area relative to nucleus	0,589713	0,4711	1,892833

'Nuclear Area' is the total of nuclear signal (Hoechst) detected in µm^2. 'Nuclear count' is the number of detected nuclei. Avg. Nuclear area is the total nuclear area divided by the number of nuclei, showing the average size of the nuclei. 'Golgi area' is the total area of Golgi apparatus signal (PAPST1-GFP) detected in µm^2. 'Golgi area nuclear average' is the average Golgi apparatus area per nucleus. 'Golgi area relative to nucleus' is the 'Golgi area nuclear average' divided by the 'avg. nuclear area'.

Section 3.3: Cell viability after incubation with DNA damage inducers

Table 3.3.1: Trypan blue, raw data for Doxo.

	Control	Control	Control	0,4 uM	0,5 uM DOX	0,75 uM	1.0 µM	1.0 µM	2.0 µM	2.0 µM	4.0 µM	5.0 µM
Total	8E+05	1E+06	1E+06	1E+06	1E+06	2E+06	1E+06	1E+06	1E+06	2E+06	2E+06	1E+06
Alive	7E+05	1E+06	1E+06	1E+06	9E+05	2E+06	1E+06	1E+06	1E+06	2E+06	1E+06	9E+05
Dead	20000	40000	40000	100000	50000	90000	30000	50000	1E+05	70000	90000	70000
Viability	0,97	0,97	0,97	0,93	0,95	0,95	0,98	0,96	0,91	0,96	0,98	0,93

Table 3.3.2: Trypan blue, avgerage data for Doxo.
This table has the average data of values from table 3.3.1 where applicable.

	Control	0.4 µM	0.5 µM	0,75 µM	1.0 µM	2.0 µM	4.0 µM	5.0 µM
Avg. Total	1E+06	1E+06	1E+06	2E+06	1E+06	1E+06	2E+06	1E+06
Avg. Alive	1E+06	1E+06	9E+05	2E+06	1E+06	1E+06	1E+06	9E+05
Avg. Dead	33333	1E+05	50000	90000	40000	85000	90000	70000
Avg. Viability	0,97	0,93	0,95	0,95	0,97	0,935	0,98	0,93
Avg. Relative	1	1,234	0,921	1,519	1,092	1,329	1,424	0,94

Table 3.3.3: Trypan blue, raw data for CPT.

	Control	Control	Control	2.0 µM	2.0 µM	2.0 µM	4.0 µM	4.0 µM	5.0 µM	6.0 µM	6.0 µM	10.0 µM
Total	2E+06	2E+06	1E+06	1E+06	1E+06	1E+06	2E+06	9E+05	4E+05	2E+06	3E+05	2E+05
Alive	2E+06	1E+06	1E+06	910000	1E+06	1E+06	1E+06	8E+05	3E+05	2E+06	3E+05	90000
Dead	40000	70000	40000	140000	1E+05	50000	70000	80000	80000	1E+05	60000	60000
Viability	0,98	0,96	0,97	0,87	0,89	0,97	0,95	0,91	0,81	0,93	0,84	0,6

Table 3.3.4: Trypan blue, average data for CPT.
This table has the average data of values from 3.3.3 where applicable.

	Control	2.0 µM	4.0 µM	5.0 µM	6.0 µM	10.0 µM
Avg. Total	2E+06	1E+06	1E+06	420000	1E+06	2E+05
Avg. Alive	1E+06	1E+06	1E+06	340000	9E+05	90000
Avg. Dead	50000	1E+05	75000	80000	90000	60000
Avg. Viability	0,97	0,88	0,93	0,81	0,885	0,6
Avg.Relative	1	0,702	0,756	0,2681	0,651	0,096

Section 3.4: Incubation with DNA damaging agents and changes in the Golgi apparatus morphology.

Table 3.4.1.1: Scintillation counts of Incorporation ^{35}S-sulphate into macromolecules by MDCK II cells and MDCK II Serglycin-GFP cells treated or not with 2.0 µM CPT for 4 and 24 h.

Basolateral			Apical			Lysate		
MDCKII	Count	Type	MDCKII	Count	Type	MDCKII	Count	Type
1.	133363	Control	1.	39735	Control	1.	15925	Control
2.	69754	Control	2.	32309	Control	2.	9498	Control
3.	64639	2uM CPT, 4H	3.	34612	2uM CPT, 4H	3.	8574	2uM CPT, 4H
4.	159948	2uM CPT, 4H	4.	30989	2uM CPT, 4H	4.	7987	2uM CPT, 4H
5.	68299	2uM CPT, 24H	5.	49288	2uM CPT, 24H	5.	10558	2uM CPT, 24H
6.	115001	2uM CPT, 24H	6.	76242	2uM CPT, 24H	6.	10262	2uM CPT, 24H
Avg Controll	101559		Avg Controll	36022		Avg Controll	12712	
Avg 4h	112294		Avg 4h	32801		Avg 4h	8281	
Avg 24h	91650		Avg 24h	62765		Avg 24h	10410	
Stdev. Ctrl	31804,5		Stdev. Ctrl	3713		Stdev. Ctrl	3214	
Stdev. 4H	47654,5		Stdev. 4H	1812		Stdev. 4H	293,5	
Stdev. 24H	23351		Stdev. 24H	13477		Stdev. 24H	148	

Basolateral			Apical			Lysate		
MDCKII-SG	Count	Type	MDCKII-SG	Count	Type	MDCKII-SG	Count	Type
1.	72943	Control	1.	22089	Control	1.	10997	Control
2.	69104	Control	2.	39193	Control	2.	21803	Control
3.	144786	2uM CPT, 4H	3.	39500	2uM CPT, 4H	3.	14615	2uM CPT, 4H
4.	79193	2uM CPT, 4H	4.	33573	2uM CPT, 4H	4.	22453	2uM CPT, 4H
5.	64056	2uM CPT, 24H	5.	34551	2uM CPT, 24H	5.	16462	2uM CPT, 24H
6.	57649	2uM CPT, 24H	6.	60210	2uM CPT, 24H	6.	13995	2uM CPT, 24H
Avg Controll	71023,5		Avg Controll	30641		Avg Controll	16400	
Avg 4h	111990		Avg 4h	36537		Avg 4h	18534	
Avg 24h	60852,5		Avg 24h	47381		Avg 24h	15229	
Stdev. Ctrl	1919,5		Stdev. Ctrl	8552		Stdev. Ctrl	5403	
Stdev. 4H	32796,5		Stdev. 4H	2964		Stdev. 4H	3919	
Stdev. 24H	3203,5		Stdev. 24H	12830		Stdev. 24H	1234	

Table 3.4.2.1: Scintillation count of MDCK II PAPST1-GFP treated with 0.25 µM, 0.5 µM or 0.75 µM Doxo.

	Apical	Basolateral	Lysate
MDCKII	Count	Count	Count
Control	13476	34794	52655
Control	14570	30770	37430
Control	13805	28109	44888
250nM	13633	27341	43268
250nM	12486	29667	24936
250nM	14295	27659	43920
500nM	12429	31027	73754
500nM	10155	42497	51361
500nM	12033	36953	56135
750nM		27771	55358
750nM	10060	31731	48706
750nM	11751	26447	47957
Avg. Control	13950,33333	31224,33333	44991
Avg. 250nM	13471,33333	28222,33333	37374,66667
Avg. 500nM	11539	36825,66667	60416,66667
Avg. 750nM	10905,5	28649,66667	50673,66667
Std. error. Ctrl	324,0629226	1943,117798	4395,380643
Std. error. 250	528,4323777	728,1431483	6222,180682
Std. error. 500	701,3786424	3311,715836	6809,579388
Std. error. 750	690,3478592	1587,367352	2352,125587

Table 3.4.2.3: SDS-PAGE signal bands of MDCK II PAPST1-GFP treated with 0.25 µM, 0.5 µM or 0.75 µM Doxo.

	Apical	Basolateral	Lysate	Lysate
MDCK II PAPST1-GFP	Volume	Volume	Top Band Volume	Middle Band Volume
Control	1359508	3946367	1208394	3000922
Control	1471742	3161074	1224623	2552187
Control	1439152	2863232	1609393	2845466
250	1624086	2766414	2125270	3597282
250	1531120	2589881	923724	1440071
250	1664879	3286051	1877695	2657652
500	1291006	3369924	4897226	4453219
500	1371574	3863581	2278311	2742204
500	1099666	3222758	3745082	4760059
750		2878330	3479055	3082264
750	768840	2562019	3049296	3006106
750	905930	2475731	3208275	2754463
Avg. Ctrl.	1423467,33	3323557,67	1347470	2799525
Avg. 250nM	1606695	2880782	1642229,667	2565001,667
Avg. 500nM	1254082	3485421	3640206,333	3985160,667
Avg. 750nM	837385	2638693,33	3245542	2947611
Std. error Ctrl	33334,788	323056,271	131045,2702	131559,5007
Std. error 250nM	39579,8883	208944,328	366292,7517	624453,8648
Std. error 500nM	80635,0347	193793,874	757832,0226	627758,8849
Std. Error 750nM	55966,7581	122380,151	125452,2771	99044,80917

Table: 3.4.3.1: Scintillation count of MDCK II PAPST1-GFP treated with 0.5 µM and 2.0 µM of Doxo, and 4.0 µM CPT.

	Lysate	Apical	Basolateral
MDCK II PAPST1-GFP	Count	Count	Count
Controll	10618	10657	14376
Controll	10134	10619	14765
Controll	10011	9990	12532
0.5 µM Doxo	10280	10914	13674
0.5uM Doxo	11283	10606	15173
2 µM Doxo	9418	7669	11113
2uM Doxo	8758	6761	9783
2uM Doxo	9381	7867	9848
4uM CPT	5786	6275	5922
4uM CPT	6038	6758	6782
4uM CPT	5186	5800	6172
Avg. Ctrl.	10254,33333	10422	13891
Avg. 0.5uM Dox	10781,5	10760	14423,5

Avg. 2uM Dox	9185,666667	7432,333333	10248
Avg. 4uM CPT	5670	6277,666667	6292
Std. error Ctrl	185,2676742	216,27837	688,716439
Std. error 0.5uM Doxo	501,5	154	749,5
Std. error 2uM Doxo	214,0999247	340,4983276	432,9068414
Std. error 4uM CPT	252,6974476	276,5539931	255,4081701

Table 3.4.3.2: SDS-PAGE of MDCK II PAPST1-GFP treated with 0.5 µM and 2.0 µM of Doxo, and 4.0 µM CPT.

	Apical	Basolateral	Lysate
MDCK II PAPST1-GFP	Volume	Volume	Volume
Control	681928	11734199	1964184
Control	716941	12887543	2317056
Control	789004	12548146	2430093
500nM Doxo	729045	13396534	1664494
500nM Doxo	792907	11402490	1938796
2.0uM Doxo	708094	9565515	1747278
2.0uM Doxo	775422	9596049	1525402
2.0uM Doxo	822121	11027229	1736976
4.0uM CPT	278744	3447084	156641
4.0uM CPT	346611	2865862	223462
4.0uM CPT	351354	3534413	202374
Avg. Ctrl.	729291	12389962,7	2237111
Avg. 500nM Doxo	760976	12399512	1801645
Avg. 2.0uM Doxo	768545,6667	10062931	1669885,33
Avg. 4.0uM CPT	325569,6667	3282453	194159
Std. error Ctrl	31520,94182	342207,087	140310,609
Std. error 500nM	31931	997022	137151
Std. error 2uM	33095,83132	482229,564	72302,8538
Std. error 4uM CPT	23452,83427	209815,502	19722,0366